



UNIVERSITY OF NAIROBI

**PROBABILISTIC SEISMIC HAZARD
ASSESSMENT OF SOUTHERN KENYA**

BY

Acholla Emmanuel Mulehane

I56/6732/2017

A Dissertation submitted in partial fulfillment of the requirements for the Degree of Master of Science in Geology (Seismology) of the University of Nairobi.

October 2022

DECLARATION


I declare that this dissertation is my original work and has not been submitted in any other University for examination, award of a degree or publication. Where other people's work or my own work has been used, this has been properly acknowledged and referenced in accordance with the University of Nairobi's requirements.


Signature 

Date 14-October-2022

Acholla Emmanuel Mulehane
I56/6732/2017

This dissertation has been submitted for examination with our approval as university supervisors:

	Signature	Date
Dr. Josphat Kyalo Mulwa Department of Earth & Climate Sciences University of Nairobi P.O. Box 30197-00100 Nairobi, Kenya jkmulwa@uonbi.ac.ke		17 th October 2022

Dr. Zachariah Njuguna Kuria Department of Earth & Climate Sciences University of Nairobi P.O. Box 30197-00100 Nairobi, Kenya zkuria@uonbi.ac.ke		18 th October 2022
---	---	-------------------------------

ABSTRACT

Kenya's Indian Ocean coastline is a passive continental margin that resulted from the breakup of the East and West Gondwanaland supercontinent during the Jurassic-Tertiary age and is consequently expected to have minimal seismic activity. However, earthquake data from 1938 to 2019 contains several shallow moderate earthquakes that occur both onshore and offshore. Previous works done in quantifying the seismic hazard in the region of Southern Kenya propose a quasi-uniform low seismic hazard or assume a uniform bedrock foundation with seismic hazard curves limited to Mombasa city. The main aim of the study was to carry out a detailed probabilistic seismic hazard assessment of the study area. The specific objectives included demarcation of the seismic source zones, computation of the peak horizontal earthquake ground accelerations and drafting an updated seismic hazard map of the area. The outputs are presented in terms of peak ground acceleration (PGA) in cm/s/s (gals) for a 10% probability of exceedance in 50 years with a return period of 475 years. Results indicate that there are three distinct seismic source zones covering the area, which align with the trends of major faults. PGA values range from 59.0 cm/s/s at Voi town in Taita-Taveta County, 68.4 cm/s/s at Malindi town in northern Kilifi County to 88 cm/s/s at Vanga town in southern Kwale County. Seismic hazard spectra indicate that PGA values are highest at short periods (<0.5seconds). Thus, the seismic hazard in the study area increases southwards. The PGA maps are an aid in seismic risk analyses for the preparation of County Seismic Building Codes. The seismic hazard curves and spectra are an aid in anti-seismic design of future critical civil engineering projects in the area of study.

ACKNOWLEDGEMENTS

This study was accomplished under a full scholarship by the University of Nairobi Graduate School. I am sincerely grateful to the University of Nairobi for this honour.

My sincere gratitude goes to my supervisors, Dr. Josphat K. Mulwa and Dr. Zachariah N. Kuria of the University of Nairobi's Department of Earth and Climate Science for their expert guidance and advice during my postgraduate research.

I recognize Dr. Edwin W. Dindi of the University of Nairobi's Department of Earth and Climate Science who inspired my interest into the seismo-tectonics of passive continental margins.

I sincerely thank Dr. Mario Ordaz of the *Instituto de Ingeniera*, Mexico, for graciously providing me access to the CRISIS 2015 v4.1 programme for my seismic hazard analysis.

I am also grateful to Anna Maria Lombardi of the *Istituto Nazionale di Geofisica e Vulcanologia*, Italy for her gracious assistance in the use of SEDA V1.0 programme for earthquake catalog analysis.

I would also like to thank the management of the Nuclear Power and Energy Agency (formerly, Kenya Nuclear Electricity Board) for facilitating my attendance of the crucial coursework classes and the field research.

Above all, I am eternally grateful to the Almighty God for his providence, blessings, care and protection throughout this research.

DEDICATION

Then the earth shook and trembled; the foundations of the hills also quaked and were shaken,
Because He was angry. (Psalm 18:7)

Table of Contents

1	INTRODUCTION	1
1.1	BACKGROUND INFORMATION	1
1.2	SCOPE OF THE RESEARCH	2
1.3	PROBLEM STATEMENT	2
1.4	AIM AND OBJECTIVES	3
1.4.1	AIM OF THE RESEARCH	3
1.4.2	OBJECTIVES	3
1.5	JUSTIFICATION AND SIGNIFICANCE	3
2	LITERATURE REVIEW	5
3	THE STUDY AREA.....	8
3.1	Location.....	8
3.2	Physiography.....	9
3.3	Coastal plate tectonics.....	10
3.4	Stratigraphy	11
3.5	Lithology	13
	Megasequence II (Sabaki Group).....	14
	Megasequence III (Tana Group)	15
	Megasequence IV (Coastal Group).....	15
3.6	Crustal thickness	16
3.7	Dynamics of The Tectono-sedimentary depo-basin	16
3.8	Seismology.....	19
3.9	Meteorology	21
3.10	Hydrology	24
3.11	Hydrogeology.....	25
3.12	Land uses.....	26
3.13	Soils.....	27
3.14	Vegetation	28
4	THEORY OF PROBABILISTIC SEISMIC HAZARD ASSESSMENT.....	30
4.1	Introduction	30
4.2	Steps Involved in PSHA	30
4.2.1	Earthquake Source Identification	31

4.2.2	Earthquake Source Characterization	32
4.2.3	Attenuation Law Selection	33
4.2.4	Calculation of Earthquake Hazard	35
5	METHODOLOGY	36
5.1	Materials Used in Research	36
5.2	Desktop Studies	40
5.2.1	Delineation of seismic sources	41
5.2.2	Earthquake data collection	43
5.2.3	Review of published seismic hazard works	43
5.3	Ground Truthing	43
5.3.1	Ground Truthing Activities	44
5.4	Computation of Seismic Hazard	49
5.4.1	Hazard Computation Procedure	50
6	DATA ANALYSIS	54
6.1	Earthquake Catalog Assembly	54
6.2	Catalog compilation	55
6.3	Catalog Homogenization	57
6.4	Catalog Declustering	57
6.5	Completeness Check	58
6.6	Magnitude-frequency relation	59
6.7	Calculation of Hazard	60
6.8	Hazard Curves & Spectra	63
6.9	Mapping of Hazard	63
7	RESULTS	64
7.1	Seismic Sources	64
7.1.1	Area Seismic Source Zone Model (ASZ)	64
7.2	Seismic Hazard	65
7.2.1	Spectrum-Dependent Hazard	67
7.2.2	Updated Seismic Hazard Map	74
7.3	Hazard Curves and Spectra	75
7.3.1	Malindi	75
7.3.2	Watamu	76
7.3.3	Kilifi	77

7.3.4	Mombasa	77
7.3.5	Voi	78
7.3.6	Kwale	79
7.3.7	Ukunda	79
7.3.8	Vanga	80
8	DISCUSSIONS	81
8.1	Seismic Sources	81
8.2	Seismic Hazard.....	82
8.3	Hazard Curves and Spectra	83
9	CONCLUSIONS AND RECOMMENDATIONS	85
9.1	Conclusions	85
9.2	Recommendations	86
9.3	Areas for Further Research	87
10	REFERENCES	88
11	APPENDICES.....	94
11.1	COMBINED EARTHQUAKE CATALOG (USGS & ISC, AD1938-2020).....	94
11.2	FIELD GROUND TRUTHING SCHEDULE	101
11.3	LOCATION OF POSTULATED OFFSHORE FAULT	102

LIST OF TABLES

Table 3-1 Deep wells drilled within the study area	11
Table 3-2 Stratigraphy of the study area (Adapted from Caswell 1953, 1956).....	13
Table 5-1 Software used in this study.....	36
Table 5-2 Hardware and logistics used in this study	37
Table 7-1 Peak Ground Accelerations for major towns in the Study Area	66

LIST OF FIGURES

Figure 1-1 Map of the study area showing faults and earthquake epicenters.....	2
Figure 3-1 The Study Area	8
Figure 3-2 Map showing the main tectonic features in the area (Adapted from Wanjala, 2020)	10
Figure 3-3 Lithological contacts of deep wells in the area (Adapted from Kivuti Nyagah, 1995).....	12
Figure 3-4 Lithology of the study area	14
Figure 3-5 Map showing instrumental earthquakes in the study area	20
Figure 3-6 Climate graph for Kilifi town.....	21
Figure 3-7 Climate graph for Malindi town.....	22
Figure 3-8 Climate graph for Mombasa City.....	22
Figure 3-9 Climate graph for Kwale town.....	23
Figure 3-10 Climate graph for Voi town	23
Figure 3-11 Hydrological features in the study area.....	24
Figure 3-12 A Map of the hydrogeological resources in the study area (Adapted from McDonald et al. 2010)	26
Figure 3-13 Land cover and use in the Study Area	27
Figure 3-14 Soils in the Study Area (Courtesy: ILRI).....	28
Figure 3-15 Vegetation in the study area.....	29
Figure 4-1 Basic steps involved in PSHA (Adapted from: Cornell-McGuire).....	31
Figure 5-1 Laptop computer used in this research (Toshiba S50W)	38
Figure 5-2 Field equipment used in this study (Left to Right: Notebook, pen, tape measure, GPS, Camera and tablet).....	39
Figure 5-3 A natural colour satellite image (bands 4,3,2) of the Study Area, showing ISC and USGS earthquake epicenters (©Used with permission from Google LLC. Google LLC's registered trademarks include Google and the Google logo.)	41
Figure 5-4 A Sentinel-2 satellite image (bands 11, 8, 2) of three sag ponds trending NE-SW located at Vitengeni, 24 Km W of Watamu town. (Courtesy: Sentinel Hub™. Downloaded: 10/02/2019)	41

Figure 5-55 Ground truthing sites in the Study Area.....	44
Figure 5-67 CRISIS 2015 v4.1 start screen and data input tab.....	49
Figure 5-7 Flowchart of Probabilistic Seismic Hazard Assessment (PSHA).....	50
Figure 5-8 CRISIS 2015 seismic hazard map output screen	52
Figure 5-9 CRISIS 2015 seismic hazard curve output screen (Mombasa Island).....	53
Figure 6-1 Temporal Distribution of events in the USGS catalog.....	54
Figure 6-2 Temporal distribution of events in the ISC catalog	55
Figure 6-3 Temporal distribution of events in the combined USGS-ISC catalog	56
Figure 6-4 Hypocentral distribution of events in the combined USGS-ISC catalog.....	56
Figure 6-5 Declustered compiled earthquake catalog for the study area.....	58
Figure 6-6 Gutenberg-Richter analysis of the earthquake catalog.....	60
Figure 6-7 Area Source Zone Seismicity Model for Source Zone 3	60
Figure 6-8 GMPE Description for Abrahamson & Silva (1997).....	61
Figure 6-9 Return Periods and Time Frame input screen	62
Figure 6-10 Spectral acceleration frequencies input window.....	62
Figure 6-11 Seismic hazard curves output window	63
Figure 7-1 Seismic Area Sources Zones (ASZ's) in the Study Area.....	65
Figure 7-2 Ground accelerations in the study area at a 0.05s structural period.....	67
Figure 7-3 Ground accelerations in the study area at 0.1s structural period.....	68
Figure 7-4 Ground accelerations in the study area at a 0.15s structural period.....	69
Figure 7-5 Ground accelerations in the study area at a 0.3s structural period.....	70
Figure 7-6 Ground accelerations in the study area at a 0.5s structural period.....	71
Figure 7-7 Ground accelerations in the study area at a 1s structural period.....	72
Figure 7-8 Ground accelerations in the study area at a 2s structural period.....	73
Figure 7-9 Seismic hazard map of the study area for a 10% Probability of Exceedance in 50 years.....	74
Figure 7-10 Seismic hazard curve & UHS for Malindi for 5% in 50-year PGA at T=0.5s.....	76

Figure 7-11 Seismic hazard curve & UHS for Watamu for a 5% in 50 year PGA at T=0.5s .76
Figure 7-12 Seismic hazard curve and UHS for Kilifi for a 5% in 50 year PGA at T=0.5s....77
Figure 7-13 Seismic hazard curve & UHS for Mombasa for a 5% in 50 year PGA at T=0.5s78
Figure 7-14 Seismic hazard curve & UHS for Voi for a 5% in 50 year PGA at T=0.5s.....78
Figure 7-15 Seismic hazard curve & UHS for Kwale for a 5% in 50 year PGA at T=0.5s79
Figure 7-16 Seismic hazard curve & UHS for Ukunda for a 5% in 50 year PGA at T=0.5s ..80
Figure 7-17 Seismic hazard curve & UHS for Vanga for a 5% in 50 year PGA at T=0.5s80

LIST OF APPENDICES

Appendix 1: Combined Earthquake Catalog (USGS & ISC, AD1938-2020)

Appendix 2: Field Ground Truthing Schedule

Appendix 3: Location of Postulated Offshore Fault

LIST OF ABBREVIATIONS AND ACRONYMS

°C	Degree Celsius
AD	<i>Anno Domini</i>
a.s.l	Above Sea Level
B.P	Before present
bgl	below ground level
DSHA	Deterministic Seismic Hazard Assessment
ETAS	Epidemic Type Aftershocks Sequence
GMPM	Ground Motion Prediction Model
GMPE	Ground Motion Prediction Equation
ILRI	International Livestock Research Institute
ISC	International Seismological Center
JICA	Japan International Cooperation Agency
KeNHA	Kenya National Highways Authority
Km	Kilometer
M	Magnitude
MW	Megawatt
M.y	Million Year
m ² /d	Square meter per day
m ³	Cubic meter
m ³ /d	Cubic meter per day
m ³ /year	Cubic meter per year
mm	Millimeter
MMI	Modified Mercalli Intensity
Mw	Moment Magnitude
MW	Mega-Watt
NEMA	National Environmental Management Authority
NTDZ	Northern Tanzania Divergence Zone
NuPEA	Nuclear Power & Energy Agency
OCHA	(United Nations) Office for the Coordination of Humanitarian Affairs
PGA	Peak Ground Acceleration
ppt	Parts per thousand

PSHA	Probabilistic Seismic Hazard Assessment
S-wave	Shear wave
™	Trade Mark
UHS	Uniform Hazard Spectrum
USGS	United States Geological Survey

1 INTRODUCTION

1.1 BACKGROUND INFORMATION

According to Fig. 1-1 below, the area of study is situated between latitudes S4°38'25" and S1°39'22" and longitudes E37°21'40" and E41°31'40", making up the southern portion of Kenya. Kibwezi town is located in its north-west, Witu town in its north-east, while Vanga town is at its southernmost tip. The western side of the area is occupied by the Western Indian Ocean coastline (NEMA, 2009) spanning about 290 kilometers in length.

The area's first seismic hazard assessments were completed by Midzi et al. (1999) and Giardini et al (1999). Both used the probabilistic seismic hazard assessment (PSHA) method to determine the study area's peak ground acceleration assuming a 50-year period with a 10% chance of exceedance. Both studies excluded the present area in their area source zone (ASZ) models and predicted maximum PGA in the study area of <20 cm/s/s. Lubkowski et al. (2014) and Hayes et al. (2014) both carried out seismic hazard assessment in the study area. Lubkowski et al. (2014) included the study area in their area source zone model, and assigned Mombasa city a PGA of 90cm/s/s for a 5% probability of exceedance in 50 years. Hayes et al. (2014) assigned the study area a PGA value of <20 cm/s/s.

The most recent seismic hazard assessment covering the study area was done by Jepkemoi (2017) and the Global Earthquake Model (Pagani et al, 2018), both of who included the study area in their area source zone model. Jepkemoi assigned the study area a maximum PGA value of 14-18 cm/s/s while the Global Earthquake Model assigned it a maximum PGA of 50-80 cm/s/s. However, GEM (Pagani et al 2018) assumed that the study area is underlain by a uniform bedrock and only used one area source zone (ASZ).

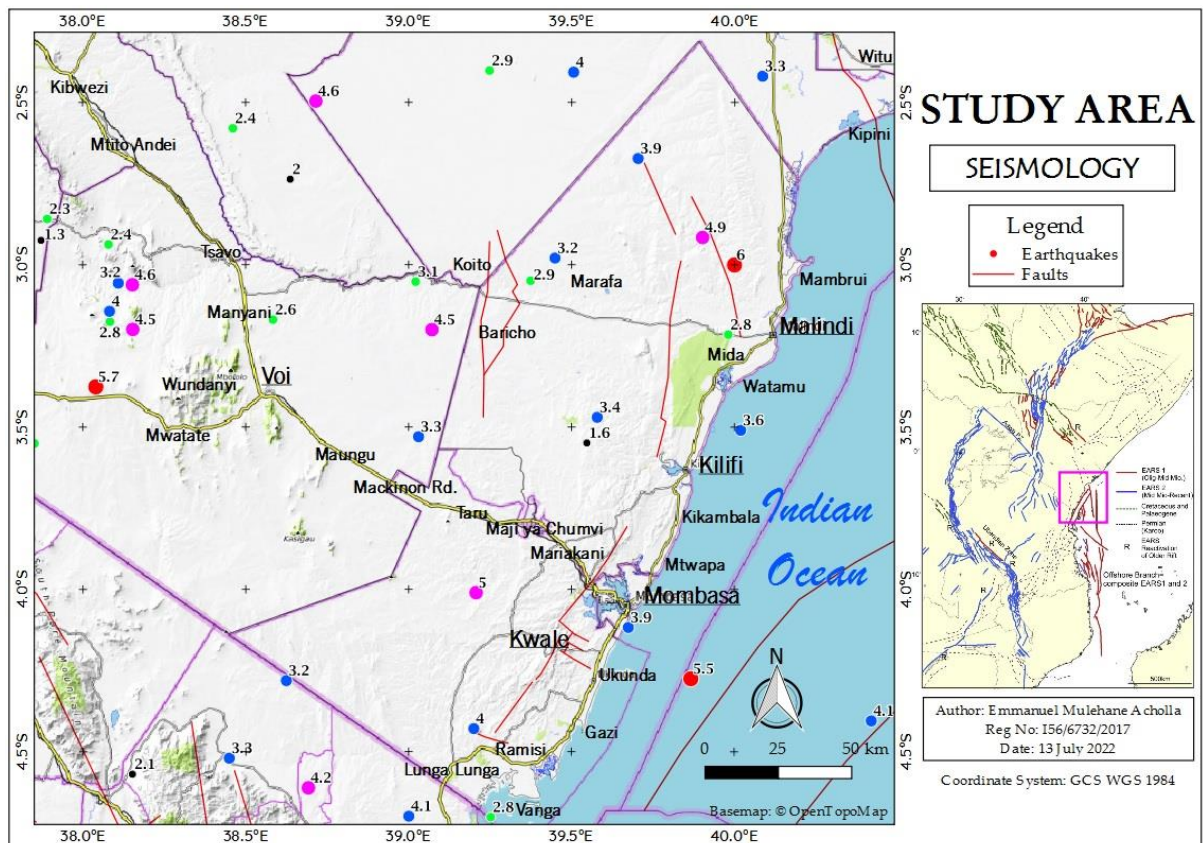


Figure 1-1 Map of the study area showing faults and earthquake epicenters

1.2 SCOPE OF THE RESEARCH

This study entails a probabilistic analysis of the hazard (maximum horizontal ground shaking) resulting from natural earthquakes in southern Kenya. It involves desktop studies, field ground truthing and data analysis.

1.3 PROBLEM STATEMENT

Based on assumptions that Kenya's Indian Ocean coastline, which forms the foundation of the area, is a passive continental margin (Phethean et al., 2016; Dirkx, 2017), there should be little to no earthquake activity along this coastline (Condie, 1997; Stein and Wyssession, 2003). Nevertheless, within a 400 km radius of the area, shallow moderate (>moment magnitude 5) crustal earthquakes have been detected in instrumental seismic data from 1938 to 2019 (ISC, 2018; USGS, 2019) as of 1995, occurring immediately north of region where the Miocene Gregory Rift partitions east into the Indian Ocean (Saria et al. 2014).

Previous works done (Midzi e al., 1999; Hayes et al., 2014; GEM, 2016, 2018; Poggi et al., 2017) in quantifying the seismic hazard in the study area have mainly utilized the probabilistic

approach. It's possible that Hayes et al. (2014) and Poggi et al. (2017) oversimplified the inherent danger when they predicted a quasi-uniform low seismic hazard. In addition, most of these works (Lubkowski, 2014; GEM, 2016; Poggi et al., 2017; Jepkemoi, 2017) assume that the study area is underlain by a uniform bedrock foundation without any field confirmation. Furthermore, some of these works (Midzi et al., 1999; Jepkemoi, 2017) do not adequately address the contribution of the juvenile Northern Tanzania Divergence Zone and the offshore Davie Fracture to the seismicity of the area, as portrayed by the extent of their seismic source zones. The seismic hazard curves derived by previous works (Lubkowski, 2014; Poggi et al., 2017; Jepkemoi, 2017) only pertain to Mombasa city and do not consider other towns and cities in the study area like Malindi, Watamu, Kilifi, Kwale and Ukunda which may be undergoing rapid growth rates and substantial infrastructure investments.

1.4 AIM AND OBJECTIVES

1.4.1 AIM OF THE RESEARCH

The purpose of this research is to conduct a thorough probabilistic seismic hazard assessment of southern Kenya.

1.4.2 OBJECTIVES

This study's particular goals are as follows:

- I. To demarcate the seismic source zones responsible for the earthquake activity in the area.
- II. To compute the peak horizontal earthquake ground accelerations for the area in terms of annual probabilities of exceedance and extract the hazard curves for all major towns.
- III. To develop an updated seismic hazard map of the area, taking into account the particular seismo-tectonics and seismic wave velocities of the area's bedrock.

1.5 JUSTIFICATION AND SIGNIFICANCE

In quantifying the hazard due to earthquakes in Kenya's Coast region, most previous works in their calculations have assumed that the study area is underlain by a reference uniform bedrock foundation, which is a significant generalization. In delineating the earthquake sources in the study region, some of these works have excluded the juvenile Northern Tanzania Divergence Zone and the offshore Davie Fracture Zone, leading to a likely under-estimation of

the earthquake hazard. Furthermore, practically all prior investigations have exclusively calculated seismic hazard curves for Mombasa city, to the exclusion of other major towns, which may need the data for planning purposes. Finally, most prior studies gave a virtually uniform, low seismic hazard level to the studied region, which may be an underestimation of the intrinsic danger.

There are proposals to build Kenya's first high-speed expressway, spanning 473 kilometers and costing around Kshs. 300 billion (Bechtel Corporation, 2017; Construction Review Online, 2018). This route is intended to expand access to the Kenyan coast and in particular, the area to further investments. There are also plans to build Kenya's first 800MW coal power station near Manda Bay in Lamu County (Amu Power, 2018) and also the cable-stayed Mombasa Gate Bridge Project (KeNHA, 2019; JICA, 2020) to link Mombasa Island to the South Coast mainland at Likoni. These two instances demonstrate Kenya's trend toward significant infrastructure expenditures, which may eventually include strategic facilities such as nuclear power stations (Nuclear Power & Energy Agency, 2022).

The present study has constrained the quantitative seismic hazard due to earthquakes in Kilifi, Mombasa and Kwale Counties, by incorporating field data on the faults and bedrock conditions, Northern Tanzania Divergence Zone and the offshore Davie fracture, and estimated seismic hazard curves for all of the area's major towns and cities. Finally, the present study has designed an up-to-date seismic hazard map of the area that reflects the unique nature of seismic activity of southern Kenya, filling the gaps in knowledge that were largely overlooked by previous works.

The results of this study have highlighted the hazard posed by moderate earthquakes that occur at passive continental margins, like the Indian Ocean Coast of Kenya, which experience moderate earthquakes stemming from the reactivation of existing faults by subsequent tectonism, like the Miocene Gregory Rift. This is an area of research interest for geoscientists working in the study area in future.

The data, maps and recommendations of this study are intended to spur concerted action by the policy makers in the respective County governments of the study area to update and implement seismic building codes in their jurisdictions. In addition, the seismic hazard curves for specific towns in the study area provide data to guide future civil engineering or public works in the study area, like the proposed cable-stayed Mombasa Gate Bridge.

2 LITERATURE REVIEW

Nyagah (1995), Condie (1997), Mbede and Dualeh (1997), Abuodha (2003), NEMA (2009), and Phethean et al. (2016) all agree that Kenya's Indian Ocean Coast, and particularly the study region, is located on an inactive (passive) continental edge with little tectonic and seismic activity. Van der Pluijm et al. (2004) assert that passive continental margins are not plate boundaries and so are not seismically active, using Africa's eastern and western borders as examples. While acknowledging that passive continental margins are often tectonically inert, Stein and Wyssession (2003) underlined that massive earthquakes might occur and speculate that these earthquakes may be related with strain at or near the continental edges. Lay and Wallace (1995) agree that the tectonic loading processes for intraplate earthquakes are poorly understood, however they hypothesize that these earthquakes occur on relict tectonic structures reactivated by fresh strains. This agrees well with Emishaw and Abdelsalam (2019) who show that the major geologic faults in the area, trending NE-SW, N-S and NNW-SSE are old, i.e. Permian to Jurassic, yet earthquake data from the USGS (2019) and ISC (2018) indicate that there are recent moderate earthquakes in their vicinity. According to Reeves et al. (2016), the Miocene East African Rift may have renewed the Davie-Walu Fracture Zone offshore of the region.

Oosterom (1988) discussed the geomorphology, geology, and geological history of southeastern Kenya, which encompasses the current research region. He characterizes the area's context as consisting of Precambrian Mozambique Belt metamorphic rocks at the base, overlain by Paleozoic-Mesozoic sedimentary layers. The fluvio-lacustrine sandstones and shales of the Karroo system are the oldest in this series, and Mesozoic marine sedimentary rocks overlie them. The formation of the Oligocene-Miocene East African rift system led in the deposition of phonolitic lavas west of the area, and the formation of the Kilimanjaro stratovolcano south of the area during the Pliocene-Pleistocene epoch. The study is consistent with previous work by Caswell et al. (1953; 1956), Nyagah (1995), Dugda et al. (2005), and Nyaberi et al (2014). The tectonism and volcanism connected with the EARS, however, persist to this day, as symbolized by the juvenile Northern Tanzania Divergence Zone, and is proven by the presence of hot springs in Mwananyamala near Godoma, north of Jombo hill in Kwale County. Previous investigations covering the area could not fully capture the relationship between this tectonism/volcanism and the instrumental seismicity.

Instrumental earthquake data from the US Geological Survey (2019) and the International Seismological Center (2018) online catalogs spanning 1938 to 2019 show that several significant events occurred in Kenya's Coast region, primarily in the southern half of the coastal strip, which is the present area. The magnitudes of the earthquakes range from 1.5 to 6.0, their depths ranging from 10 km to 38 km, and they occurred between 1938 and 2019. The USGS catalog includes events from 1979 to 2019, but is incomplete for events less than M3. On the other hand, the ISC reviewed catalog contains events from 1938 to 2018 and incorporates events with magnitudes as low as M1.5. Gupta (2002) ascribes this incompleteness to inadequate instrumentation in the early years in addition to the fact that $M < 3$ earthquakes are excluded from the USGS catalogue for earthquakes outside the United States of America. Because the area has a typically low level of seismic activity, these $M < 3$ events are very vital in computing the inherent hazard, because they illuminate areas that may have active faults. The shallow epicenters of the moderate earthquakes, as well as their closeness to heavily populated Mombasa, Malindi, and Ukunda towns, pose a significant risk. The strain responsible for these events could be due to tectonic reactivation (Lay and Wysession 1995) of relict Jurassic-Tertiary faults described by Morley (1999), the offshore Davie Fracture Zone described by Saria et al. (2014) and Mulwa et al. (2013), or the Northern Tanzanian Divergence Zone described by Ring (2014). Delvaux et al. (2010) used an inversion of earthquake focal mechanism data to examine the tectonic stress regime covering the area and concluded that the coastal region of Kenya is experiencing expansion within a normal faulting regime. This is consistent with the area's geological structure and reported seismic activity.

Gupta (2002), Baker (2008), Ahmad (2016), and Poggi et al (2017) all agree that a seismic hazard analysis begins with the collection and analysis of earthquake data, followed by seismic source zonation, calculation of recurrence intervals, and finally the assignment of ground motion prediction models before calculating hazard. The authors indicated above used the probabilistic method to seismic hazard analysis (PSHA), which is also the approach used in this study because CRISIS-2015TM is a PSHA-based program (Ordaz et al., 2015). The probabilistic method is preferred by Gupta (2002), Baker (2008), Lubkowski et al. (2014), and Poggi et al. (2017) because it incorporates the effect of all earthquakes that are expected to occur at a specific geographical region within a certain timeframe and with a specified degree of confidence. This is in contrast to the deterministic seismic hazard analysis (DSHA) approach, which is constrained by a subjective estimate of the magnitude of the largest possible earthquake (also known as the 'maximum credible earthquake' or 'scenario' earthquake) and the assumption that this earthquake will occur near the site (Baker 2008).

Several projects have been completed in the past to gauge the seismic hazard in the area. According to the United Nations OCHA (2007) earthquake intensity zones map for Africa, the area has a 'strong' acceleration rating. This figure may be an accurate assessment of the risk posed by the stated earthquake activity. However, the Mercalli intensity scale may not be the best estimate of earthquake risk because it is based on human observations of earthquake damage to civil structures, which depends on factors such as distance from the epicenter, construction quality, soil and bedrock characteristics, among others. The studies of Giardini (1992), Hayes et al. (2014), the Global Earthquake Model (2016), and Poggi et al. (2017) all indicate an invariable low seismic hazard. Given the significant seismic activity, this may not be an accurate representation of the inherent threat. The Global Earthquake Model's subsequent work (Pagani et al., 2018) gives a higher resolution of the underlying seismic hazard in the area. Despite this, Lubkowski et al. (2014), Poggi et al. (2017), Jepkemoi (2017), and Pagani et al. (2018) all assume a reference hard rock foundation for Mombasa, the area's principal metropolis, without field verification. Furthermore, Lubkowski et al. (2014), Poggi et al. (2017), and Jepkemoi (2017) computed seismic hazard curves for Mombasa city alone, excluding other fast rising towns like as Malindi, Watamu, Kilifi, and Kwale that may require this information for planning purposes. As a result, the Global Earthquake Model (2018) cautions that places depicted in their global seismic hazard map as having low seismic hazard may nonetheless be vulnerable to potentially destructive earthquakes.

According to Worku (2017), the Kenyan seismic code uses the modified Mercalli Intensity (MMI) scale to depict the earthquake risk in Kenya. According to the MMI Scale, the resulting map divides Kenya into four earthquake zones. He is accurate in stating that seismic hazard mapping based on earthquake intensity is out of date. Furthermore, the Intensity scale is a subjective assessment that provides no information on the magnitude of the earthquakes involved, recurrence times, or exceedance possibilities. This necessitates a re-evaluation of Kenya's seismic code, which should incorporate state of the art in seismic hazard analysis, ostensibly the probabilistic approach, and the deployment of new seismic networks covering the entire country, which should be cascaded down to the County levels for appropriate planning purposes.

3 THE STUDY AREA

3.1 LOCATION

The area is bound by longitudes 37°53'32"E and 40°25'27"E and by latitudes 2°17'07"S and 4°44'48"S and encompasses the southern tip of Kenya, as shown in Fig 3-1 below.

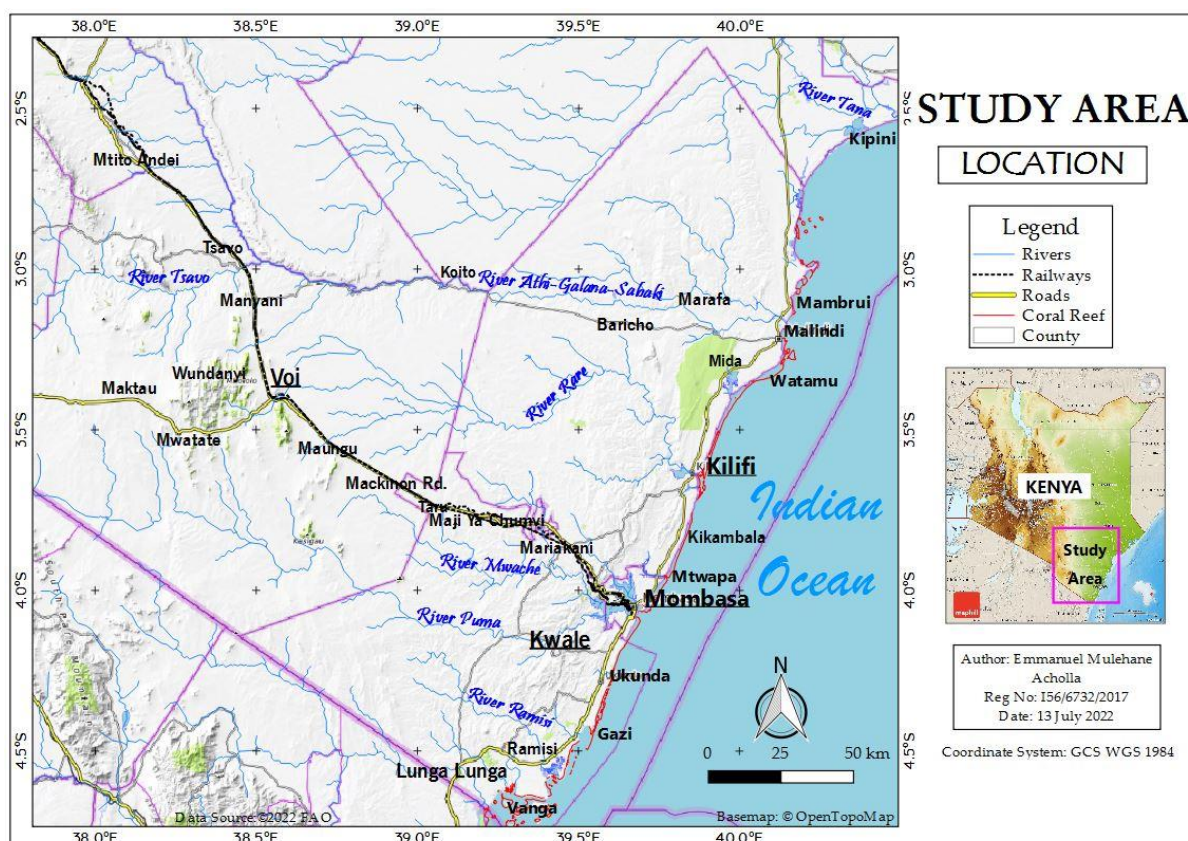


Figure 3-1 The Study Area

The area is accessible by car through the main A109 Nairobi-Mombasa highway, the A14 South Coast road, and the B8 Mombasa-Malindi road. However, a new Nairobi-Mombasa expressway is planned (Bechtel Corp., 2017). Moi International Airport in Mombasa, Ukunda Airport in Ukunda, and Malindi Airport in Malindi are the primary airfields. The railway network is comprised of the old Nairobi-Mombasa railway and the new Nairobi-Mombasa Standard Gauge Railway (SGR), both of which include Mombasa stations.

The research region slopes towards the Indian Ocean through the Coastal Plain. Accordingly, the rivers in the area, such as Tana, Athi, and Sabaki, drain from the north east to

the south west. Dzombo Hill in Kwale County is the highest point in the study region at 406 meters above sea level.

The coastline underlying the study region is a passive continental margin (Bosworth et al., 1993; NEMA, 2009; Mbede et al., 1997; Phethean et al., 2016) formed by the middle Jurassic to early Triassic (Mcloughlin, 2001; Kapilima, 2002) breakup of the East and West parts of the Gondwanaland supercontinent (NEMA, 2009; Dirkx, 2017). (Mcloughlin, 2001; Kapilima, 2002). The coastline is projected to experience low seismic activity (Condie, 1997; Stein et al., 2003).

The region's stratigraphy grows younger towards the Indian Ocean. Late Paleozoic sedimentary units are unconformably overlain on the Precambrian rock formations (Taru Formation). Meso-Cenozoic formations of continental margin origin follow the sequence.

3.2 PHYSIOGRAPHY

The following units, which parallel the shoreline, might be used to summarize the physiography of the study area:

- a) The Coast Plain
- b) The Foot Plateau
- c) Coastal Range
- d) The Nyika

The Coast Plain is made up of 3–4 km wide late Cainozoic strata and often falls below the 30 m contour. The Pleistocene coral reef lines the seaward edge of the plain.

The Foot Plateau is 60 to 130 meters above sea level. The Jurassic rocks form the Foot Plateau's foundation. A long ridge of sandy hilts made of Magarini Sands, which continue west to the Duruma Sandstones and conceal the Jurassic Rocks, rests on the eastern edge of the plateau.

A 150-meter rise leads into the Coastal Range. They are part of the Shimba Hills, which dominate the topography of the region and are made of Mazeras Sandstone with a topping of Shimba Grit.

The Nyika climbs steadily from 180 meters to roughly 300 meters at the western edge of the region. It extends far to the north-west of the region and is primarily underlain by rocks that underwent Precambrian metamorphism. The Taita Hills interrupt the undulating terrain of the Nyika near the Tsavo National Park, with the Dawida Massif rising to more than 2000m. North

of the Taita hills is the unique Yatta Plateau phonolitic lava flow, trending north-west to south-east.

3.3 COASTAL PLATE TECTONICS

The sedimentary wedge which thickens toward the sea and is characterized by listric faulting and salt tectonics makes up the basic structure of the area, which is typical of passive margin development. North-South, Northeast-Southwest, and Northwest-Southeast lineaments formed on the basement platform before continental breakup. This formed the structural fabric over which the earliest rifts were superimposed and progradational sediments deposited. Four unconformity-bound megasequences were deposited during four distinct rifting episodes and include Karoo, Cretaceous, Eocene, and Miocene-Recent (Kivuti Nyagah, 1995).

The Mombasa-Tana Hingeline, the Tana and Pate Synclines, and the Walu-Kipini High are the principal structural tectonic features in the research area. The N-S trending geologic border that separates the Karoo rocks from the exposed Precambrian basement is seen on the western side of the research region. (Dugda et al. 2005)

This is illustrated in Fig 3-2 below.

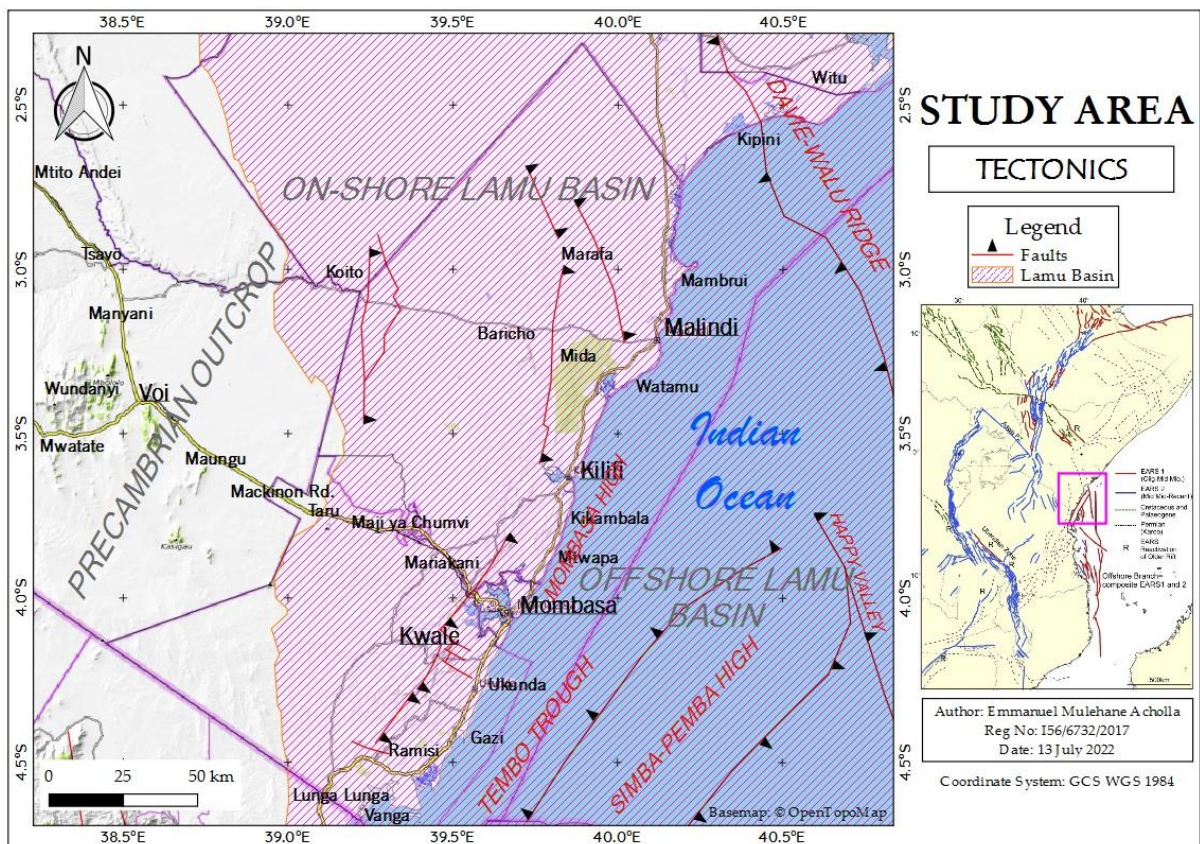


Figure 3-2 Map showing the main tectonic features in the area (Adapted from Wanjala, 2020)

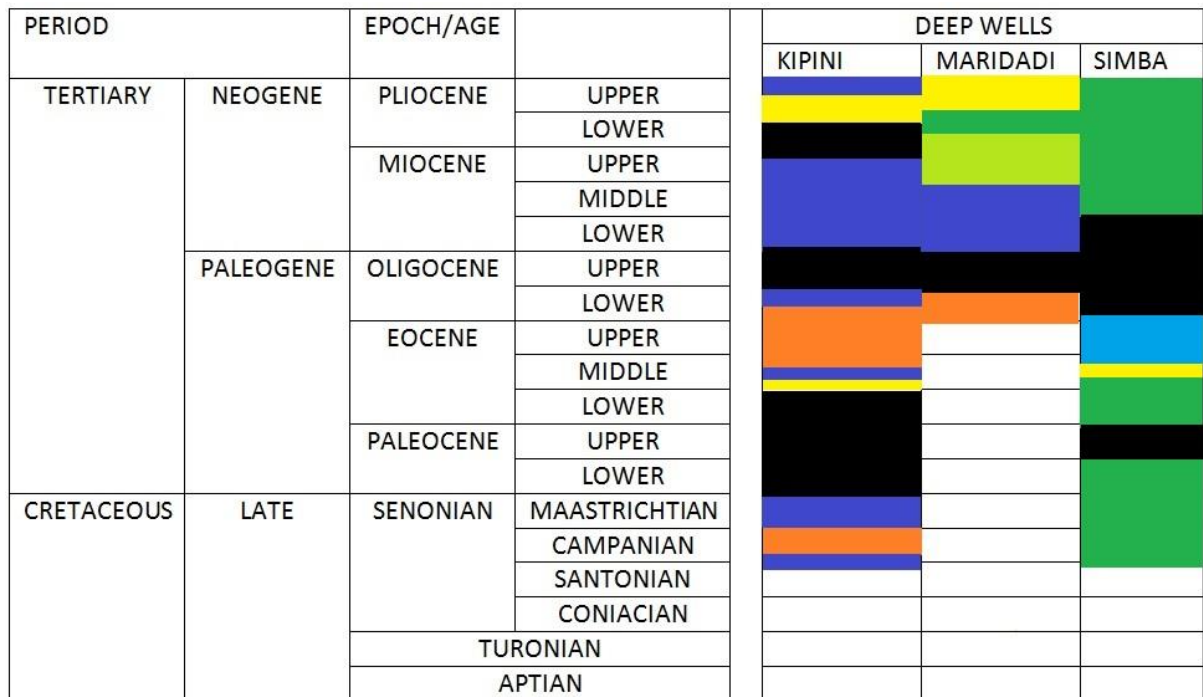
3.4 STRATIGRAPHY

International oil corporations have drilled a total of 16 subsurface wells in the Lamu basin, which have proven the lithologies present in the study region (Kivuti Nyagah, 1995; Dugda et al. 2005). According to the drilling campaigns, the thickness of the sedimentary prism in the onshore depocentre ranges from 3250 meters to 10,000 meters. The sedimentary column in the offshore depocentre is 12,000 to 13,000 meters thick. (Kivuti Nyagah 1995; Dugda et al. 2005)

The deep wells that occur within the study area (from North to South) are illustrated in Table 3-1 and Fig 3-3 below:

Table 3-1 Deep wells drilled within the study area

Well	Operator	Drilled Depth	Date Drilled
Kipini-1	BP/SHELL	3663	1971
Maridadi-1B	CITIES SERVICE	4196	1982
Simba-1	TOTAL	3604	1978
Sunbird-1	AFRICA OIL	2952	2014



Adapted from: Kivuti Nyagah (1995)

Key	
Sand/Sandstone	Yellow
Sandy Mud	Orange
Shale-1	Green
Shale-2	Light Green
Clastic/Limestone interbed	Blue
Limestone	Dark Blue
Unconformity	Black

Figure 3-3 Lithological contacts of deep wells in the area (Adapted from Kivuti Nyagah, 1995)

Table 3-2 below summarizes the geological sequence of lithologies in the area:

Table 3-2 Stratigraphy of the study area (Adapted from Caswell 1953, 1956)

ERA				REPRESENTATIVE		LITHOLOGY
CAINOZOIC	Quaternary	Recent		River Deposits		Alluvium
		Pleistocene		Coral Reef Lagoonal Deposits		Reef limestone, calc. sands, qtz. sands. <u>300ft</u>
	Tertiary	Pliocene		Magarini Sands		Sands, gravel. <u>400 ft</u>
		Miocene				
		Oligocene				
Eocene						
MESOZOIC	Cretaceous		Upper			
			Lower	Freretown Limestones		Limestone & Shale
	Jurassic		Upper	Changamwe Shales		Limestones, Sandstones, Shales <u>4000-5000ft</u>
			Middle	Rabai Shales Mombasa Limestone Miritini Shale Kibiongoni Beds Kambe limestone		
			Lower			
	Karoo	Triassic	Upper	Duruma Sandstone	Shimba Grits Mazeras Sandstone	Grits, Arkosic sand stone <u>1000ft</u>
			Lower		Mariakani Sandstone Maji Ya Chumvi Beds	Thin Sandstones and Shale <u>6500ft</u> <u>[3500 ft?]</u>
Permian		Upper	Taru grits			Grits and Arkosic Sandstone <u>500ft</u>
		Lower				
Carboniferous		Upper				
PALEOZOIC	Basement System				Gneisses and Schists	
ARCHEAN						

3.5 LITHOLOGY

At 132,770 km², the Lamu Basin is Kenya's largest basinal area. It is situated in southeast Kenya and includes the nearby continental shelf and Indian Ocean slope regions. It stretches offshore from a restricted onshore graben to comprise the majority of Kenya's continental shelf and slope, making up the eastern portion of the area. Crystalline Precambrian metamorphics from the Late Precambrian and Early Palaeozoic phases of the Pan-African thermo-tectonic episode make up the western half. They are made up of the Mozambiquean belt's linearly folded high-grade metamorphics, such as quartzites, granites, granitoid gneisses, migmatites, biotite and hornblende gneisses, and amphibolites as shown in Fig 3-4 below (Kivuti Nyagah, 1995; Dugda et al 2005)

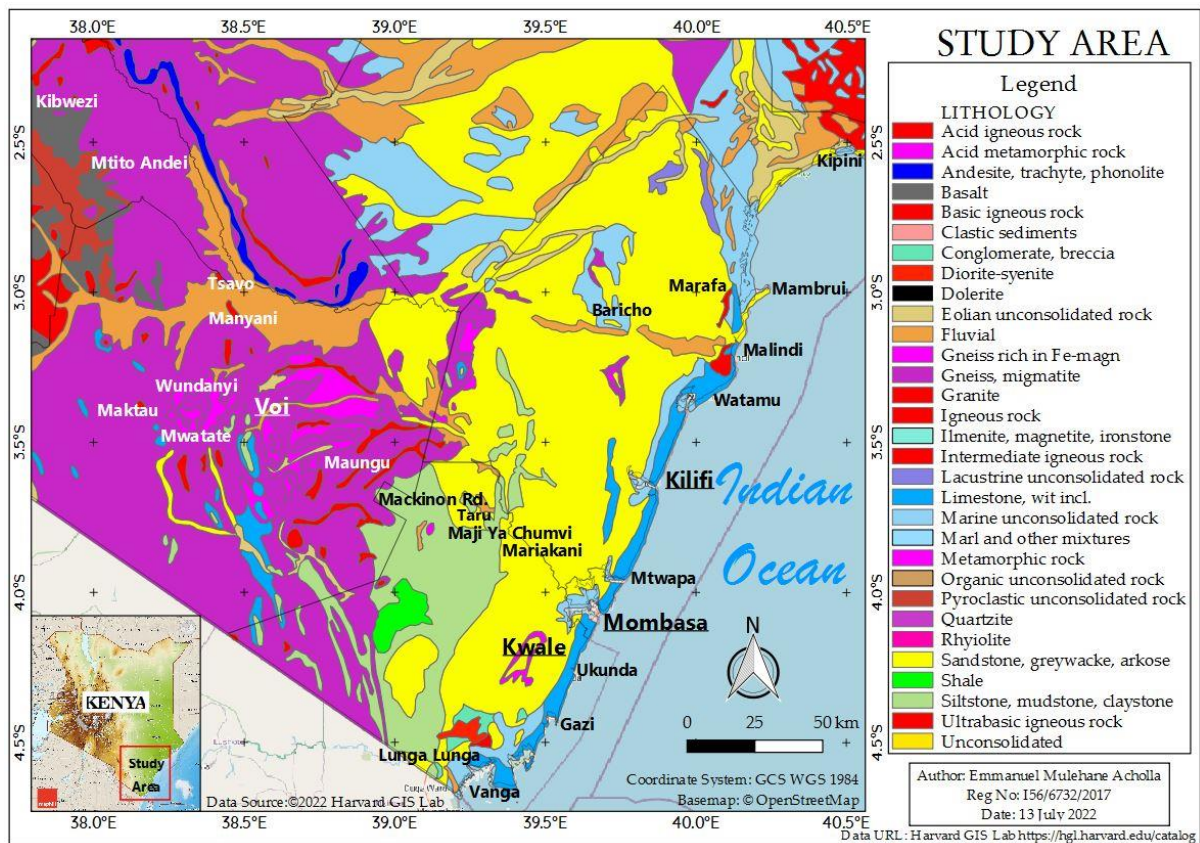


Figure 3-4 Lithology of the study area

The sedimentary column in the offshore depocentre is 12,000 to 13,000 meters thick. These sediments are made up of carbonates, fluvio-deltaic sandstones, marine shales, and sandstones from the Permo-Carboniferous to Tertiary continental rift basin. (Kivuti Nyagah 1995)

The majority of the rocks in the study area's eastern portion are sedimentary in nature and range in age from the Permian (perhaps Upper Carboniferous) to the Recent. It is possible to identify three distinct divisions (Caswell 1953, 1956):

- The rocks of the Cainozoic era.
- Rocks from the Upper Mesozoic
- The series of Duruma sandstone.

The Cretaceous and Tertiary sediments of the Lamu Basin can be divided into three megasequences, each of which is connected by local unconformities and has a particular architecture that is the consequence of the interaction between the sediment supply, basin tectonics, and eustatic sea level change. The three megasequences and events of extension and sinking during the Cretaceous, Eocene-Oligocene, and Miocene to Recent have a relationship. (Kivuti Nyagah, 1995; Dugda et al. 2005) These are as follows:

MEGASEQUENCE II (SABAKI GROUP)

All of the rock units between the Late Jurassic and Late Paleocene unconformities are collectively referred to as the Sabaki Group. They contain fossils, which date from the Early Cretaceous to the Early Paleocene, resulting from two marine regressions and a transgression that occurred in between.

i. ***Freretown Limestone***

One and a half kilometers west of the Mombasa-Kilifi road and south of the Bamburi shale quarry, close to Freretown, the Freretown Limestone outcrops over a very small area at an old quarry site. Shell fragments can be found in the calcarenite limestones.

MEGASEQUENCE III (TANA GROUP)

This consists of rocks from the Palaeogene (Eocene to Oligocene), whose deposition occurred over the course of three sea-level rise pulses and one regressive phase. The regional unconformity where strata of Early or Middle Eocene age lay unconformably on strata of Late Cretaceous age is where the lithostratigraphic assemblage is found. The Kipini Formation, which includes the Pate Limestone, Linderina Limestone, and Dodori Limestone Members, and the Barren Beds Formation are the lithostratigraphic units that make up this group.

i. ***Kipini Formation***

The Tana Group is made up of rocks from the Palaeogene (Eocene to Oligocene), whose deposition occurred over the course of three sea-level rise pulses and one regressive phase. The regional unconformity where strata of Early or Middle Eocene age lay unconformably on strata of Late Cretaceous age is where the lithostratigraphic assemblage is found. The Kipini Formation, which includes the Pate Limestone, Linderina Limestone, and Dodori Limestone Members, and the Barren Beds Formation are the lithostratigraphic units that make up this group.

MEGASEQUENCE IV (COASTAL GROUP)

This carbonate sequence is connected to marine shale and a siliciclastic sequence underneath it. The Baratumu Formation, Lamu Reefs, Simba Shales, and Marafa Formation are among the lithostratigraphic units that belong to this group.

i. ***Baratumu Formation***

This occurs as surface exposures of yellowish foraminiferal layers found in Lake Baratumu in Malindi's Goshi region. At Kilifi Creek, a sizable portion of the formation is exposed. Putting down the Baratumu Between the Early and Late Miocene, sinking gradually accompanied formation. In the offshore Maridadi-1 well, limestone grades into a 376-meter-long chunk of shale as one moves toward the sea.

ii. ***Lamu Reefs***

The Lamu Reefs correlate to the Kipini-1 (1533 m) well's Baratumu Formation. Crystalline limestone breaks up the nearly continuous limestone build-up.

iii. ***Simba Shales***

The Miocene to Pliocene interval of the Simba-1 well contains what are known as the lateral deep-marine analogues of the Lamu Reefs. They are made up of green-gray to dark grey pyritic shales of 1508 m thickness. The Miocene–Pliocene age is constrained by the fossils.

iv. ***Marafa Formation***

They are a series of sandstones and sands that have been eroded and exposed in a scarp north of Marafa town. An outcrop of the unit north of Marafa has a badlands topography and is composed of medium- to coarse-grained, poorly cemented quartz sands with sandstones and kaolinitic clays that range in color from a very light orange to a greyish orange. (Kivuti Nyagah 1995)

3.6 CRUSTAL THICKNESS

The thickness of the crust has been measured in numerous studies in the research region using a variety of methods.

In order to better understand the deep structure under the Kenya rift, the Kenya Rift International Seismic Project (KRISP 90) was an integrated seismic-refraction/teleseismic survey. The study discovered that, assuming that the crust thins toward the Indian Ocean coastline, crustal thickness varies from 42 km beneath the Chyulu Hills to 40 km beneath the Taita Hills and less than 35 km for the remainder of the Study Area. The average P wave velocity varies from 6.2 to 6.7 km/s to the east of the rift, while the crustal thickness shifts from 20 km along the coast to 44 km just north of Mount Kilimanjaro.

Using receiver function analysis of broadband seismic data, Dugda et al. (2005) studied the crustal structure in Kenya and Ethiopia. Results from two seismic stations in the research area, BOKO and NDEI, showed that Mohorovicic discontinuity (“moho”) depths ranged from 38.7 km to 42 km and that p-wave velocities ranged from 6.3 km/s to 6.8 km/s. The study calculated that the depth along the coastline was roughly 20 Km despite their being no station at the coastline.

3.7 DYNAMICS OF THE TECTONO-SEDIMENTARY DEPO-BASIN

The Mozambiquean belt's linearly folded high-grade metamorphics, which include quartzites, granites, granitoid gneisses, migmatites, biotite and hornblende gneisses, and

amphibolites, make up the crystalline basement that is connected to the Late Precambrian and Early Palaeozoic phases of the Pan-African thermo-tectonic episode.

The Cretaceous-Tertiary basin's overall structure, which consists of a seaward-thickening sedimentary wedge marked by listric faulting and salt tectonics, is characteristic of passive margin evolution. North-South, Northeast-Southwest, and Northwest-Southeast lineaments formed on the basement platform before to continental breakup, forming the structural fabric over which the earliest rifts were superimposed and progradational sediments deposited. The four unconformity-bound megasequences were deposited during four distinct rifting episodes that have been identified. Karoo, Cretaceous, Eocene, and Miocene-Recent are these. (Kivuti Nyagah, 1995)

The Lamu Basin, which extends offshore from a relatively small onshore graben to include most of Kenya's continental shelf and slope, makes up half of the study area. (Kivuti Nyagah, 1995; Dugda et al 2005)

The failed arm of a tri-radial rift system that occurred during continental rupture gave rise to the basin during the early phases of the development of the Indian Ocean. The basin passively grew during the Mesozoic era after Madagascar subsequently migrated from the east coast of Africa. Karoo (Permo-Carboniferous to Triassic) and Jurassic rocks illustrate the rifting and early post-rifting history of the basin. (Kivuti Nyagah, 1995; Dugda et al 2005)

The Karoo Group sediments were deposited in areally constrained linear grabens that were part of a significant Palaeozoic-Mesozoic tri-radial rift system that ran northeast-southwest from Lake Malawi to southeast Kenya. This rifting episode most likely has a connection to the beginnings of continental split. Lacustrine shales and fluvio-deltaic sandstones make up the majority of the rocks. Palaeo-Tethyan sea flooded the Trans-Erytrean trough in the Early to Middle Jurassic after Madagascar moved along the Davie Fracture. Carbonates were deposited in the Ogaden, Manderu, Anza, and Lamu Basins. Megasequence I is formed from the Karoo and Jurassic rocks of this depositional phase. (Kivuti Nyagah, 1995)

Following Madagascar's separation and southeastward drift during the Cretaceous period, marine recession left a trailing edge shoreline. Large coastal plains, well-developed drainage basins, and progradational shelves are features of these types of coasts. Both an extensional and strike-slip initial margin configuration emerged as a result of Madagascar's drift. The orthoquartzitic sandstones that make up the Ewaso Sands are progradational deposits of a delta that was created in a supratidal environment under the action of tides. In regions west and northwest of the depositional center, this depositional phase coincided with the uplift of strata from the Megasequence I Group and the Precambrian Basement. (Kivuti Nyagah, 1995)

The fracturing of the India-Madagascar-Antarctica block, the movement of India along the Owen Fracture, and a global eustatic event all contributed to a rise in sea level that started in the Aptian. As a result, deep-water facies of the Walu Shale, Hagarso Limestone, and Freretown Limestone were deposited in the Lamu Basin (Fig. 11). The Cenomanian sea level decline may have something to do with the conclusion of this transgressive phase of deposition. Further erosion in the west and concurrent deltaic deposition (Kofia Sands) to the east were caused by the renewed uplift of the basement that created the Walu-Kipini and Garissa axis during the Turonian to Early Paleocene periods. The Tana and Pate sub-basins formed as distinct synclinal depressions concurrently with the uplift. Along the line of this uplift, Megasequence II's Upper Cretaceous successions experienced the most severe later (Late Paleocene) erosion. With the buildup of the Kipini Formation, depositional conditions were once again present during the Eocene (Megasequence III). The Kipini Formation's sediments may have originated from an ancient Tana river distributary system that was restricted by tectonic activity in the basin. Due to the disequilibrium brought on by the fast deposition of sand wedges on undercompacted shales, growth faults, clay and salt diapirs, and listric faults were likely formed during the development of this regressive deltaic-offlap sequence. (Kivuti Nyagah, 1995)

A new depositional regime has been established on the continental shelf as a result of the Megasequence III sediments. The existence of a northeast-trending basement ridge may help explain the constrained maritime environment that predominated at the beginning of the Palaeogene depositional phase. Sediments from the delta front may have been redistributed in a shore-parallel manner by wave action and longshore currents, which were likely caused by tides that were similar to those that are active today on the coast. Nutrients were transported by upwelling seas to shelf environments, promoting the biogenic synthesis of pelagic sediments. Thus, under totally marine conditions, the Pate Limestone predominantly formed as an upward-shoaling carbonate sequence that was occasionally interrupted by modest influxes of terrigenous material to form localized cycles of carbonate-clastic couplets. The Walu-2 well has lateral accretion deposits from the Barren Beds Formation, which is made up of "red beds" that were produced in a fluvial, oxidizing environment. (Kivuti Nyagah, 1995)

The dramatic reduction in sea level linked to the massive glacial that occurred in Antarctica may connect with the Oligocene unconformity, which represents the top of Megasequence III. (Kivuti Nyagah, 1995)

The Neogene shared the same sedimentary facies and basic environmental conditions as the Palaeogene. An upward-shoaling inner-shelf facies, the Baratumu Formation was deposited

through periods of subsidence and sea-level changes. The Lamu Reefs were formed as a result of these conditions together with reefal buildups in middle- to outer-shelf and shelf-edge regions, while the Simba Shales accumulated in the deeper subsiding areas of the basin. The Marafa Formation was created as clastics were deposited under fluvial circumstances throughout the Late Miocene and Pliocene phases of uplift and the high rates of sea-level decline. This coincided with increased river gradients. (Kivuti Nyagah, 1995)

The newly formed structural components shared a genetic connection with the growing rift valley in central Kenya, which had a strong northward and southeastward drainage pattern when it first started to develop in the Miocene. The expanded capacity of the Indian Ocean basin following the collision of India and Eurasia coincides with this regressive depositional era and marine regression. (Kivuti Nyagah, 1995)

The temporary sea-level rise observed in the Late Miocene may be related to the Carlsberg Rift system's extension to the north, which connects the Red Sea with the Indian Ocean. The ultimate and most severe deformation linked to the rift valley tectonic paroxysm corresponded with the sudden regressive episode that took place in the Late Pliocene. Following these final stages of clastic progression, there may have been extensive diapiric movement in the salt deposited offshore. (Kivuti Nyagah, 1995)

3.8 SEISMOLOGY

The study area experiences a moderate level of earthquake activity, despite its location on a passive continental margin. The US Geological Survey and the International Seismological Center instrumental catalogs from 1938 to 2020 reveal that the magnitude of these earthquakes ranges from 1.3 to 6.0, from 10 km to 35 km deep, both onshore and offshore. This is illustrated in Fig 3-5 below.

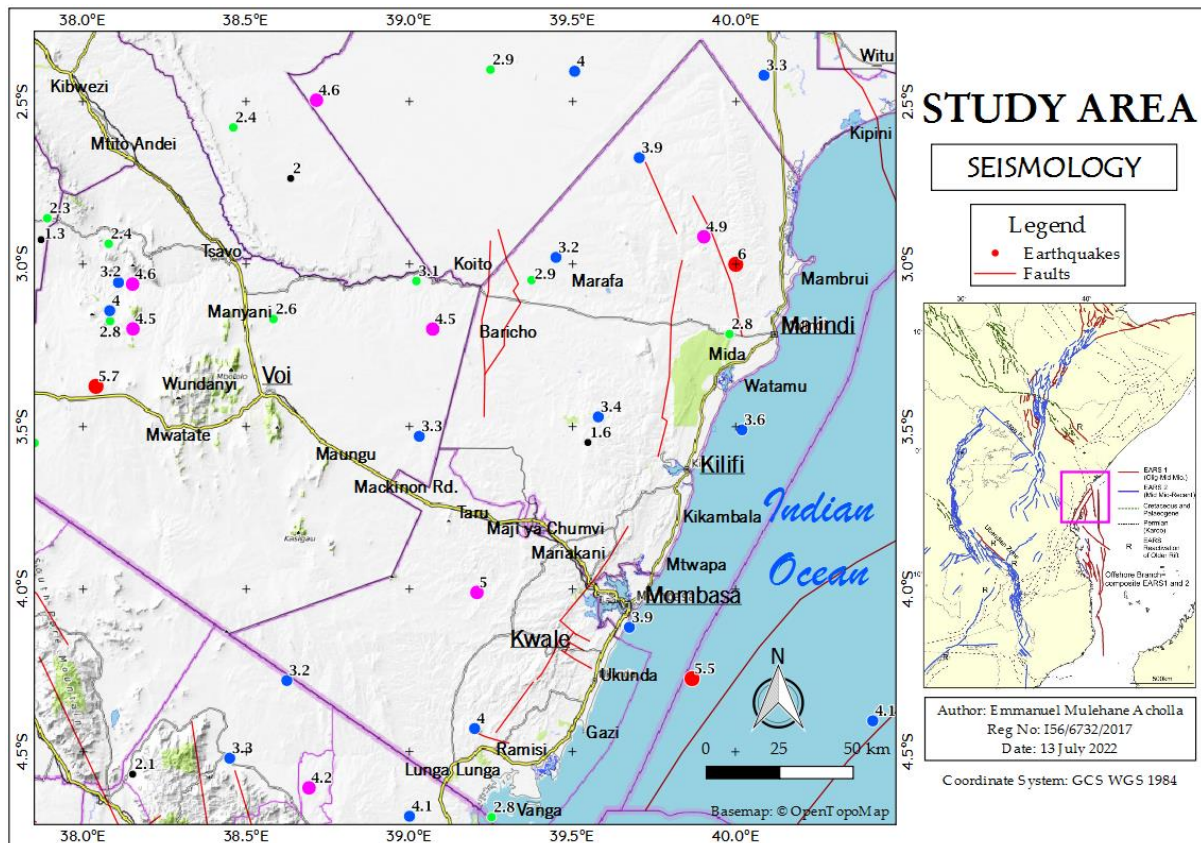


Figure 3-5 Map showing instrumental earthquakes in the study area

These earthquakes are generally distributed in a NNE-SSW corridor, in line with the trend of the geologic faults in the study area, especially the boundary faults of the Tertiary-Paleocene-Pliocene Lamu Embayment. Beyond the southern border of the study area, the NW-SE trending Manyara rift of the Northern Tanzania Divergence Zone of the Oligocene-Miocene Gregory Rift does experience a higher rate of seismicity, likely due to the juvenile nature of the rift.

This seismicity could be caused by a number of factors, including tectonic reactivation (Lay et al., 1995) of Jurassic-Tertiary faults described by Morley et al. (1999), the offshore Davie-Walu Fracture described by Saria et al. (2014) and Mulwa et al. (2013), or the Northern Tanzanian Divergence Zone described by Ring (2014).

The main earthquake hazard in the study area due to this seismic activity is ground shaking. This is especially so for Kwale County, around which several M5 earthquakes have occurred in the past, and which is underlain by sandstones, siltstones overlain by Magarini sands. The southernmost part of Kwale County is particularly exposed to this shaking hazard due to its proximity to the Manyara Rift and the prevalent M5 earthquakes. The densely populated

Mombasa City in Mombasa County has an above average seismic hazard due to the moderate earthquakes that occur offshore, likely as a result of motion within the Davie Fracture.

3.9 METEOROLOGY

A tropical humid climate prevails throughout the area. Kilifi town has an annual mean temperature of approximately 25.0°C and an annual rainfall of about 1,060mm. As seen in Figs 3-6 and 3-7 below, Malindi town has an annual mean temperature of 26.0°C and a yearly mean rainfall of 1,090mm (Climate Data.org, 2018).

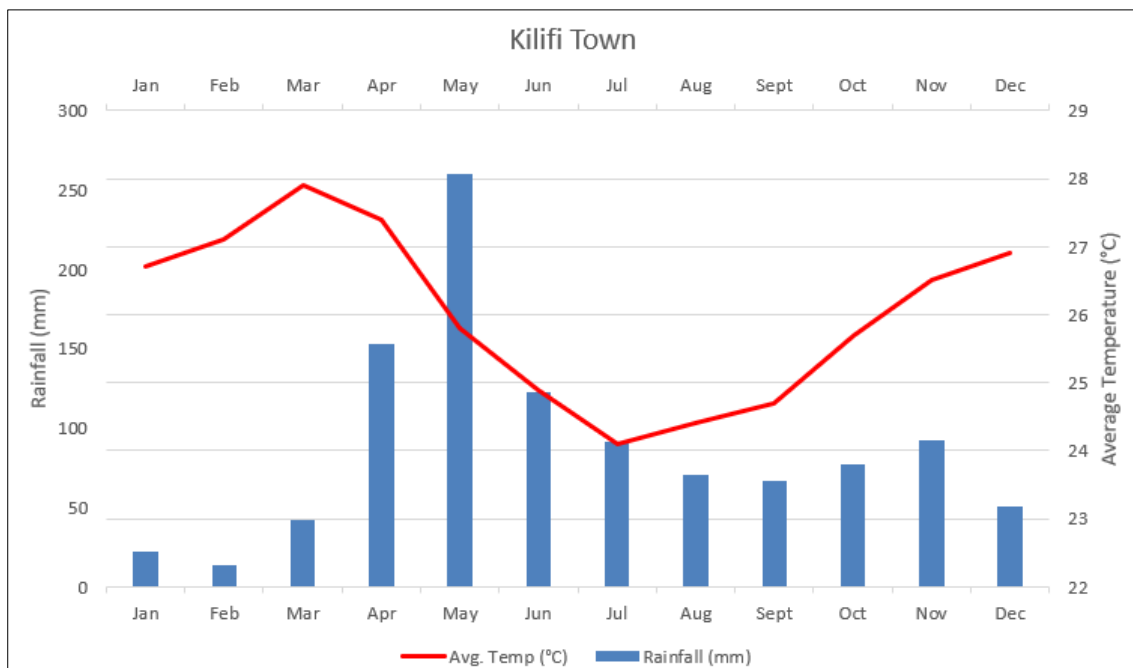


Figure 3-6 Climate graph for Kilifi town

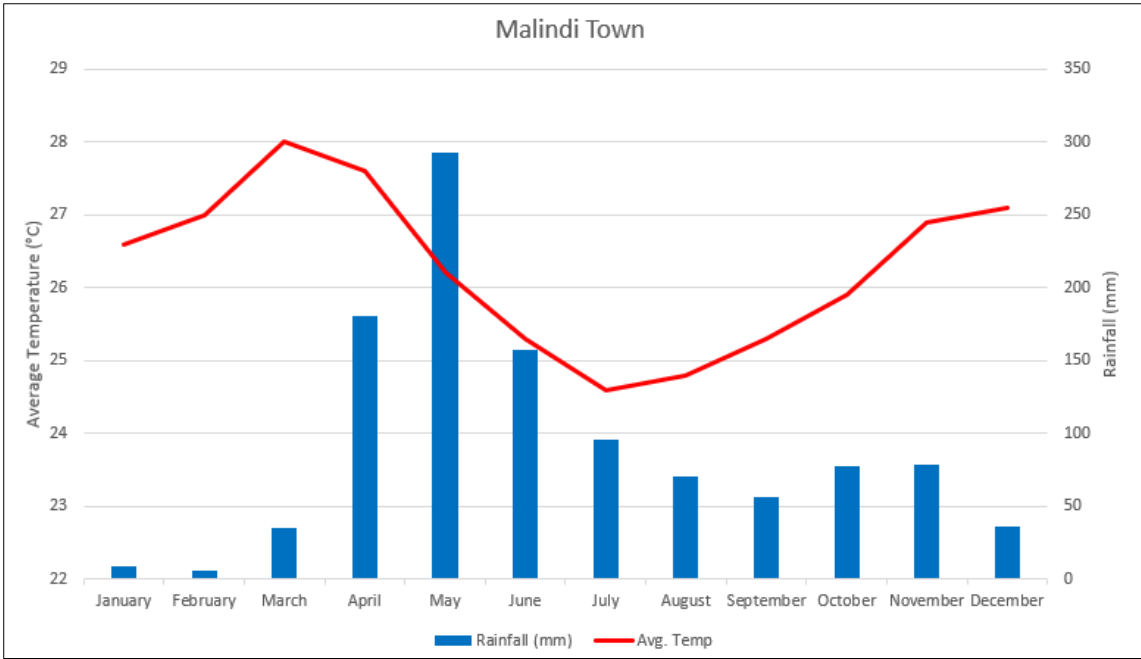


Figure 3-7 Climate graph for Malindi town

Mombasa has an annual mean temperature of 26.6°C and an annual rainfall of 1,190mm. The yearly mean temperature in Kwale is 23.5°C, with a yearly mean rainfall of 1,117mm. The yearly mean temperature in Ukunda is 26.4°C, with a yearly mean rainfall of 1,260 mm, as shown in Figs 3-8 and 3-9 below.

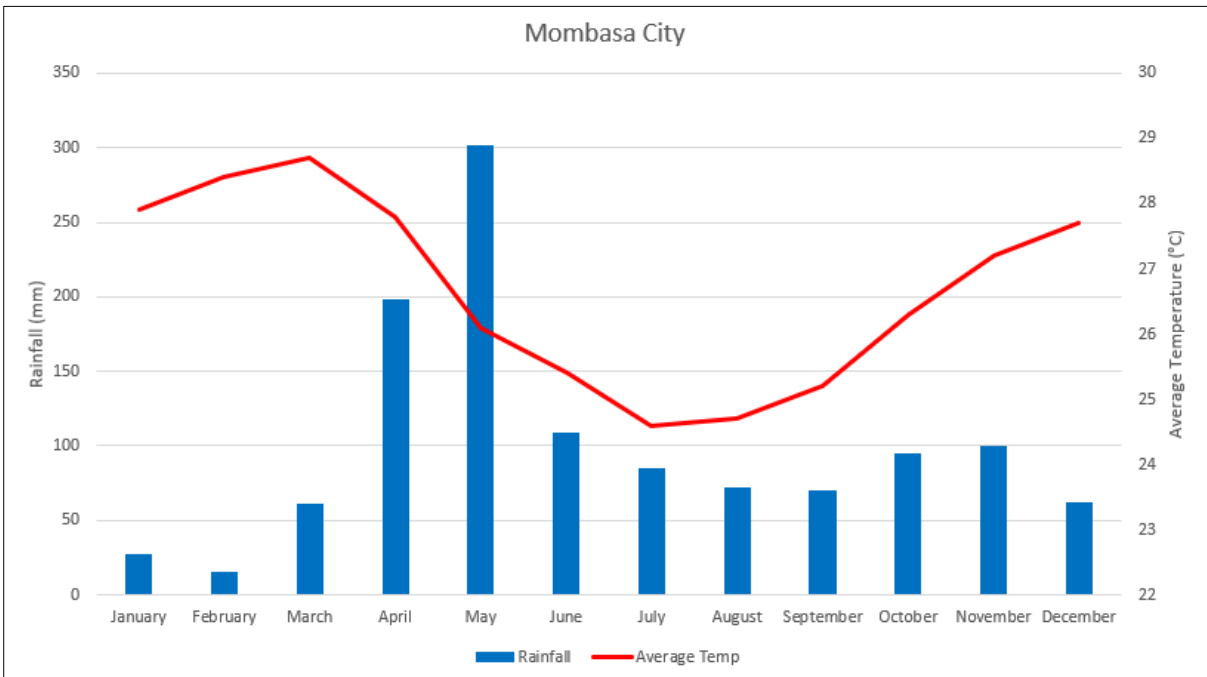


Figure 3-8 Climate graph for Mombasa City

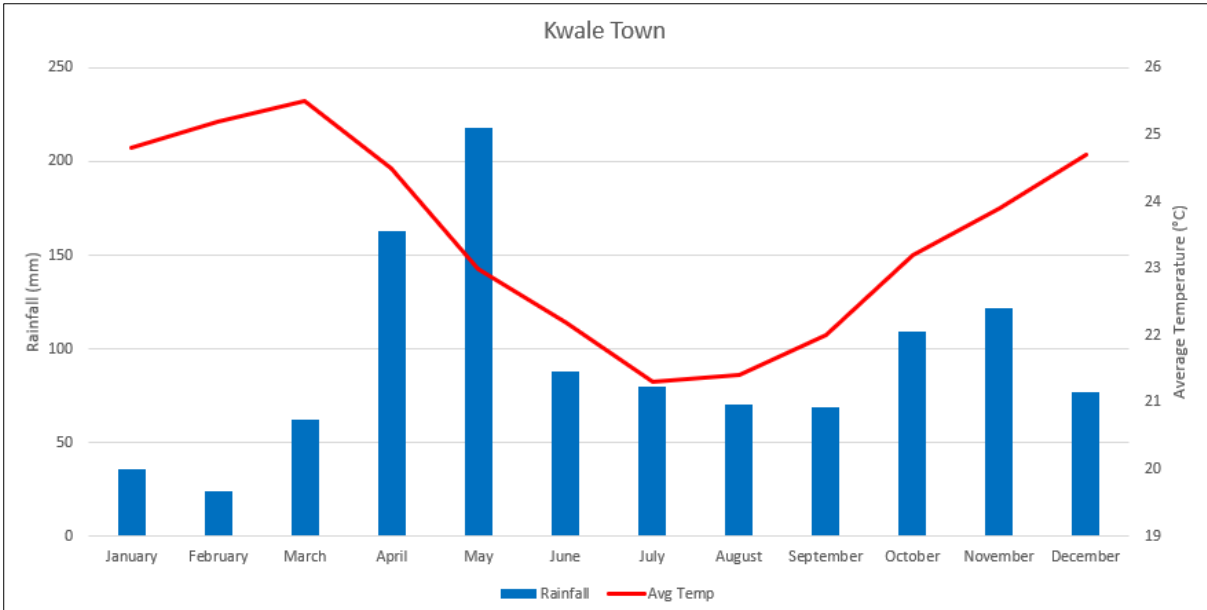


Figure 3-9 Climate graph for Kwale town

The yearly mean temperature in Voi is 24.1°C, with a yearly mean rainfall of 589mm, as shown in Figs 3-8 and 3-9 below.

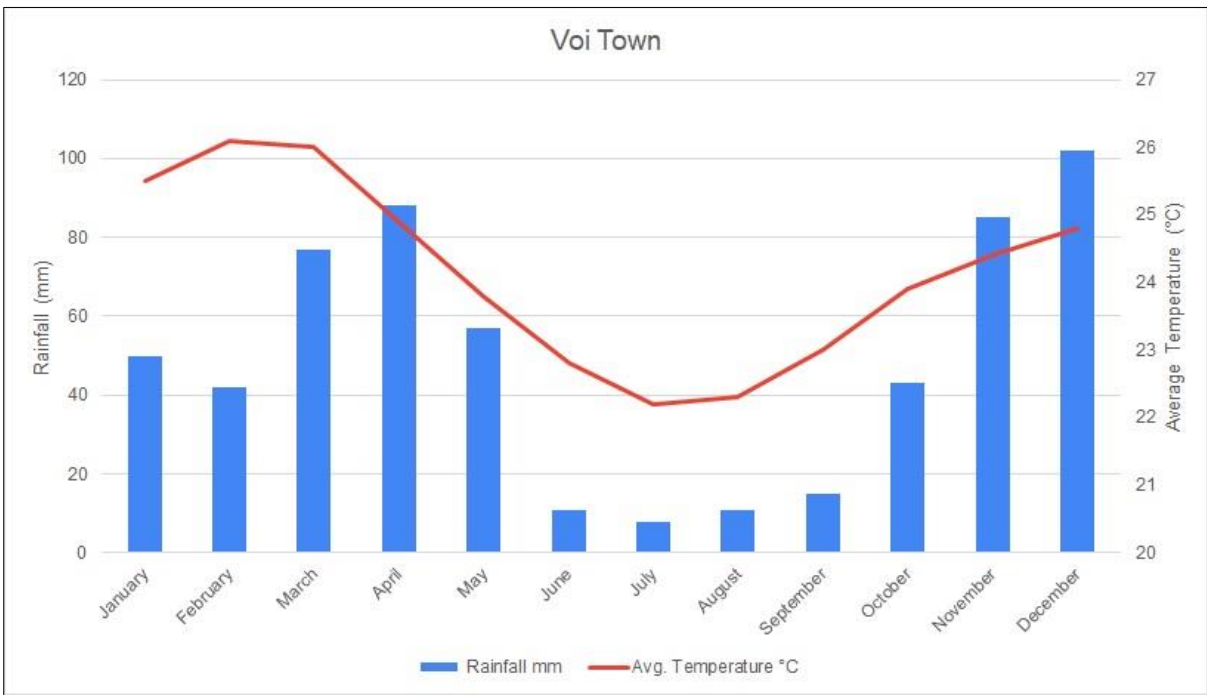


Figure 3-10 Climate graph for Voi town

3.10 HYDROLOGY

The drainage features in the Study Area comprise of rivers and streams, which generally flow from the north-western part of the Study Area, to the Indian Ocean, on the east side, as shown in Fig 3-11 below.

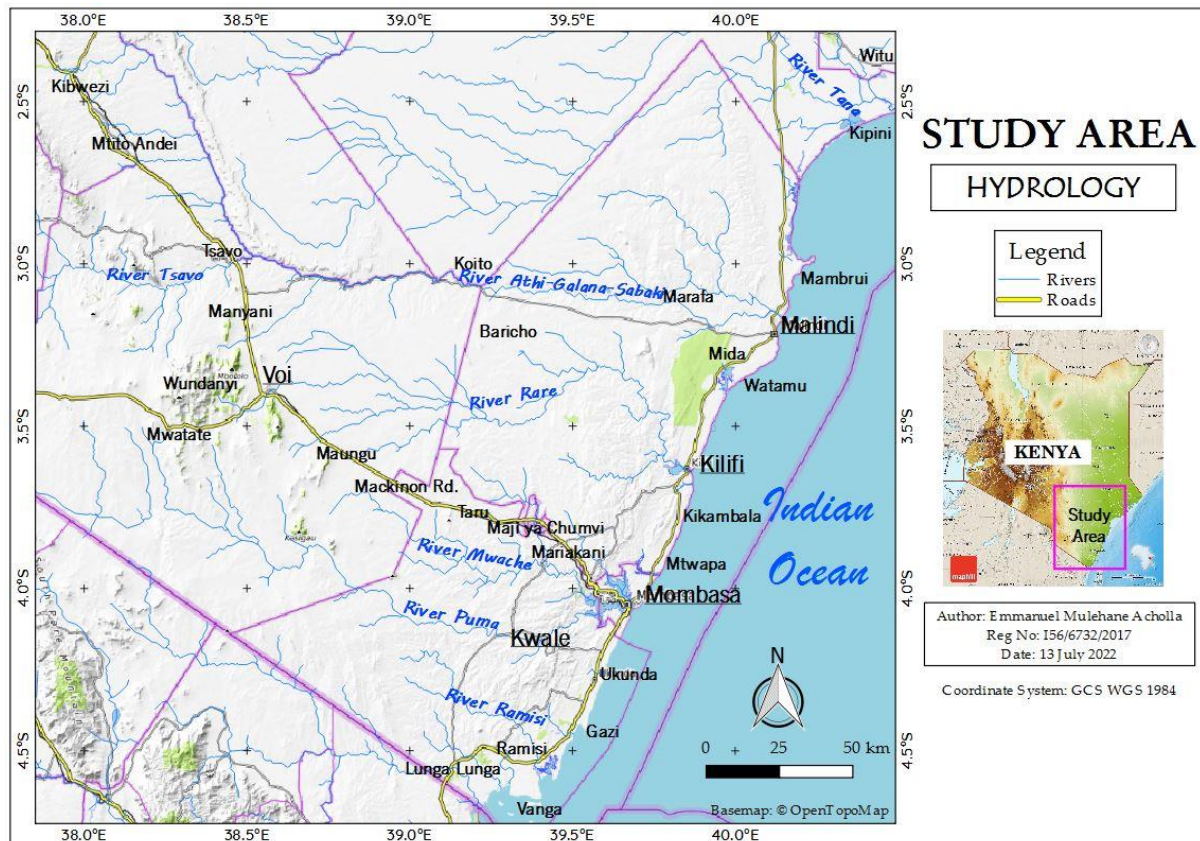


Figure 3-11 Hydrological features in the study area

Tana and Sabaki are the two primary rivers that drain the area. Ramisi, Uмба, Mkurumudzi, and Kidongoweni are smaller rivers. River Tana is the longest, originating from the Mount Kenya region with a catchment area of 127,000 km², an annual flow of approximately 4 billion m³ of freshwater and 6 million tons of sediments. It empties into the Indian Ocean near Kipini in Ungwana Bay.

The Athi-Sabaki River flows from the hills around Nairobi. It merges with the Tsavo River in its lower basin to form the Galana River. This system spans 380 kilometers and drains around 70,000 square kilometers. The Athi-Sabaki River has an annual fresh water flow of around 6 million m³. Other large rivers are the Ramisi and Uмба, which discharge over 6 million m³ and 16 million m³ of water into Funzi and Shirazi Bays, respectively. Mkurumudzi and Kidongoweni are two smaller rivers that enter the sea near Gazi Bay (NEMA, 2009).

3.11 HYDROGEOLOGY

Numerous lakes exist in the study region, principally within the Tana delta, shown in Fig 3-12 below. The bulk of them, like lakes Bilisa and Shakabobo, are oxbow lakes replenished by groundwater percolation or temporary overflows from the Tana River.

All of the primary water sources that serve the population in the area are underground (like the sand dune aquifers in Lamu, the aquifer at Baricho, the springs at Mzima and Marere and the aquifer at Tiwi). Many households and businesses in the study area rely on these subsurface water sources.

The Tiwi aquifer spans 147km² between the Mwachema River to the south and Matuga to the north. It is bound to the East by Pleistocene coral limestone, while the western boundary is 2 kilometers west of the Likoni-Ukunda road. The aquifer is made up of Kilindini lagoon sands from the Pleistocene epoch, with a water rest level of 25-30m bgl. It is replenished from the west, and from overlying seasonal swamps and lakes. The average yearly recharge is around 27,000m³/d. Discharge occurs at the marine front.

The Baricho aquifer crosses the Lango Baya fault, which forms an unconformable interface between the Mazeras sandstones and the Kambe limestones. The lowest unit is roughly 40m thick, with another 20m of sand, silt, and clay above. Surface water flow replenishes the system, while underflow into the Sabaki River discharges it. The aquifer covers 1.9km² and has an annual recharge rate of 83 million m³/year (Mumma et al., 2011).

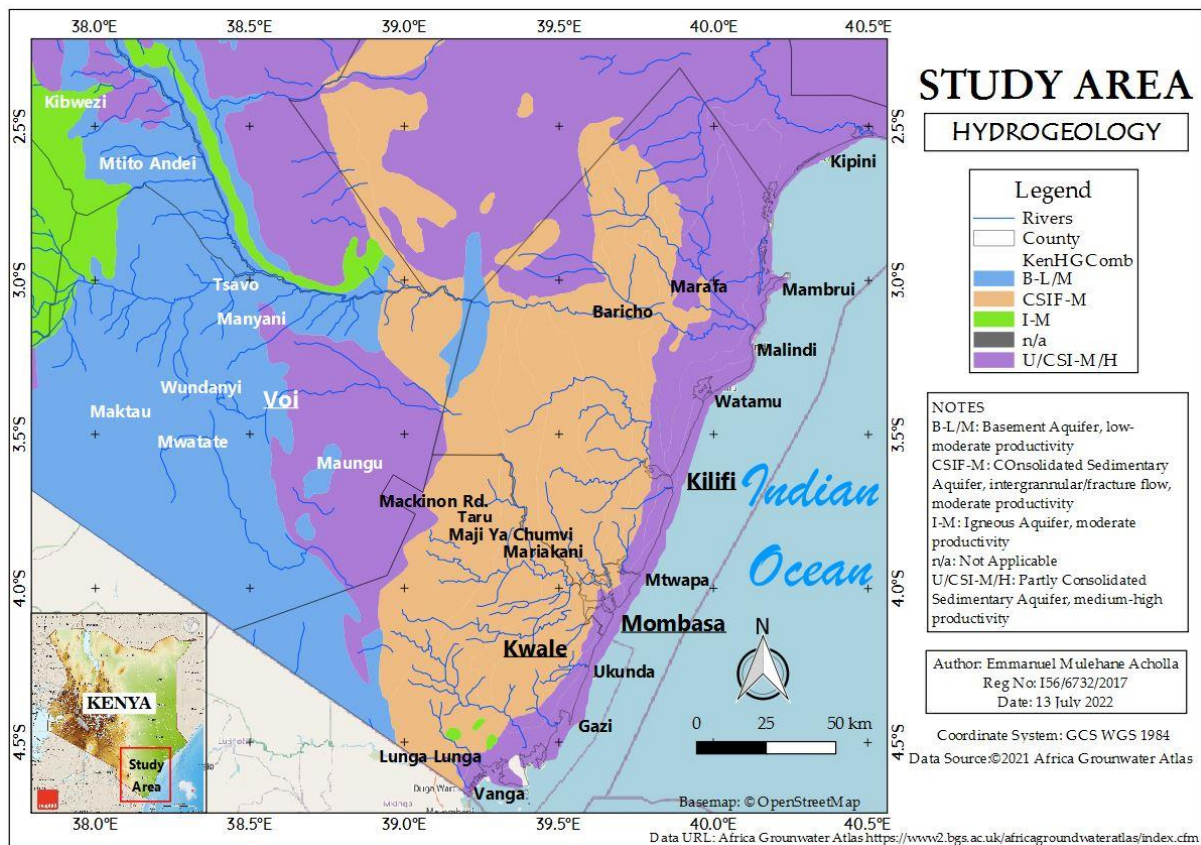


Figure 3-12 A Map of the hydrogeological resources in the study area (Adapted from McDonald et al. 2010)

3.12 LAND USES

The area's land use includes animal ranches, agricultural settlements in plots, privately held property next to the sea, and defined civic space. Livestock accounts for around 50% of the current countryside, while agriculture accounts for 25%. Protected areas includes National Parks and Reserves such as Shimba Hills and Mwaluganje Elephant Reserve (NEMA, 2009), as seen in Fig 3-13 below.

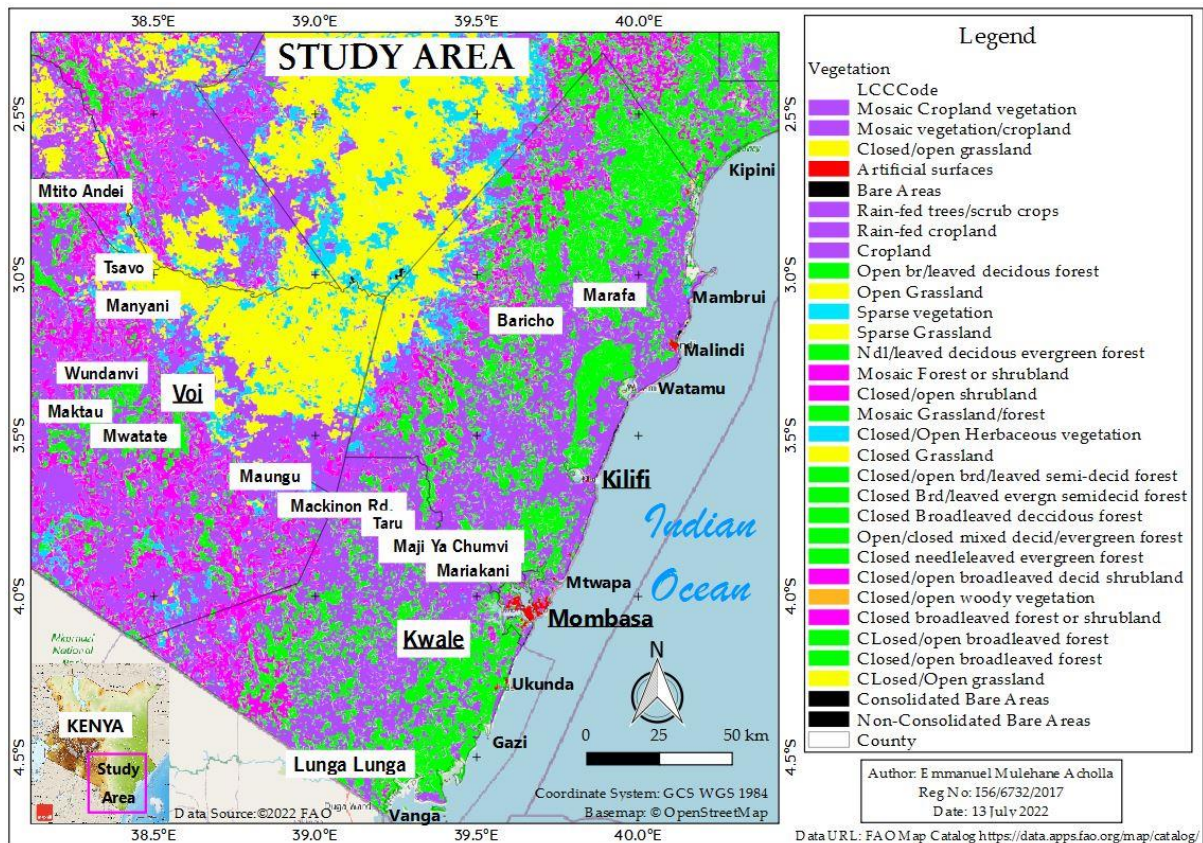


Figure 3-13 Land cover and use in the Study Area

3.13 SOILS

As shown in Fig 3-14 below, the soils in the area can be categorized as sandy, clayey, or loamy. The sandy and clayey soils are found along the coast, whilst the loamy soils are found inland and at higher elevations. Clayey soils are found in river valleys and floodplains north of the research area in the Tana River delta, as well as in protected coves such as Gazi Bay and Vanga.

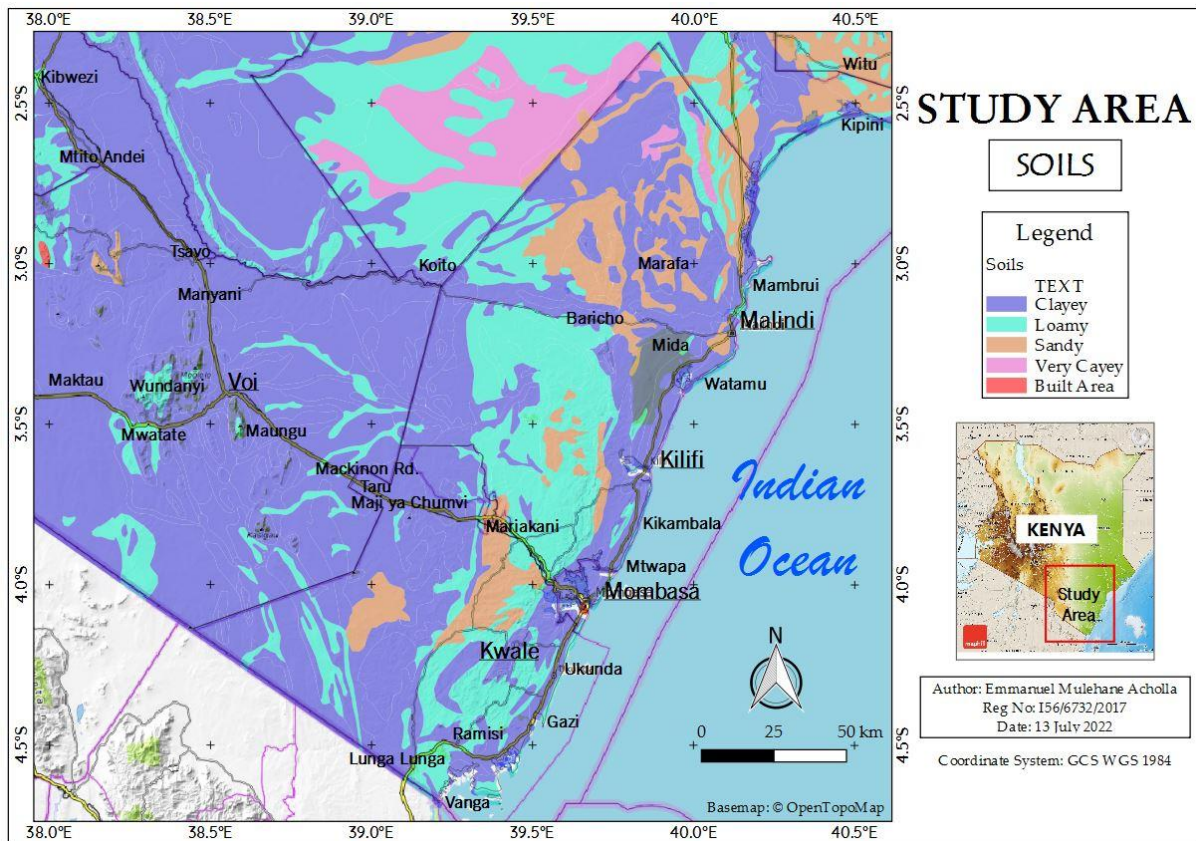


Figure 3-14 Soils in the Study Area (Courtesy: ILRI)

3.14 VEGETATION

The area's vegetation comprises of the following, as illustrated in Fig. 3-15 below, from west to east:

- I. Somalia-Maasai thickets and deciduous bushland
- II. Mangrove
- III. Edaphic vegetation

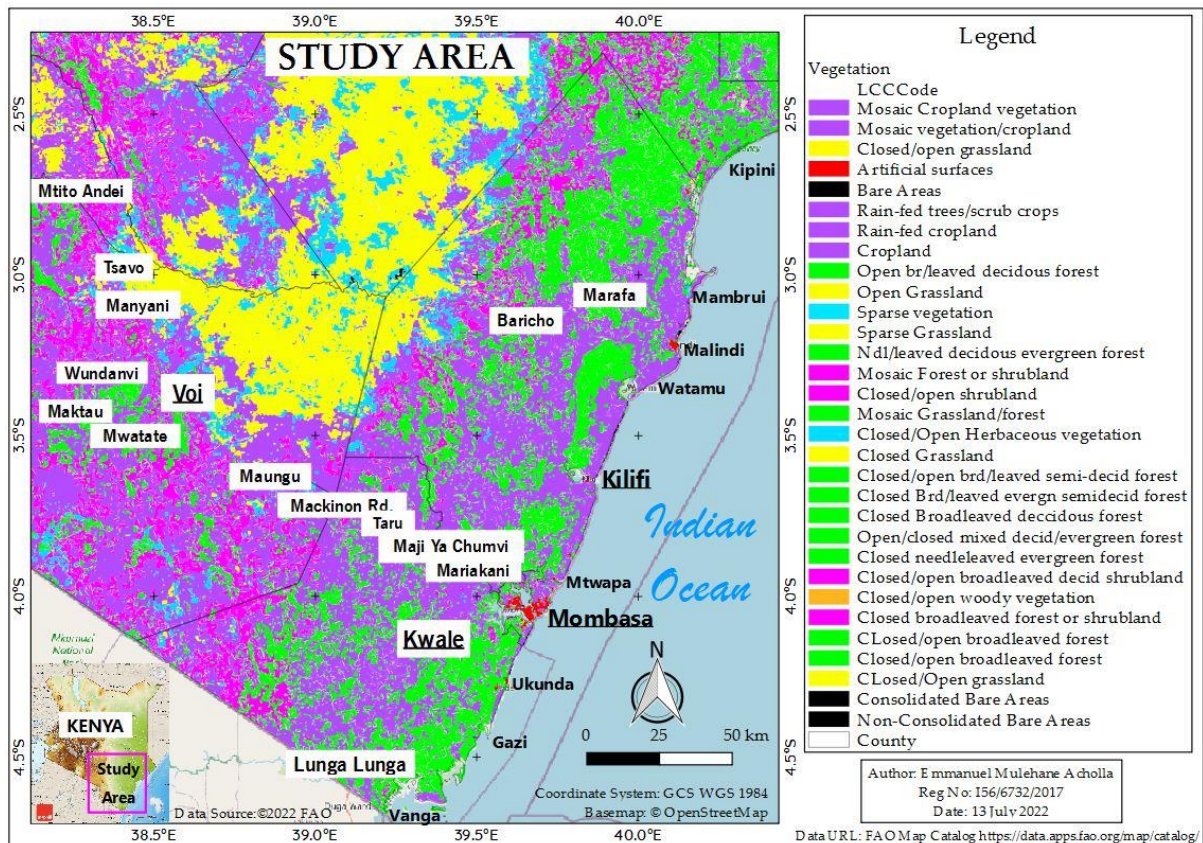


Figure 3-15 Vegetation in the study area

The deciduous scrubland and thicket of Somalia-Maasai consists of dense scrub with scattered trees, and includes *Acacia*, *Commiphora*, and *Grewia*, while palm tree species predominate along the shore.

Mangroves thrive on the area's coastlines, which are sometimes inundated by brackish water. The most common grasslands are connected with periodically or continuously wet soils in places with highly seasonal rainfall, such as the area. Floodplain grasslands are found in valleys of big rivers, such as the Tana River, where erosion has deposited alluvium on the valley bottoms. (Kindt et al., 2015)

4 THEORY OF PROBABILISTIC SEISMIC HAZARD ASSESSMENT

4.1 INTRODUCTION

Many earthquake engineering analyses seek to verify that a particular structure can withstand a certain range of ground shaking while maintaining a certain level of functionality. The sensible question is how strong the ground shaking should be for this sort of examination. Similarly, there is considerable uncertainty on the location, magnitude, and severity of future earthquakes. Using the Total Probability Theorem, the probabilistic seismic hazard assessment (PSHA) approach seeks to quantify these uncertainties and consolidate them to provide a realistic range of future shaking that may occur at a particular site.

Consider event A and a succession of separate but complementary occurrences. E1, E2 ... En. According to the Total Probability Theorem:

$$P(A) = \sum_{i=1}^n P(A|E_i)P(E_i) \dots\dots \text{Equation 4.1 (Baker, 2008)}$$

This entails the capacity to estimate the probability of event A given the probability of the independent factors (A's) and the ability to compute the likelihood of X given any of the A's.

This theorem allows the option to divide a given analysis into segments (such as earthquake magnitude and structural competency), compute the individual probabilities of these segmented sections, and then assemble them in a fashion that answers the initial problem. This expedites the solution in stages and allows various specialists (such as geologists, seismologists, and civil/structural engineers) to focus on different aspects of the computation. Baker (2008).

4.2 STEPS INVOLVED IN PSHA

PSHA evaluates all likely earthquake events and associated ground shaking, as well as their occurrence likelihoods, in order to determine an intensity of ground shaking that may be surpassed with a particular amount of certainty. PSHA approach comprises of determining earthquake sources, defining seismic sources, choosing attenuation relations (ground motion prediction equations), and lastly computing seismic hazard, as shown in Fig. 4-1 below: -

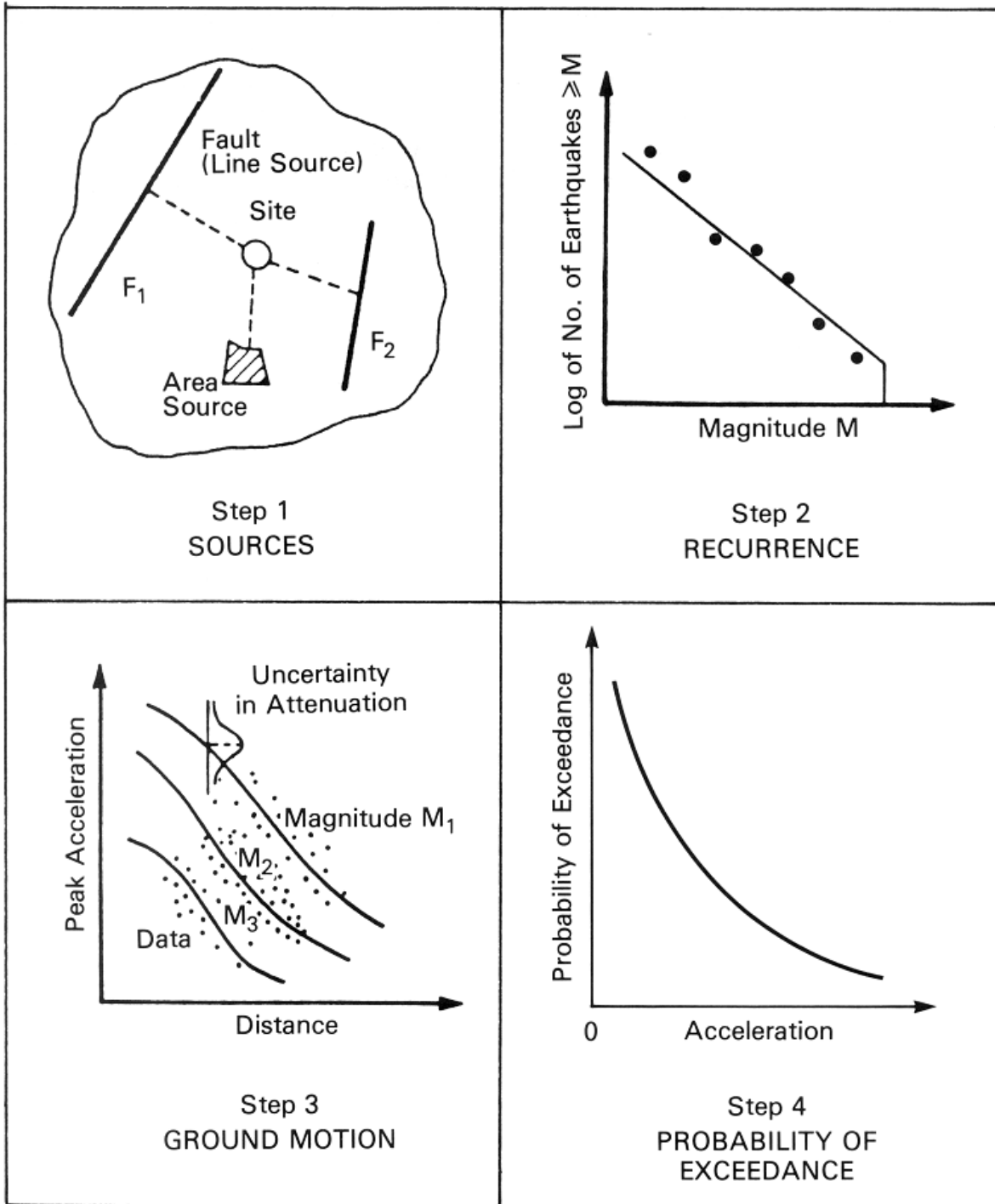


Figure 4-1 Basic steps involved in PSHA (Adapted from: Cornell-McGuire)

4.2.1 EARTHQUAKE SOURCE IDENTIFICATION

PSHA focuses on any source that could result in hazardous ground shaking in a specific place, as shown in Step 1 of Fig 4-1 above. These might be faults, that are typically thought to be planar and can be distinguished using a variety of approaches, such as examination of

instrumental earthquake epicenters and field geology or geophysical data. In circumstances when individual faults are not apparent (for example, in seismically inactive locations), seismic sources can be shown using geographic zones with a similar likelihood of seismic activity.

To determine ground shaking at a particular place, the distances from earthquake epicenters to that site must be calculated. The assumption for a certain seismic source is that earthquakes occur with equal probability at every position. Subsequently, it is quite simple to determine the source-to-site distances in relation to the dimensions of the specific source. It should be noted that the expert's judgment on the definition of these distances is dependent on what input is necessary for the specific ground motion prediction model selected.

4.2.1.1 Area Source

This kind of earthquake source is presumed to create earthquakes randomly, with equal chances everywhere within a certain distance of a site. In practice, they are widely utilized to portray diffuse earthquakes or seismicity that cannot be directly assigned to a single fault. Because of the widespread tectonic and seismic activity in the area, the area source model will be used in this study.

4.2.1.2 Line Source

The source is presumed to be of straight dimension (Ordaz et al., 2014). It is very useful for constraining precisely defined faults, such as those that occur at defined tectonic plate borders, whether convergent, divergent, or transform. Because of the diffuse character of the geological setting of the area, little or no data is available to precisely tie the instrumental seismicity to the continental edge faults. This may necessitate future paleo-seismic research, that is beyond the scope of the current investigations.

In this study, data on the locations, sizes, and kinds of faults in the area were utilized to create an earthquake source geometry model in the PSHA software CRISIS2015 (Ordaz et al. 2015). The bedrock lithologies' identities were matched with their seismic shear-wave velocities and utilized to define the site effects model.

4.2.2 EARTHQUAKE SOURCE CHARACTERIZATION

Active tectonic faults can cause earthquakes of varying size. Gutenberg & Richter (1944) popularized the observation that the graph of earthquake magnitudes in a certain region follows

a consistent pattern. The model is depicted in Eq. 4.2 by the Gutenberg-Richter Recurrence Law as:

$$\log \lambda_m = a - bm \dots \dots \text{Equation 4.2 (Baker, 2008)}$$

Where:

λ_m = frequency of occurrence of earthquakes with magnitudes greater than m

a, b = constants

The a and b factors above are derived from a statistical analysis of historical earthquakes in conjunction with other geologic indicators. The a-coefficient denotes the total frequency of seismic events in a certain region, whereas the b-coefficient denotes the ratio of minor and big earthquake magnitudes (generally, the b-value seldom surpasses 1).

In addition, the following parameters have to be specified for each seismic source modeled, as shown in Step 2 of Fig 4-1 above:

- i. Earthquake activity rate λ , which is the number of earthquakes per year
- ii. Catalog completeness, including the minimum magnitude (M_{\min})

Maximum possible earthquake magnitude (M_{\max})

- iii. The b -value, a parameter which indicates the relation between large and small earthquakes
- iv. Focal depth of earthquakes

4.2.3 ATTENUATION LAW SELECTION

The primary goal of this study is to analyze ground vibrations rather than earthquakes. The next inevitable step is to construct a model that can estimate ground shaking caused by earthquakes (GMPM, also known as Attenuation Laws/Models or Attenuation Relations). As illustrated in Step 3 of Fig 4-1 above, these equations calculate the probability and severity of ground shaking considering a number of crucial criteria, such as the size of the earthquake, its distance from a place, the rupture mechanism involved, and the foundation characteristics at a location. The statistical analysis of records from large catalogs of actual or computed ground shaking data and historical earthquakes yielded attenuation equations. These models in Eq. 4.3 have the overall form depicted below: -

$$\ln IM = \overline{\ln IM}(M, R, \theta) + (M, R, \theta) \cdot \varepsilon \dots \dots \text{Equation 4.3 (Baker, 2008)}$$

Where:

$\ln IM$ = Natural log of the ground motion acceleration

$\overline{\ln IM}(M, R, \theta)$ and $\sigma(M, R, \theta)$ = the GMPM results (the expected average and standard deviation of $\ln IM$). They are contingent on the magnitude of the earthquake (M), its distance from a certain site (R), and any extra limits (expressed by θ).

ε = a typical random factor indicating the $\ln IM$ inconsistency.

Finally, it is possible to calculate the likelihood of surpassing a ground motion acceleration level (say x), caused by a future earthquake of undetermined size and distance from a single source, using the Total Probability Theorem in Eq. 4.4, illustrated below: -

$$P(IM > x) = \int_{m_{min}}^{m_{max}} \int_0^{r_{max}} P(IM > x/m, r) f_M(m) f_R(r) dr dm \dots \dots \text{Equation 4.4(Baker, 2008)}$$

Where:

$P(IM > x/m, r)$ = Derived from the attenuation relation

$f_M(m)$ and $f_R(r)$ = Likelihood factors for magnitude and distance

This method combines the set probability of exceeding associated with all conceivable earthquake magnitudes and epicentral distances. The preceding equation does not include data regarding the frequency of earthquake occurrences or the source of interest. The method, as described in Eq. 4.5, can be modified to estimate the frequency of any ground shaking (IM) larger than level x rather than the likelihood of any ground motion (IM) bigger than x in the case of a specific earthquake:

$$\lambda(IM > x) = \lambda(M > m_{min}) \int_{m_{min}}^{m_{max}} \int_0^{r_{max}} P(IM > x/m, r) f_M(m) f_R(r) dr dm \dots \dots \text{Equation 4.5(Baker, 2008)}$$

Where:

$\lambda(M > m_{min})$ = the frequency of earthquake occurrence surpassing m_{min}

$\lambda(IM > x)$ = the frequency of ground shaking (IM) surpassing x

In situations involving more than one source, the frequency of ground acceleration (*IM*) exceeding a value *x* will be the summation of the frequencies of ground accelerations (*IM*) exceeding *x* from every discrete source as in Eq. 4.6, such that: -

$$\lambda(IM > x) = \sum_{i=1}^{n_s} \lambda(M_i > m_{min}) \int_{m_{min}}^{m_{max}} \int_0^{r_{max}} P(IM > x/m, r) f_M(m) f_R(r) dr dm$$

Equation 4.6 (Baker, 2008)

Where:

n_s = number of the sources

M/R =the proportion of magnitude to distance for each source

This formula is generally associated with PSHA. It integrates current knowledge on earthquake incidence rates, magnitudes, epicentral distances, and the duration of ground shaking. After analyzing instrumental earthquake catalogs, each of these contributions may be identified. This will result in a higher frequency of exceeding IM degrees by variable amounts, which is critical for technical decision making in engineering research. (Baker, 2008).

4.2.4 CALCULATION OF EARTHQUAKE HAZARD

The result of probabilistic seismic hazard analyses includes seismic hazard curves (SHC) and uniform hazard spectra (UHS). In addition, maps can be generated, depicting the spatial distribution of ground vibration in an area, for various frequencies, probabilities of exceedance and return periods, as shown in Step 4 of Fig 4-1 above.

PSHA computations may quickly become lengthy due to the inherent complexity of geological settings and earthquake events in actual conditions. As a result, PSHA is accomplished utilizing specialized software applications. These programs do advanced PSHA calculations, particularly for complex projects involving many seismic origins, while including the most recent attenuation equations.

In this work, Ordaz et al. (2015)'s CRISIS 2015 software was utilized to carry out the calculations for the PSHA in the area and to generate the seismic hazard curves.

5 METHODOLOGY

This study included retrospective desktop investigations, outdoor ground truthing of the area's outcrops and prominent faults, secondary earthquake data gathering, and statistical analysis. The information regarding the rock types and geologic faults in the area was included in the CRISIS 2015 PSHA software site impacts module, the magnitude-frequency relations derived from the seismicity characteristics of the earthquake catalogs were incorporated in the source seismicity module of CRISIS 2015, the probabilistic earthquake ground accelerations computed and thereafter seismic hazard curves for all significant towns in the area were generated.

Data on earthquake hazard was imported into ArcGIS Pro 2.3.3 software, and used to develop an improved seismic hazard map of the area. Following that, a comparison was carried out on the data, methodology, and outcomes of this study to earlier studies, illustrating the parallels and contrasts, and conclusions and recommendations prescribed.

5.1 MATERIALS USED IN RESEARCH

This study utilized several open-source software (CRISIS, SEDA, SPSS, Google Earth, Surfer) and 1 commercial software (ArcGIS) during the desktop studies and subsequently for data analysis. They are listed in Table 5-1 below.

Table 5-1 Software used in this study

	Software	Developer	Version/Year
1	CRISIS2015	Mario Ordaz	4.1
2	SEDA	Anna Maria Lombardi	1.0
3	IBM SPSS	IBM Systems Incorporated	2021
4	Google Earth Pro	Google Incorporated	2021
5	Surfer	Surfer Systems	14
6	ArcGIS	ESRI Incorporated	2.2.3

This study utilized several hardware for desktop studies and data analysis (Computer, loaded with digital maps and earthquake data, and software), ground truthing (GPS set, camera,

tablet, measuring tape, writing materials) and logistics during the ground truthing (hired field vehicle). They are listed in Table 5-2, and illustrated in the Plates below.

Table 5-2 Hardware and logistics used in this study

Category	Materials
Computer	1. Toshiba Radius S50W laptop
Maps	1. Google Earth maps 2. SentinelHub satellite imagery 3. Ministry of Energy (1986) digital geological map of Kenya
Earthquake data	1. United States Geological Survey online catalog 2. International Seismological Center online reviewed catalog
Ground Truthing equipment	1. Garmin GPSMap64 GPS 2. Canon EOS200D Camera 3. Samsung Galaxy tablet 4. Measuring tape 5. Field notebook and pen
Ground Truthing logistics	1. Field vehicle (hired)- Toyota Ractis



Figure 5-1 Laptop computer used in this research (Toshiba S50W)

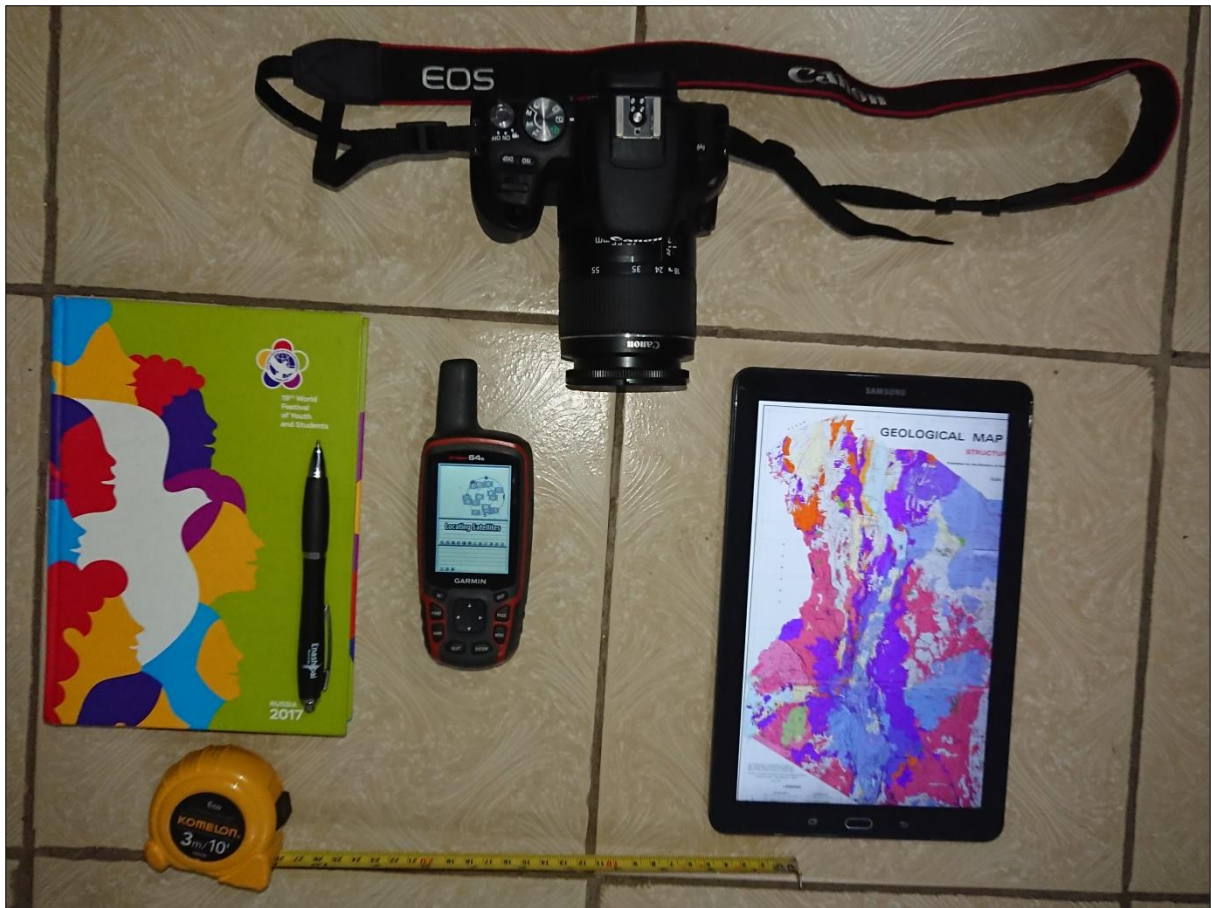


Figure 5-2 Field equipment used in this study (Left to Right: Notebook, pen, tape measure, GPS, Camera and tablet)



Plate 5-1 Vehicle used during the field ground truthing

5.2 DESKTOP STUDIES

According to conventional PSHA procedure (Gupta, 2002; Baker, 2008; Poggi et al., 2017), instrumental seismicity data from 1900 to 2019 was retrieved from the US Geological Survey and ISC web - based reviewed catalogs and analyzed using IBM SPSS statistical tools, while the catalog kml files were mapped on Google Earth, as illustrated in Fig 5-3 below.

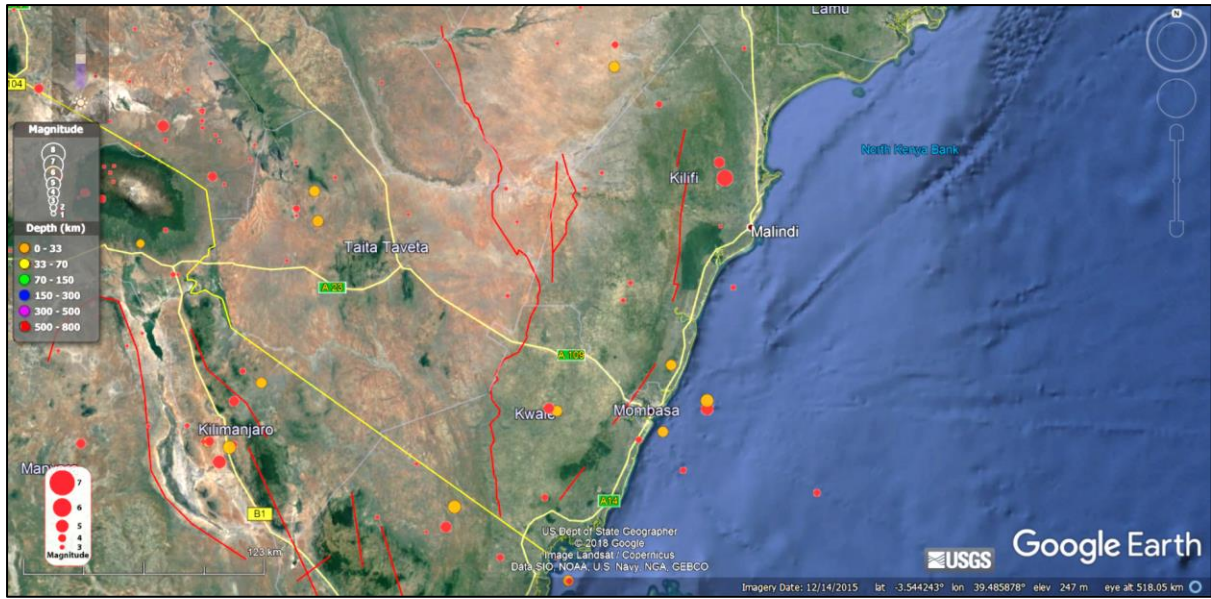


Figure 5-3 A natural colour satellite image (bands 4,3,2) of the Study Area, showing ISC and USGS earthquake epicenters (©Used with permission from Google LLC. Google LLC's registered trademarks include Google and the Google logo.)

5.2.1 DELINEATION OF SEISMIC SOURCES

A detailed review of the geology, seismology and tectonics of the Indian Ocean coast of Kenya was carried out from published geological maps, detailed satellite images and published literature in order to identify the area of interest (the Study Area) and its geologic faults as illustrated in Fig 5-4, 5-5 and 5-6 below, in relation to earthquake epicenters.

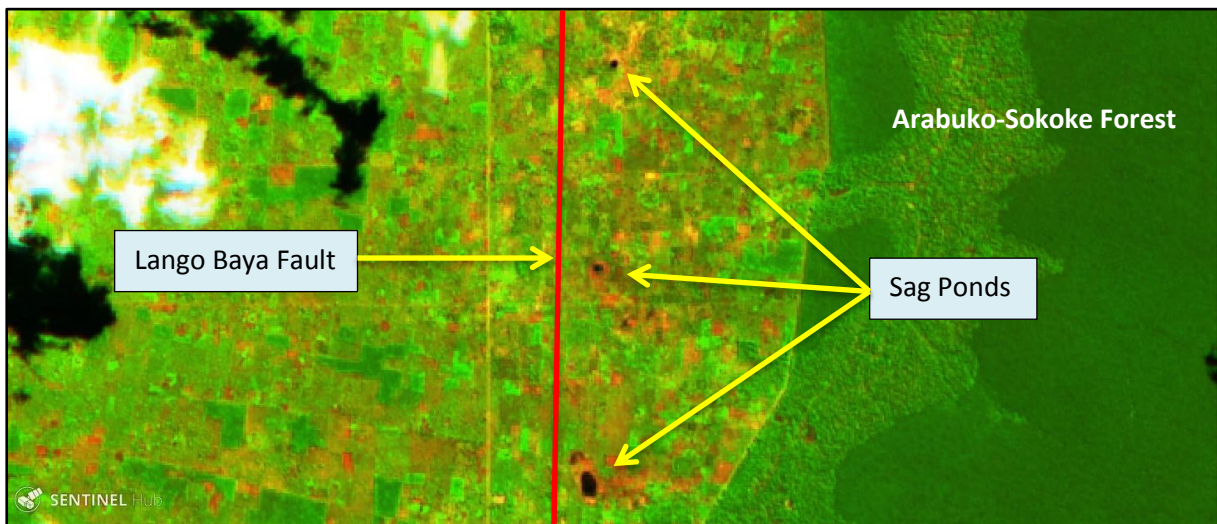


Figure 5-4 A Sentinel-2 satellite image (bands 11, 8, 2) of three sag ponds trending NE-SW located at Vitengeni, 24 Km W of Watamu town. (Courtesy: Sentinel Hub™. Downloaded: 10/02/2019)

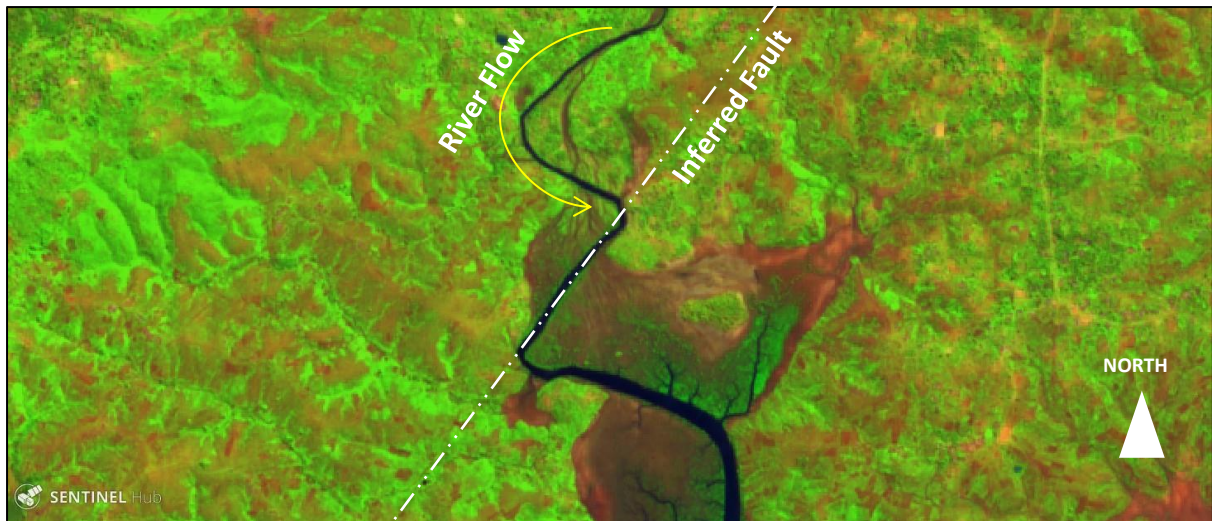


Figure 5-3 A Sentinel-2 satellite image (bands 11, 8, 2) of an elbow bend on river near Tudor Creek, Mombasa County (Courtesy: Sentinel Hub™ Downloaded on 18-12-2018)



Figure 5-4 A natural colour satellite image (bands 4,3,2) of NE-SW trending knick points within a fault zone intersecting River Marere bed, north of Kwale town. (©2019 Used with permission from Google LLC. Google LLC's registered trademarks include Google and the Google logo.)

The main reference geological map used was a structural geological map by the Ministry of Energy (1987), while the latest satellite imagery was obtained from the Sentinel Hub website (<https://apps.sentinel-hub.com/sentinel-playground/>). The main literature reference used was the geological report of South Eastern Kenya by Oosterom (1988). From these sources, it is clear that Kenya's Coast region, and particularly the south Coast, is passive continental margin with an unusual level of earthquake activity, which merits investigation.

5.2.2 EARTHQUAKE DATA COLLECTION

From available literature, a study of earthquake catalogs, catalog assembly and analytics, PSHA calculation, and the generation of earthquake hazard curves was performed. This also involved a review of the data inputs, methodologies, assumptions and results.

The main sources of earthquake catalog data were the USGS (2019) and ISC (2018) online reviewed catalogs. SEDA v1.0 user manual by Lombardi (2016) was the main reference and program used for the analysis of the catalog. The main reference for the PSHA computation was the CRISIS 2015 user manual by Ordaz et al (2014), because CRISIS 2015 was the program adopted for PSHA computation.

5.2.3 REVIEW OF PUBLISHED SEISMIC HAZARD WORKS

A critical review of the latest published seismic hazard maps covering the study area was carried out, including their data, methodologies, assumptions and results.

The Global Earthquake Model (GEM) Foundation's worldwide earthquake hazard map served as the primary reference (2018). The methodology applied by GEM (2018) in designing the map is PSHA, similar to the present study. The data sources, analysis, assumption and results were also very similar to the present study, except for the field ground truthing.

5.3 GROUND TRUTHING

A ground truthing field visit was carried out to the study area from the 16th to 23rd March 2019 (Appendix 11.2). The specific objective of this research that this ground truthing addressed was “*To delineate the seismic source zones responsible for the earthquake activity in the study area.*” The ground truthing involved field visits to sites of interest shown in Fig 5-5 below, including open quarries, rock outcrops, river bends, sag ponds and river rapids/knick points.

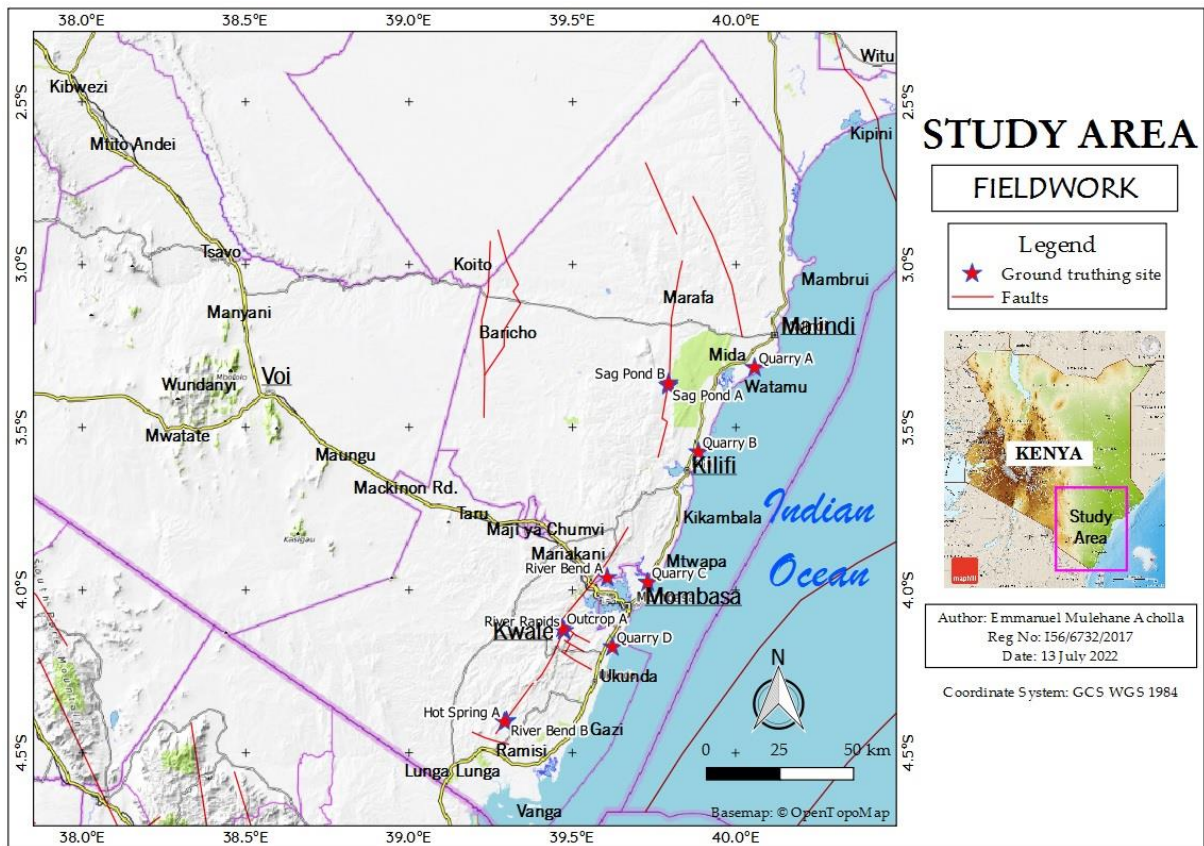


Figure 5-55 Ground truthing sites in the Study Area.

5.3.1 GROUND TRUTHING ACTIVITIES

The direct investigation of open pit quarries, rock formations, and river valleys to define the type, stratigraphy, structural linkages, and features of geologic strata was the target of the field visits. In addition, sag ponds, knick points and elbow bends on river beds were physically examined to deduce the nature, trends and orientation of faulting in the study area. Volcanic features like hot springs close to inferred faults were also physically examined to deduce any structural relationships. These are illustrated in the plates below.

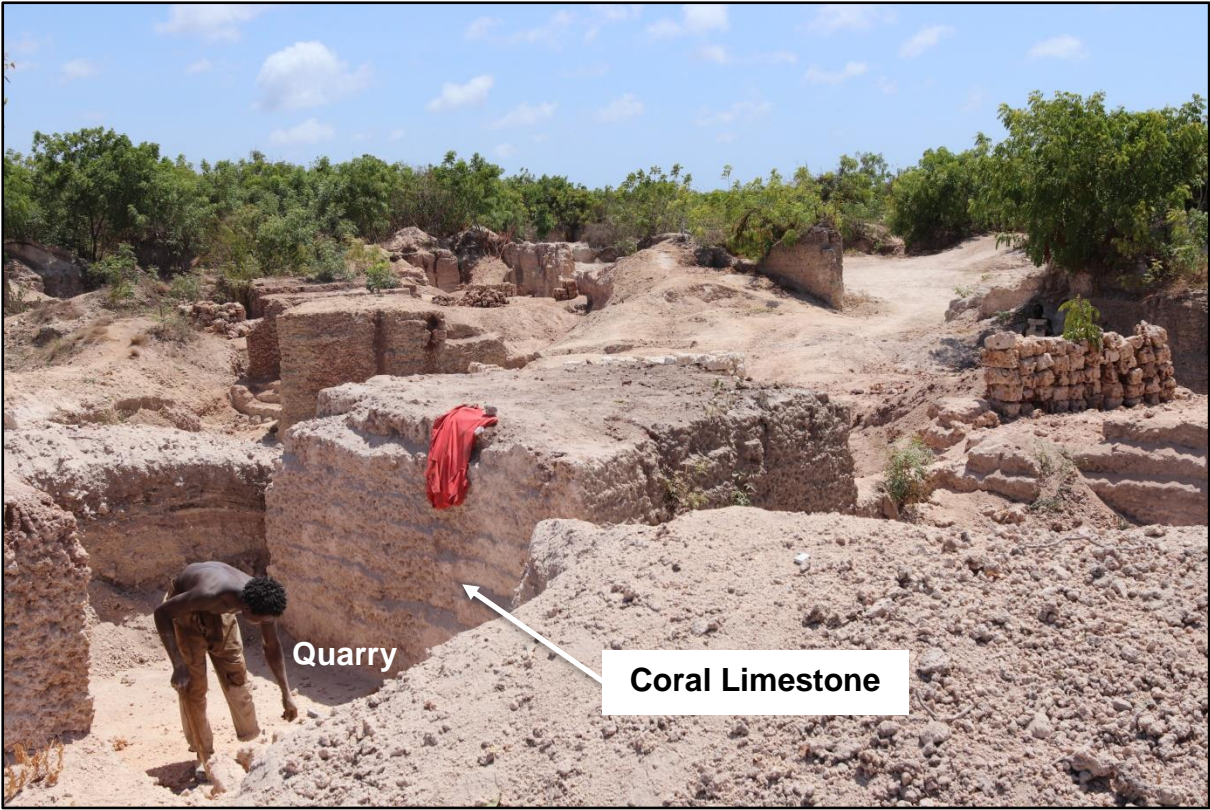


Plate 5-2 Artisanal quarry at Gede, south of Malindi Town



Plate 5-3 A NE-SW trending knick-point (KP) at Marere riverbed, north of Kwale town

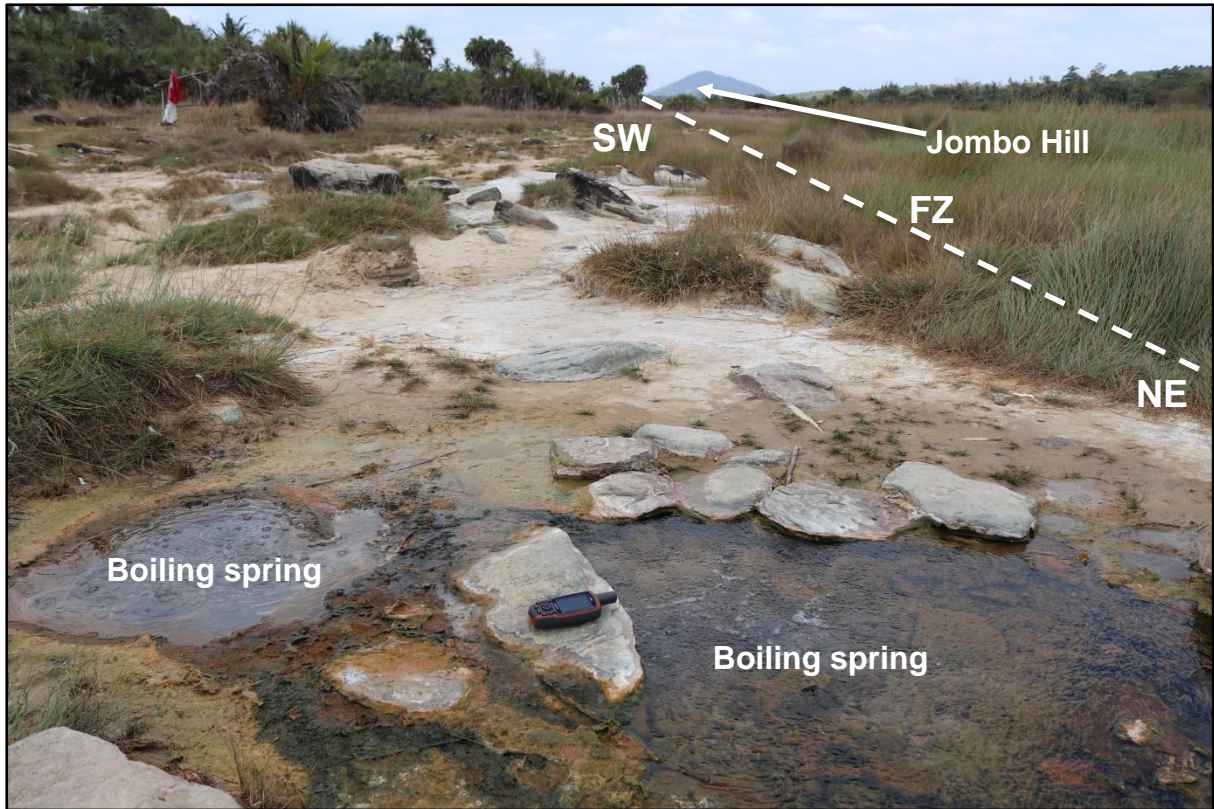


Plate 5-4 Hot Springs in a NE-SW trending fault zone (FZ), Mwananyamala, Kwale

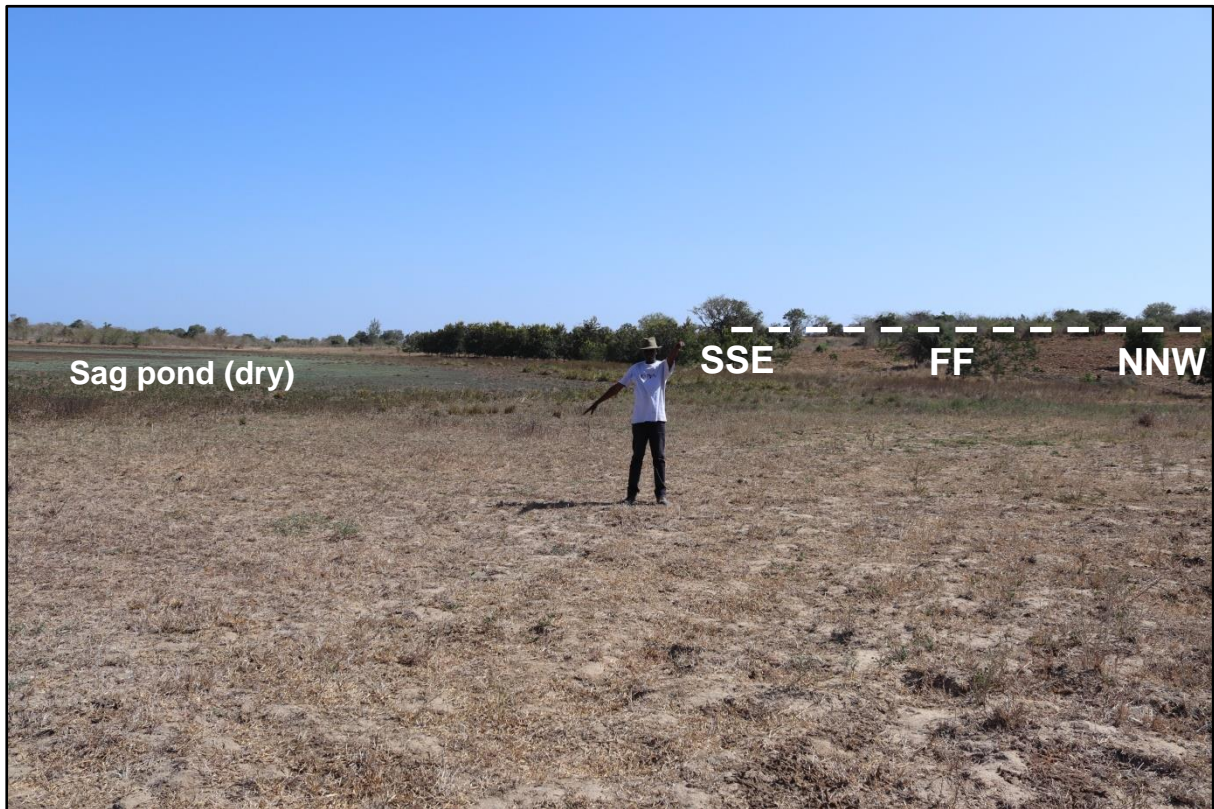


Plate 5-5 A sag pond (SP) on the hanging-wall side of a NE-SW trending fault at Vitengeni, Kwale.

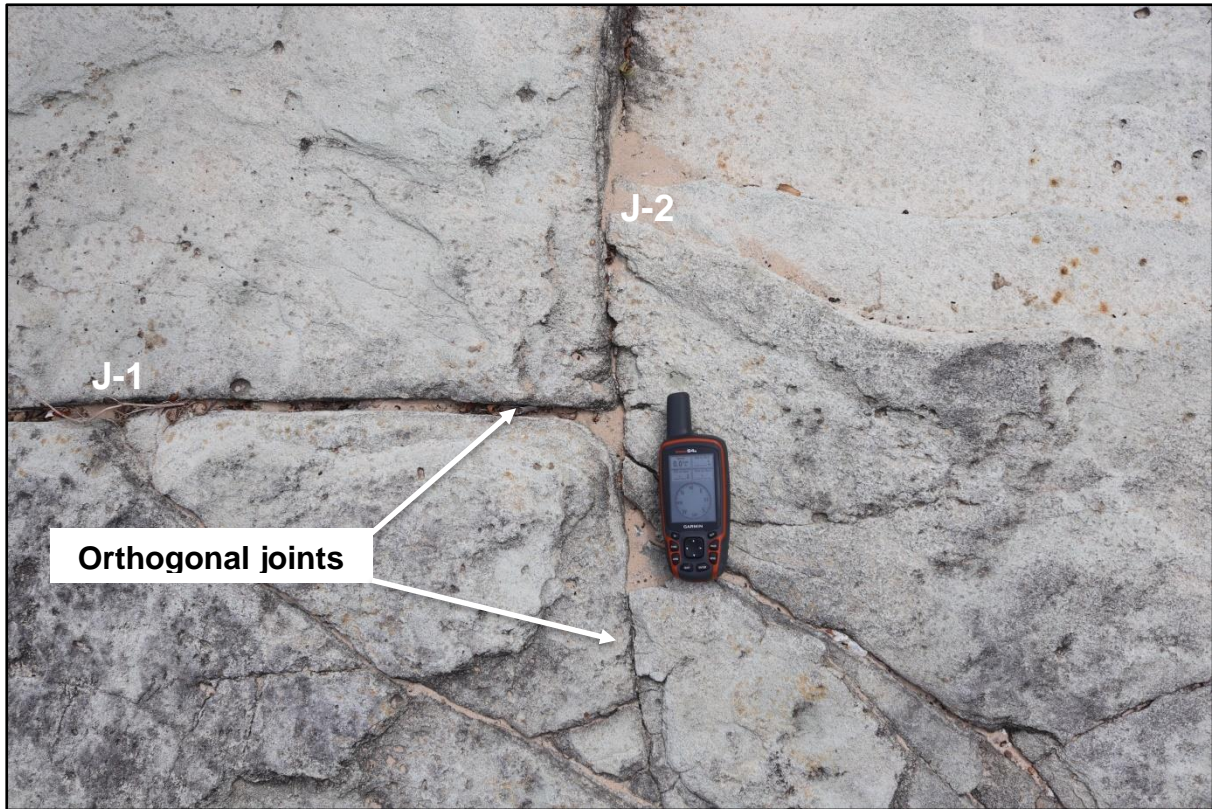


Plate 5-6 A sandstone outcrop at river Marere north of Kwale Town (GPS is 16cm long).

The information acquired during field visits assisted in the identification of geologic faults in the area, as well as the zones with equal probability of earthquakes when coupled with earthquake epicenters. The information on the extent and faulting characteristics of the source zones were then incorporated into the seismic source geometry model in the main probabilistic seismic hazard computation software, CRISIS 2015™.

In addition, the field data and observations guided the determination of the faulting characteristics prevalent in the study area, in terms of the style of faulting (normal, reverse, strike-slip) and thus, the tectonic regime (extensional, compressional, shear) which are inputs in the seismic source model.

5.4 COMPUTATION OF SEISMIC HAZARD

In this research, the CRISIS 2015 program by Ordaz et al (2015) was used to run the calculations for the PSHA in the area, calculate peak ground accelerations (PGA), and generate seismic hazard curves and spectra for significant towns (see Fig 5-9 below).

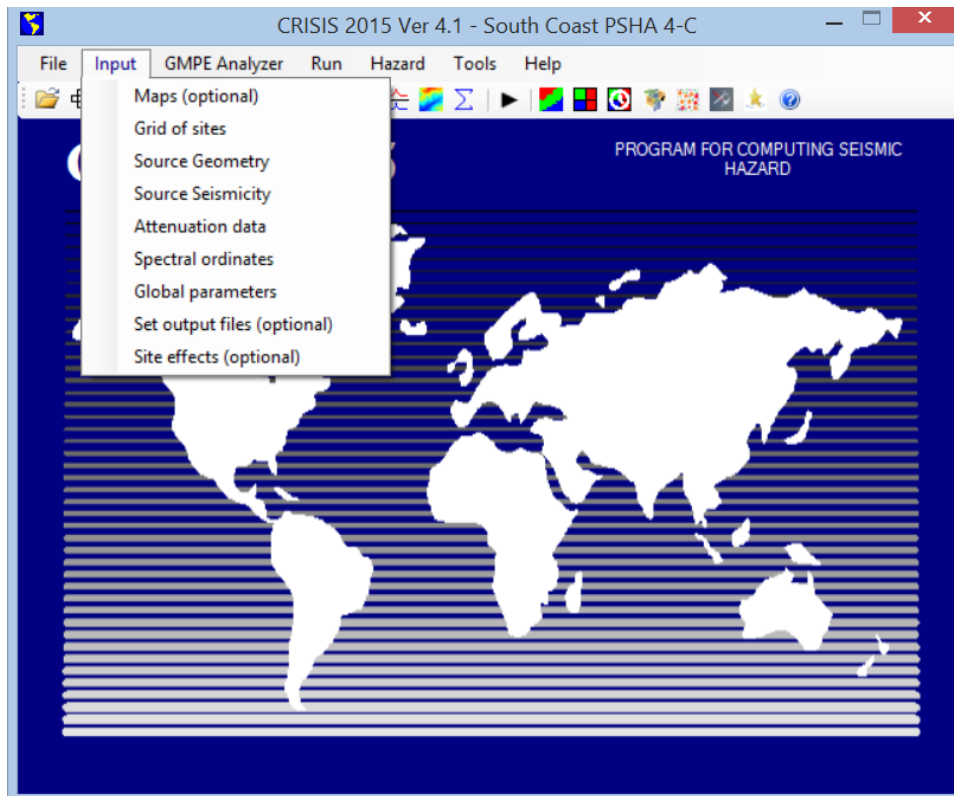


Figure 5-67 CRISIS 2015 v4.1 start screen and data input tab

5.4.1 HAZARD COMPUTATION PROCEDURE

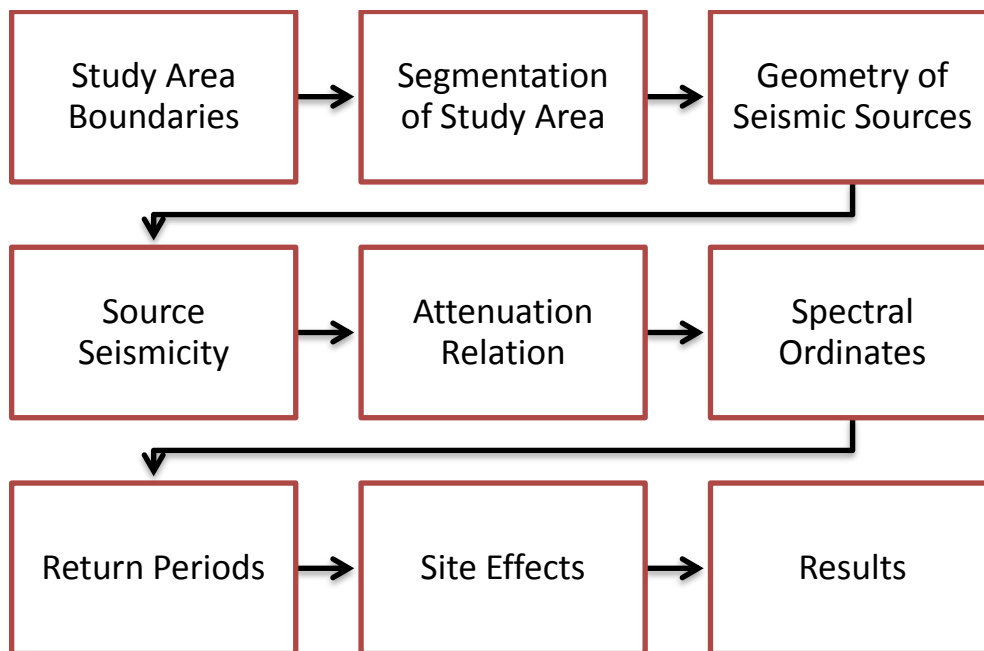


Figure 5-7 Flowchart of Probabilistic Seismic Hazard Assessment (PSHA)

As shown in Fig 5-10 above, the data required to initiate a PSHA computation involves the boundaries of the study area in question. In this study, this consisted of a map of Kenya, together with its towns in ESRI shapefile (.shp) format.

The second step was to segment the Study Area into spatial areas over which the PSHA computation would be made, through the *Grid of Sites* tab. This involved specification of a number of points within the specified study area, for which PSHA computations will be made. In this study, a mesh of 95x92 lines was used, separated by a distance of 0.1°.

The third step was to define the dimensions of the seismic sources in the study area. Here, the coordinates of the seismic area source zones delineated in Google Earth Pro were loaded into the *Geometry of Seismic Sources* tab, together with their approximate thicknesses and rupture parameters.

The fourth step was to define the seismicity parameters of the seismic sources specified in the previous step in the *Source Seismicity* tab. The parameters include the maximum (m_{\max}) and Minimum (m_{\min}) magnitudes and the Gutenberg-Richter (G-R) a - and b -values. These parameters were obtained from a statistical analysis of the combined earthquake catalog of the study area by SEDA v6.0 software.

The fifth step is to define the attenuation relations for each specified seismic source zone. This involved selection of an appropriate attenuation relation from the database contained in

CRISIS 2015 in the *Attenuation Relation* tab. In this study, the Abraham & Silva (1997) attenuation relation was selected because it applies to shallow crustal earthquakes worldwide, and has parameters for ground acceleration, spectral range, magnitude range and tectonic regime that are suitable to the study area.

The sixth step involved the definition of structural periods (in Seconds) for which the PSHA will be computed, in the *Spectral Ordinates* tab. Related to this is the *Global Parameters* tab, in which specifications of the time frame of the PSHA and return periods of the maps generated were input. Seismic hazard was calculated in this study assuming a 10% likelihood of exceedance in 50 years, in the form of maximum horizontal ground acceleration (PGA) in cm/s/s, for return periods of 25, 50, 100, 150, and 200 years. Oscillation durations of 0.05, 0.1, 0.15, 0.3, 0.5, 1.0, and 2.0 seconds were used to account for all potential shaking events, ranging from short-period oscillations to long-period oscillations.

The final step is the *Site Effects* tab, wherein the seismic wave velocity of the bedrock observed in the study area is defined. In this study, given the observed predominantly limestone foundation formations underlying the major cities in the study area, the seismic shear wave velocity was conservatively set at 750 m/s taking into consideration velocity losses from attenuation.

After this, the *Set Output Files* tab was used to define the types and locations of PSHA files will be generated by CRISIS 2015, and the *Run* tab used to execute the PSHA computation. In this study, the software generated seismic hazard data in grid (*.grid*) format, together with a map of the distribution of seismic hazard in and around the study area, for various return periods (years) and spectral frequencies, as shown in in Fig 5-11 below.

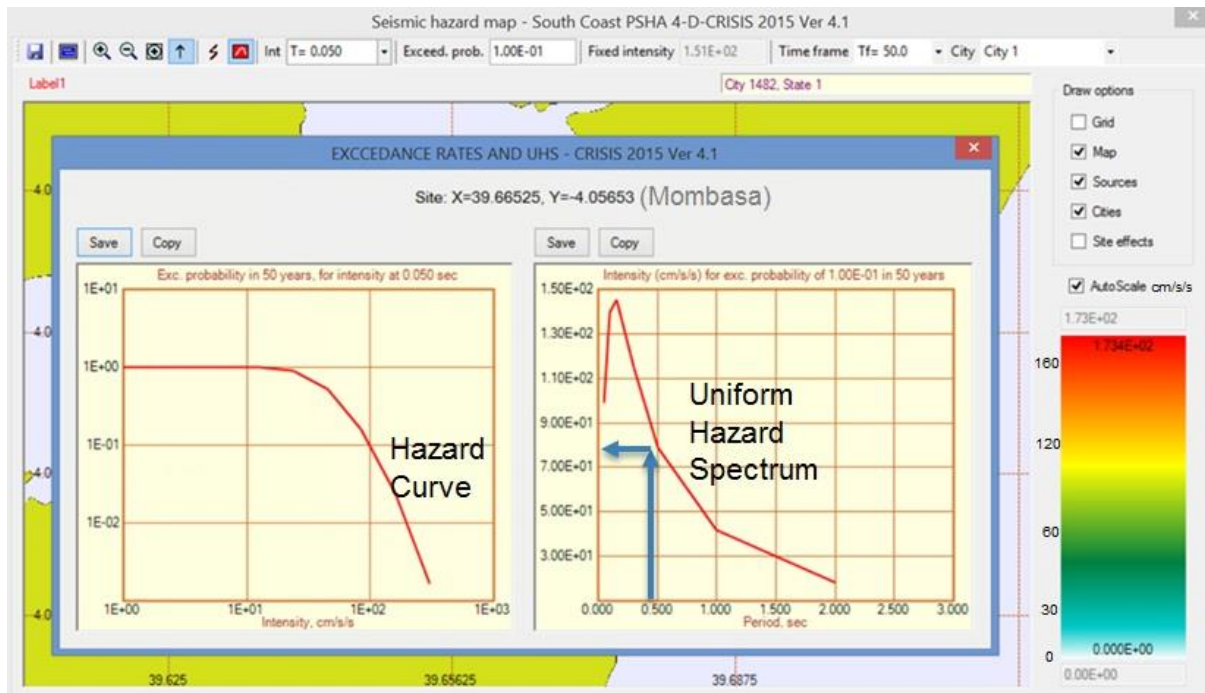


Figure 5-8 CRISIS 2015 seismic hazard map output screen

The seismic hazard curves for towns and cities on the map was viewed by first specifying the relevant ground acceleration period, exceedance probability and time frame. Clicking on the desired town location opened a window titled *Exceedance/Non-Exceedance Rates and Uniform Hazard Spectra*. The window featured two charts: the left-hand chart presented the chance of exceedance within 50 years for a 0.5s interval, while the right-hand one displayed the maximum horizontal ground accelerations for a 10% likelihood of exceedance in 50 years, as shown in Fig 5-12 below.

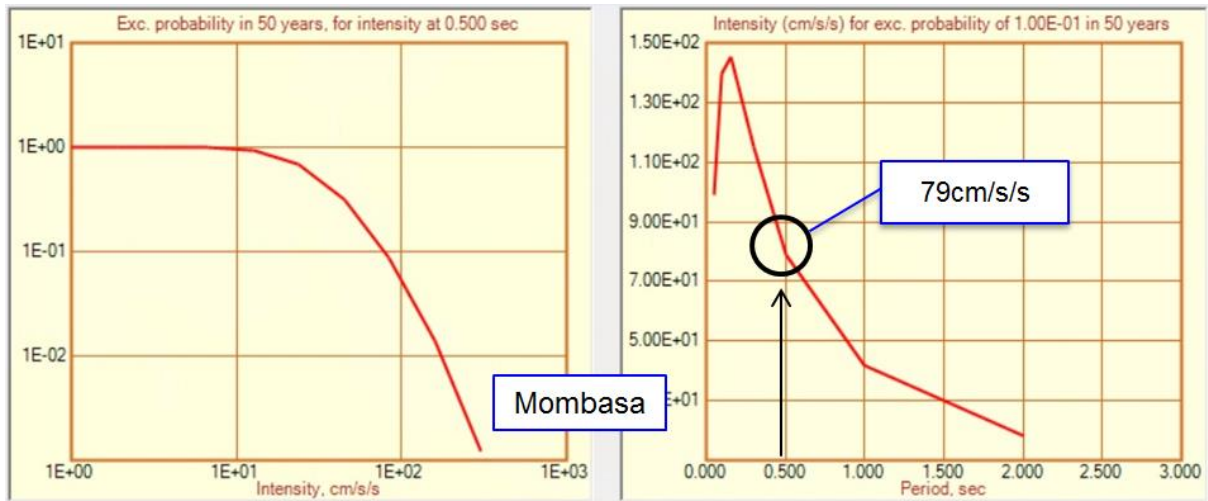


Figure 5-9 CRISIS 2015 seismic hazard curve output screen (Mombasa Island)

The seismic hazard grid data files saved during the PSHA computation were then imported to Surfer 14™ software for contour analysis..

The seismic hazard contour map generated by Surfer 14 program was then exported as an ESRI .shp file for viewing and final editing on ArcGIS Pro 2.2.3.

6 DATA ANALYSIS

6.1 EARTHQUAKE CATALOG ASSEMBLY

Instrumental natural seismicity data were retrieved from the United States Geological Survey (<https://earthquake.usgs.gov/earthquakes/search/>) and the International Seismological Center (<http://www.isc.ac.uk/iscbulletin/search/catalogue/>) validated catalogs in accordance with the established PSHA technique (Gupta, 2002; Baker, 2008; Poggi et al., 2017). Events with magnitudes less than 2.0 were considered insignificant with regards to seismic hazard (ground shaking), but still serve to illuminate geologic faults that may be still be active.

The magnitudes vary from 1.2 to 6.0, the depths from 10 km to 38 km, and the years span from 1938 to 2020. The US Geological Survey inventory covers occurrences from 1975 through 2019, although it is lacking for events smaller than M3, as seen in Fig 6-1 below. This is because the USGS established a cut-off magnitude of M3, below which occurrences are deemed insignificant.

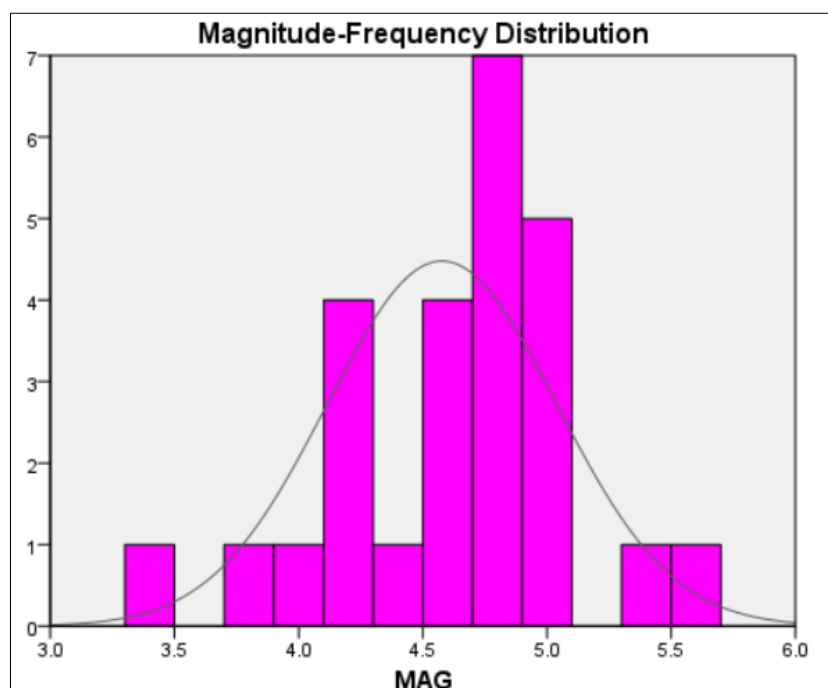


Figure 6-1 Temporal Distribution of events in the USGS catalog

On the other hand, the ISC reviewed catalog contains events from 1938 to 2018 and incorporates events with magnitudes as low as M1.3 as shown in Fig 6-2 below. The decision by the ISC not to impose a lower cut-off magnitude is appropriate for this study and particularly

the study area, which is a passive continental margin, with more small earthquakes than moderate earthquakes.

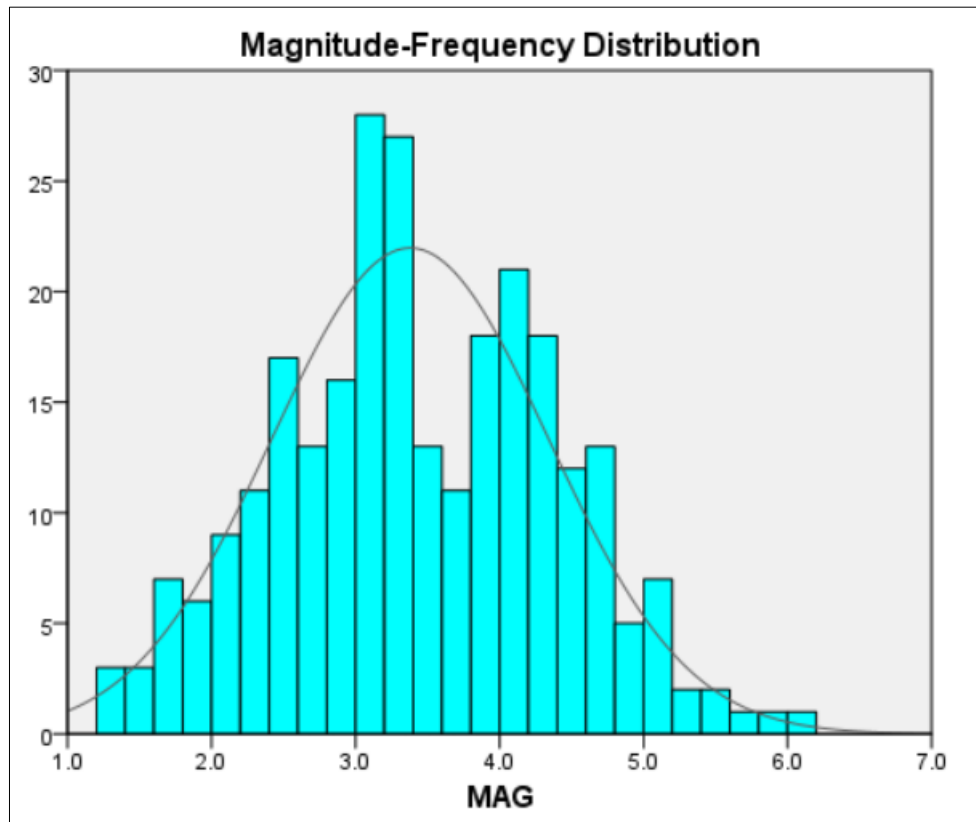


Figure 6-2 Temporal distribution of events in the ISC catalog

6.2 CATALOG COMPILATION

Because of the gap in data in the USGS catalog from 1938 to 1975, and in the ISC Catalog from 2018 to 2019, the two catalogs were combined to obtain a compiled earthquake catalog spanning from 1938 to 2019 and containing a total of 291 events from M1.3 to 6.0 as shown in Fig 6-3 below.

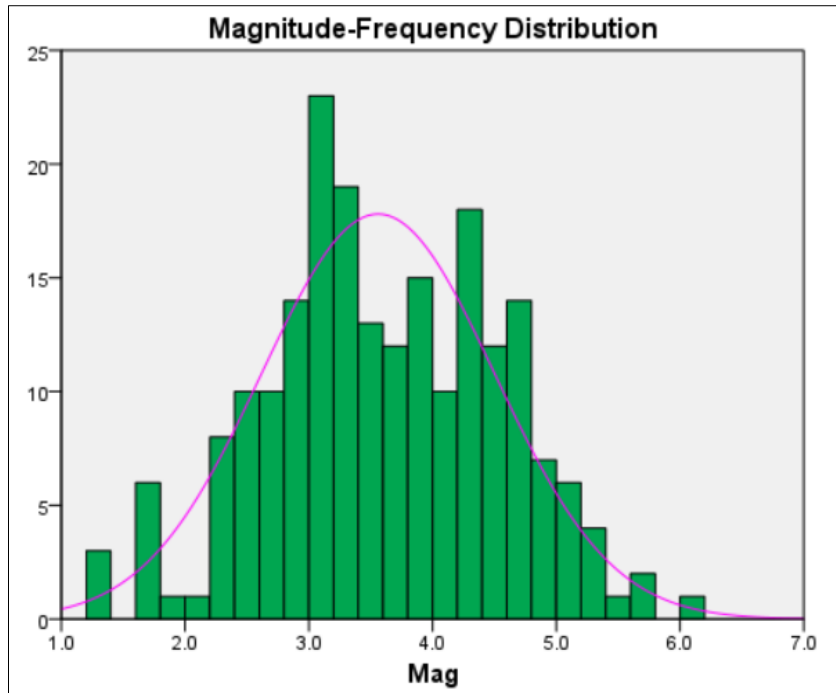


Figure 6-3 Temporal distribution of events in the combined USGS-ISC catalog

The events in the combined catalog vary in depth from 8 km to as deep as 38km, but are predominantly in the 10 to 15 Km depth range, as shown in Fig 6-4 below.

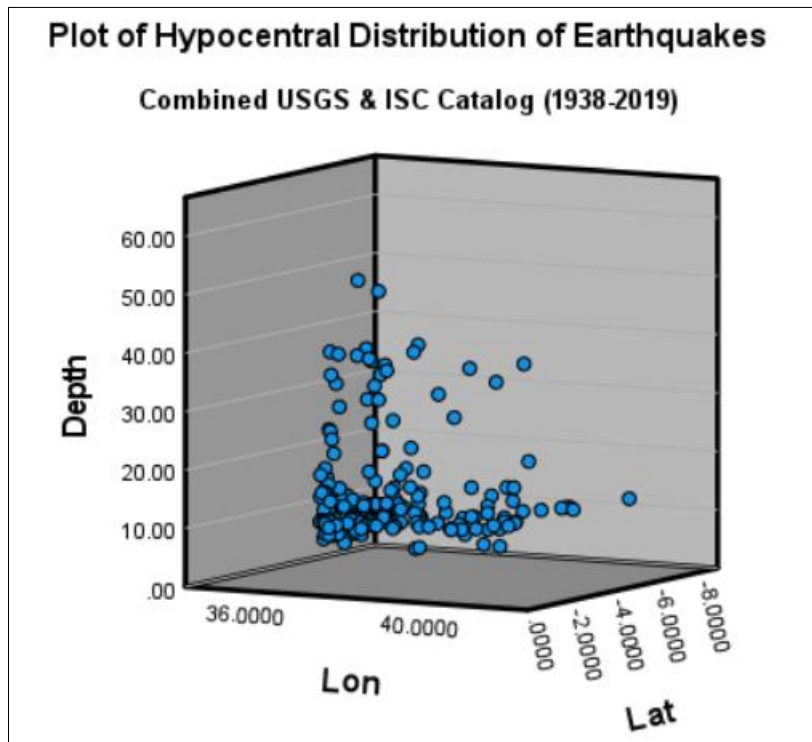


Figure 6-4 Hypocentral distribution of events in the combined USGS-ISC catalog

The result was then used to build a homogenized earthquake catalog, shown in Appendix 1 using the SPSS program by IBM.

6.3 CATALOG HOMOGENIZATION

The combined catalog, shown in Appendix 1 containing 210 earthquake events, recorded between 1938 and 2019 contained events with various magnitude scales. An objective seismicity analysis warrants that the earthquake record is represented with a uniform magnitude scale in order to avoid inconsistencies because different processing methods are used to calculate the different magnitude scales. The best homogeneous magnitude scale that can be used is the moment magnitude (M_w) scale, because it directly relates the size and energy of an earthquake and does not saturate at high magnitudes. Most events in the USGS (2019) were represented in the mb scale, unlike the ISC (2015) catalog, thus requiring conversion to a common magnitude scale.

This study employed the Akkar & Bommer (2007) and Weatherhill et al. (2016) relations, because they envelope the maximum earthquake magnitudes recorded. The following are the magnitude conversion relations:

$$M_w = 0.616M_s + 2.369 \quad \text{for } M_s < 6.0$$

$$M_w = 1.084M_b - 0.142 \quad \text{for } M_b < 6.5$$

$$M_w = 0.953M_L + 0.421 \quad \text{for } M_L < 6.8$$

$$M_w = 0.760M_d + 1.302 \quad \text{for } M_d < 6.0$$

6.4 CATALOG DECLUSTERING

This study employs the standard PSHA assumption that the rate of occurrence of earthquakes is independent of the observation time and that their probability distribution conforms to a Poissonian distribution. But earthquake catalogs do have correlated events like foreshocks and aftershocks and even earthquake swarms in volcanic areas. Such events are highly dependent spatially and temporally and have therefore to be removed through catalog filtering before performing any statistical occurrence relations. This is referred to as catalog declustering.

This study used the SEDA v1 earthquake analysis program by Anna Maria Lombardi (2017) which has embedded catalog declustering models. This tool enables the detection of background seismicity from an earthquake catalog, by employing a Time-Magnitude Relationship (TMR)TM or Time-Magnitude-Space (TMS) Epidemic Type Aftershocks

Sequence (ETAS) model. The technique involves attributing the probability pr_i^B of becoming a background event to each target event in the catalog. The algorithm then detects the background events using the calculated probability. The formulae are used by the system to determine the background probabilities pr_i^B :

$$pr_i^B = \frac{\mu}{\lambda_{TM}(T_i|H_{T_i})} \text{ and } pr_i^B = \frac{\mu \cdot u(X_i, Y_i)}{\lambda_{TMS}(T_i, X_i, Y_i|H_{T_i})}$$

for the afore-mentioned TM and TMS ETAS models.

The declustered catalog contains 210 earthquake events, recorded between 1938 and 2019..

The result is as displayed in Fig 6-5 below.

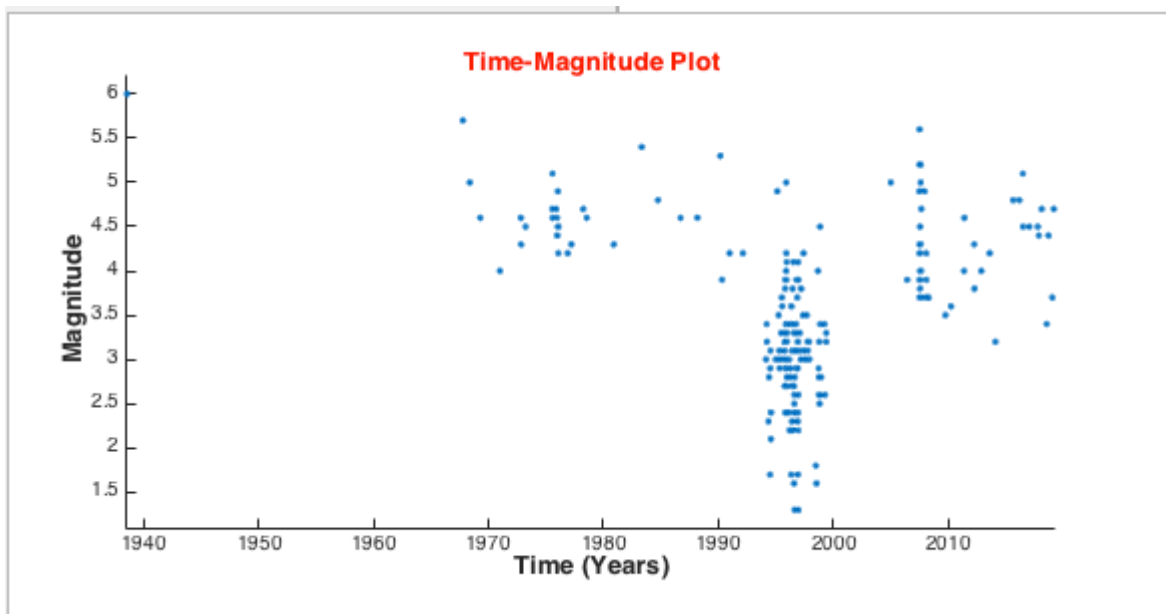


Figure 6-5 Declustered compiled earthquake catalog for the study area

The gaps observed in Fig 6-5 above can be attributed to the declustered fore- or aftershock events in the original catalog which were recorded as earthquake events.

6.5 COMPLETENESS CHECK

An earthquake catalog is considered complete if all the recorded events occurred within the temporal period of interest and are effectively reported. This is usually done through comparison of the annual frequency of occurrence of events with respect to time in regular steps of magnitude and time.

From Fig 6-5 above, it is clear that the data compiled for this study is discontinuous. This is not uncommon in Sub-Saharan Africa and can be attributed to the sparse seismic network in Kenya, particularly so in the early days. Therefore, there are more recorded events in the 1990-2010 period *vis a vis* the 1940.

6.6 MAGNITUDE-FREQUENCY RELATION

The catalog was then subjected to statistical analysis using SEDAv1.0 earthquake catalog analysis program to derive seismicity characteristics (*a*-value, *b*-value) of the earthquakes in the area, shown in Fig 6-6 below.

The *a*-value is proportional to seismicity for a given region and is an index of seismicity. Coefficient *a* can be interpreted as the seismicity value. The *b*-value is the slope of a graph depicting the number of seismic events versus their magnitudes. It is commonly referred to as the Gutenberg-Richter relationship. (Pamukcu et al., 2021)

SEDA v1.0 applies the Gutenberg-Richter Law to compute the magnitude-frequency distribution of earthquakes in a catalog. The probability density function is defined as:

$$f(m) = \beta \cdot \exp[-\beta \cdot (m - Mc)]$$

Where: $\beta = b \cdot \ln(10)$ is a factor and *Mc* is the completeness magnitude for the catalog.

The system assumes an earthquake size difference of 0.1 and applies two approaches to estimate the *b* and *Mc*:

- a) The *Mc* and *B* value Stability Method (MBS)
- b) The Goodness of Fit Test Method (GFT)

The GFT Technique is used at both 90% and 95% probabilities, as seen in Fig 6-6 below. Furthermore, SEDAv1.0 uses an earthquake size range of 0.5 to determine the *b*-value required to use the MBS approach.

The *a*-value and *b*-value are direct inputs into the “source seismicity” module of the CRISIS 2015 software, shown in Fig 6-7 below, for hazard computation.

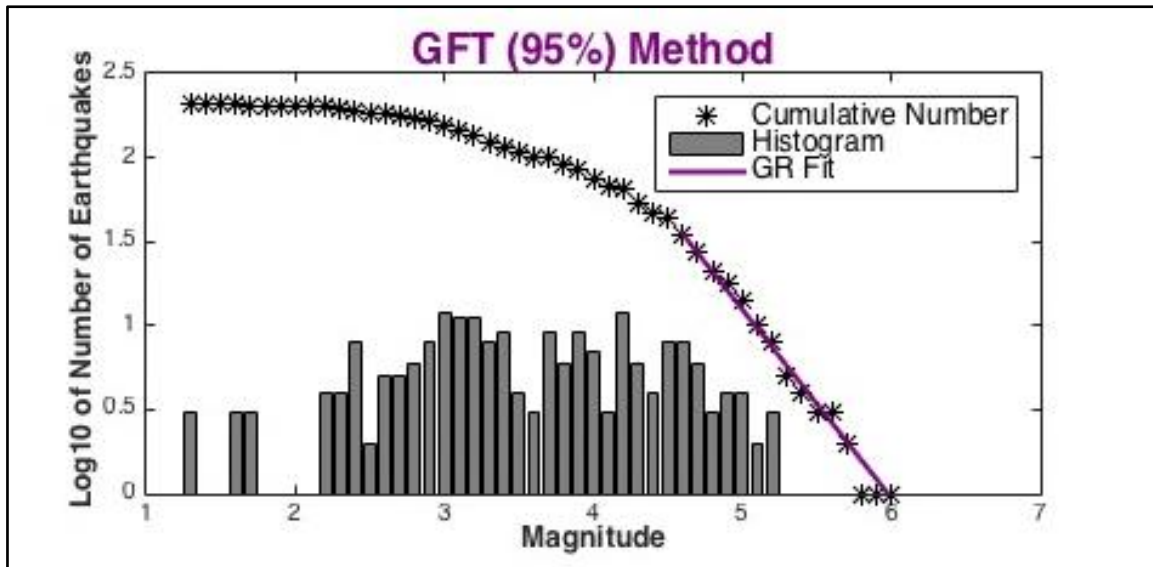


Figure 6-6 Gutenberg-Richter analysis of the earthquake catalog

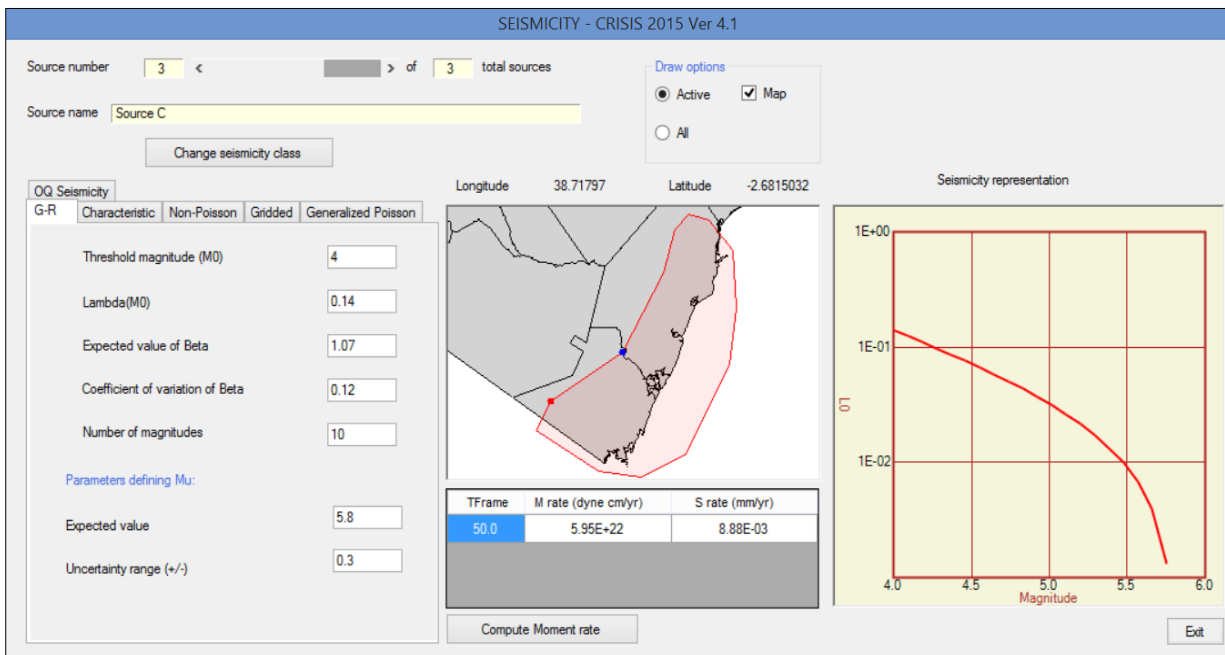


Figure 6-7 Area Source Zone Seismicity Model for Source Zone 3

6.7 CALCULATION OF HAZARD

As a first step, the dimensions and faulting characteristics of the respective earthquake source zones in the study area were estimated from an analysis of published geological maps, the distribution of seismicity and confirmed through field observation. These were then translated onto CRISIS 2015 v4.1.

The Gutenberg-Richter magnitude-frequency relations of these earthquake source zones was calculated from statistical analysis of the combined earthquake catalog using Statistical Earthquake Data Analysis (SEDA) v1.0 computer programme.

The attenuation relation (ground motion prediction equation) adopted in this study is Abrahamson & Silva (1997) and was selected from the list of GMPEs embedded within CRISIS-2015™ software, shown in Figure 6-8 below. This GMPE was selected because it applies to shallow crustal earthquakes worldwide, and has parameters for ground acceleration, spectral range, magnitude range and tectonic regime that are suitable to the study area.

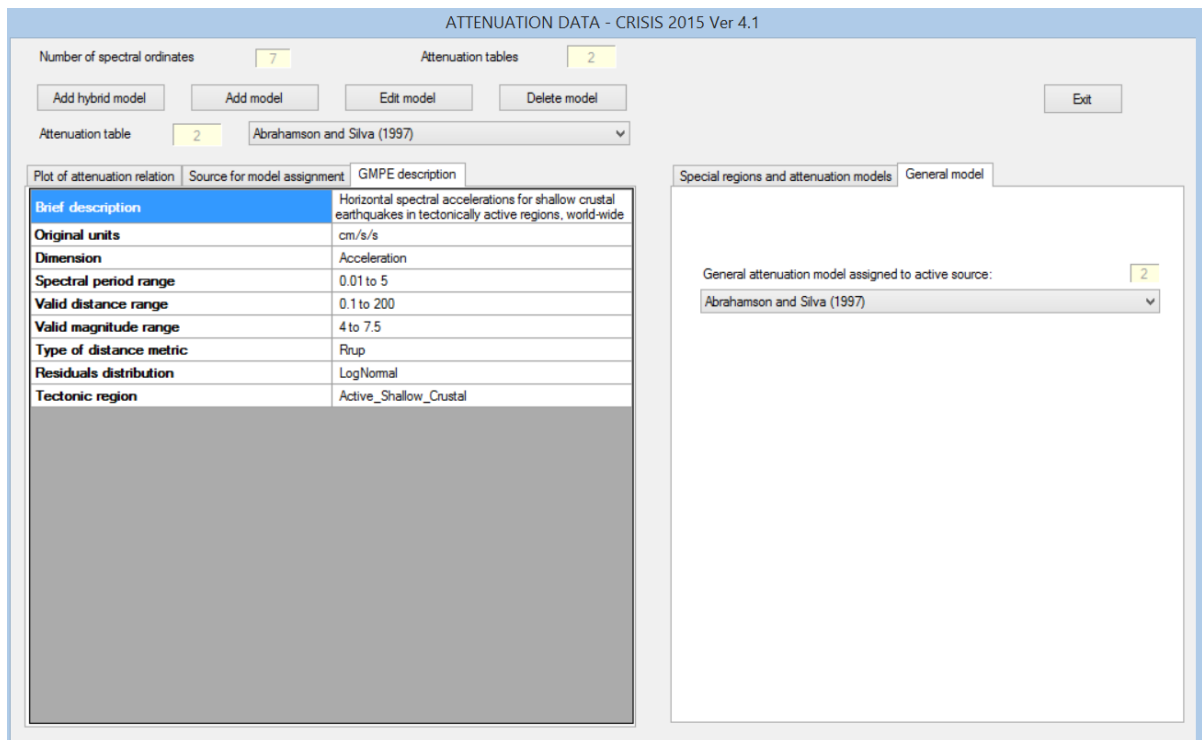


Figure 6-8 GMPE Description for Abrahamson & Silva (1997)

Ground accelerations in the study area were calculated in units of cm/s/s, for return periods of 25, 50, 100, 150 and 200 years. The period in consideration was conservatively fixed at 50 years (6.32E-01), as shown in Fig 6-9 below.

GLOBAL PARAMETERS - CRISIS 2015 Ver 4.1

Integration parameters

Maximum integration distance: km

Minimum triangle size: km

Minimum Distance/Triangle Size ratio:

CAV filter

None

Time frame	Map return period (years)	PE in 50 years
50	25	8.65E-01
	50	6.32E-01
	100	3.93E-01
	150	2.83E-01
	200	2.21E-01

Figure 6-9 Return Periods and Time Frame input screen

The maximum earthquake ground shaking was calculated considering periods of 0.05, 0.1, 0.15, 0.3, 0.5, 1.0 and 2.0 seconds, as shown in Fig 6-10 below.

INTENSITIES FOR EACH SPECTRAL ORDINATE - CRISIS 20...

Spectral ordinates

Total number of spectral ordinates:

Actual spectral ordinate:

Structural period of actual spectral ordinate:

Lower limit of intensity level:

Upper limit of intensity level:

Spacing

Log Linear PEER Large PEER

General values

Units:

Number of levels of intensity for which seismic hazard will be computed:

Figure 6-10 Spectral acceleration frequencies input window

6.8 HAZARD CURVES & SPECTRA

Following that, the earthquake hazard profiles for all major the towns in the area were retrieved, as shown in Fig 6-11 below. This was accomplished by selecting the locations of each of the towns on the PGA map resulting from the PSHA computation.

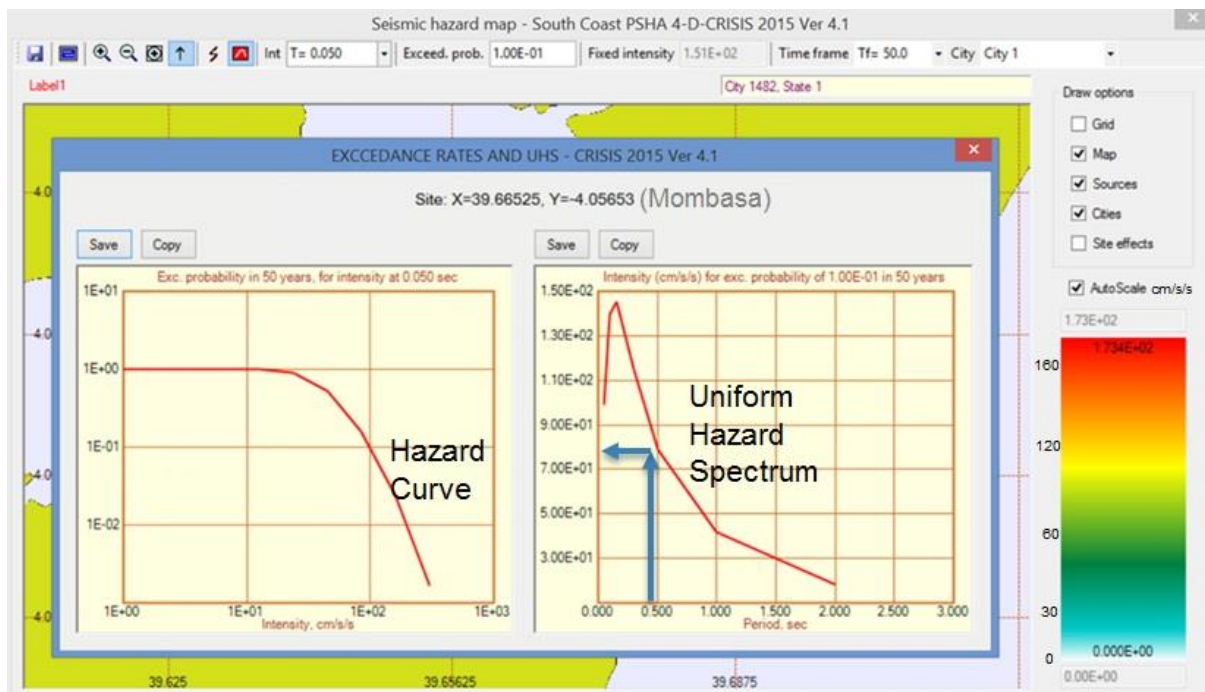


Figure 6-11 Seismic hazard curves output window

6.9 MAPPING OF HAZARD

CRISIS-2015TM seismic hazard results were transferred to Surfer 14TM program and contour analysis was performed.

The results were imported into ArcGIS ProTM 2.3.3 and an updated earthquake hazard map of the area developed.

7 RESULTS

7.1 SEISMIC SOURCES

The field ground truthing visits confirmed that the geologic faults in the study area are predominantly normal faults, albeit with a component of shearing. They are mostly buried under Recent sediments, except in a few cases where they are exposed by river valleys.

The surface manifestations of these faults are mostly benign and include aligned sag ponds, elbow bends on rivers, numerous aligned river rapids and geothermal hot springs. These surficial manifestations are well aligned to the general strike of geological faults mapped on published geological maps of the study area, which in north-east to south-west.

A plot of the earthquake epicenters for events from M1.2- 6.0, from 1938 to 2019 in a compiled earthquake catalog derived from the ISC (2018) and USGS (2019) websites reveals the earthquake epicenters are not located directly above the mapped geologic faults. This is not unusual, given that these may be normal faults with steep dip angles, so that the epicenters of earthquakes generated by their movement are horizontally off-set from the surface trace of the fault itself, by several Km.

7.1.1 AREA SEISMIC SOURCE ZONE MODEL (ASZ)

The earthquakes in the study area occur in a diffuse pattern, within a 100 Km N-S trending corridor starting from southern Kwale to northern Malindi, both on-shore and offshore. This follows the trend of the southern boundary faults of the Tertiary Lamu Embayment.

The earthquakes in the Manyara Rift area of the Northern Tanzania Divergence Zone (NTDZ) of the Gregory Rift system, south of the Study Area occur in a curvilinear NW-SE trending corridor, in line with the active faults of the Manyara Rift.

Similarly, the earthquakes in the Chyulu Hills-Wundanyi-Voi area, west of the Study Area occur in a curvilinear NNW-SSE trending corridor, a similar trend to that of the Aswa Shear Zone (Katumwehe et al., 2015). These earthquakes may result from stress transfer from the Juvenile Northern Tanzania Divergence Zone or may be volcano-seismic, resulting from the passive volcanism of Chyulu hills.

In view of the aforementioned, the Area Source Zone (ASZ) Model approach was applied to the delineation of the seismic sources. Each of the earthquake areal sources, as indicated in Fig 7-1 below, is considered to have an equal likelihood of seismicity inside its boundaries.

The depth of each area source zone was conservatively estimated from the focal depths of the deepest earthquakes recorded within each Area Source Zone.

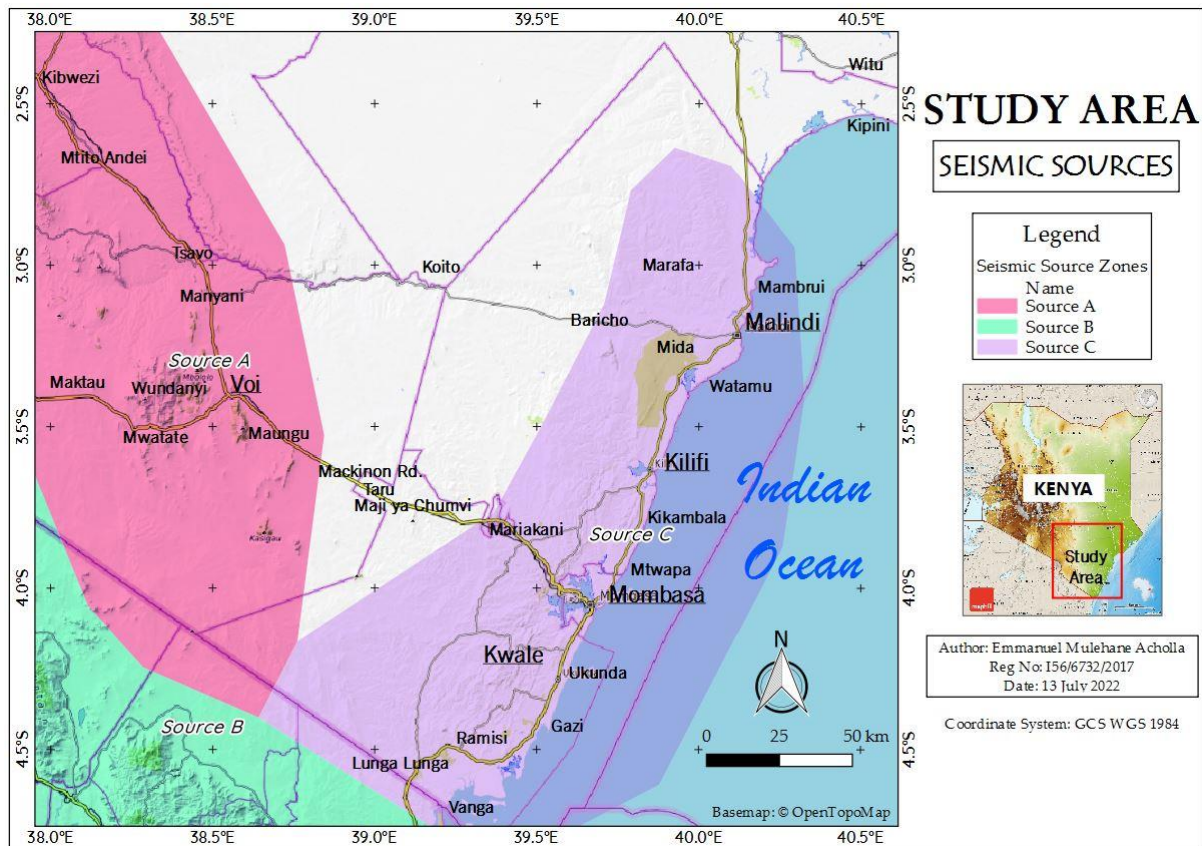


Figure 7-1 Seismic Area Sources Zones (ASZ's) in the Study Area

7.2 SEISMIC HAZARD

Maximum horizontal earthquake shaking (PGA) for the counties in the area was calculated with a 10% likelihood of exceedance in 50 years, leading to a recurrence interval of 475 years. Specifically, PGA values were derived for major towns in the study area like Malindi, Watamu, Kilifi, Mombasa, Voi, Kwale, Ukunda and Vanga towns. The results are displayed in Table 7-1 below.

Table 7-1 Peak Ground Accelerations for major towns in the Study Area

TOWN	Peak Ground Accelerations in cm/s/s for fixed Spectral Frequencies						
	0.05s	0.1s	0.15s	0.3s	0.5s	1.0s	2s
Malindi	91.94	126.70	130.40	102.80	68.47	35.81	15.66
Watamu	95.49	133.00	137.40	108.10	72.75	38.13	16.57
Kilifi	97.54	136.80	141.90	122.00	76.51	40.48	17.60
Mombasa	98.99	139.60	145.10	115.10	79.14	42.14	18.34
Voi	106.5	154.9	143.8	96.98	59.08	29.20	12.91
Kwale	99.18	140.00	145.50	115.40	79.43	42.34	18.44
Ukunda	99.24	140.10	145.60	115.50	79.43	42.29	18.40
Vanga	124.60	178.00	178.70	1342.00	88.55	45.41	19.02

Malindi town on the northern end of the study area has PGA values ranging from as low as 15.6 cm/s/s at structural period T=2s to 130.4 cm/s/s at T=0.15s. Watamu town, south of Malindi has PGA values ranging from as low as 16.57cm/s/s at T=2s to 137.4 cm/s/s at T=0.15s. Kilifi town has PGA values ranging from as low as 17.6 cm/s/s at T=2s to 141.9cm/s/s at T=0.15s.

Mombasa city has PGA values ranging from 18.34 cm/s/s at T=2s to 145.1cm/s/s at T=0.15s. Voi town has PGA values ranging from 12.91cm/s/s at T=2s to 154.9cm/s/s at T=0.1s. Kwale town has PGA values ranging from 18.44cm/s/s at T=2s to 145.5cm/s/s at T=0.15s. Ukunda town has PGA values ranging from 18.4cm/s/s at T=0.2s to 145.6cm/s/s at T=0.15s. Vanga town, the southernmost town in the Study Area, has PGA values ranging from 19.02 cm/s/s at T=2s to 1342 cm/s/s at T=0.3s. This is the highest ground acceleration in the entire study area.

From Table 7-1, it is clear that the lowest ground accelerations are expected at spectral frequency T=2 seconds. The highest expected ground accelerations are expected for spectral frequency T=0.15 seconds and 0.3 seconds. The structural period of T=0.5 seconds was selected for extracting seismic hazard curves because it is a representative median.

7.2.1 SPECTRUM-DEPENDENT HAZARD

The seismic hazard grid data files for each structural period ($T=0.05, 0.1, 0.15, 0.3, 0.5, 1.0$ and 2.0 seconds) were then used to design seismic hazard maps for each structural period, using ArcGIS Pro 2.2.5 in terms of peak ground acceleration (PGA) for a 10% probability of exceedance in 50 years. These are detailed below:

7.2.1.1 PGA at $T=0.05$ seconds

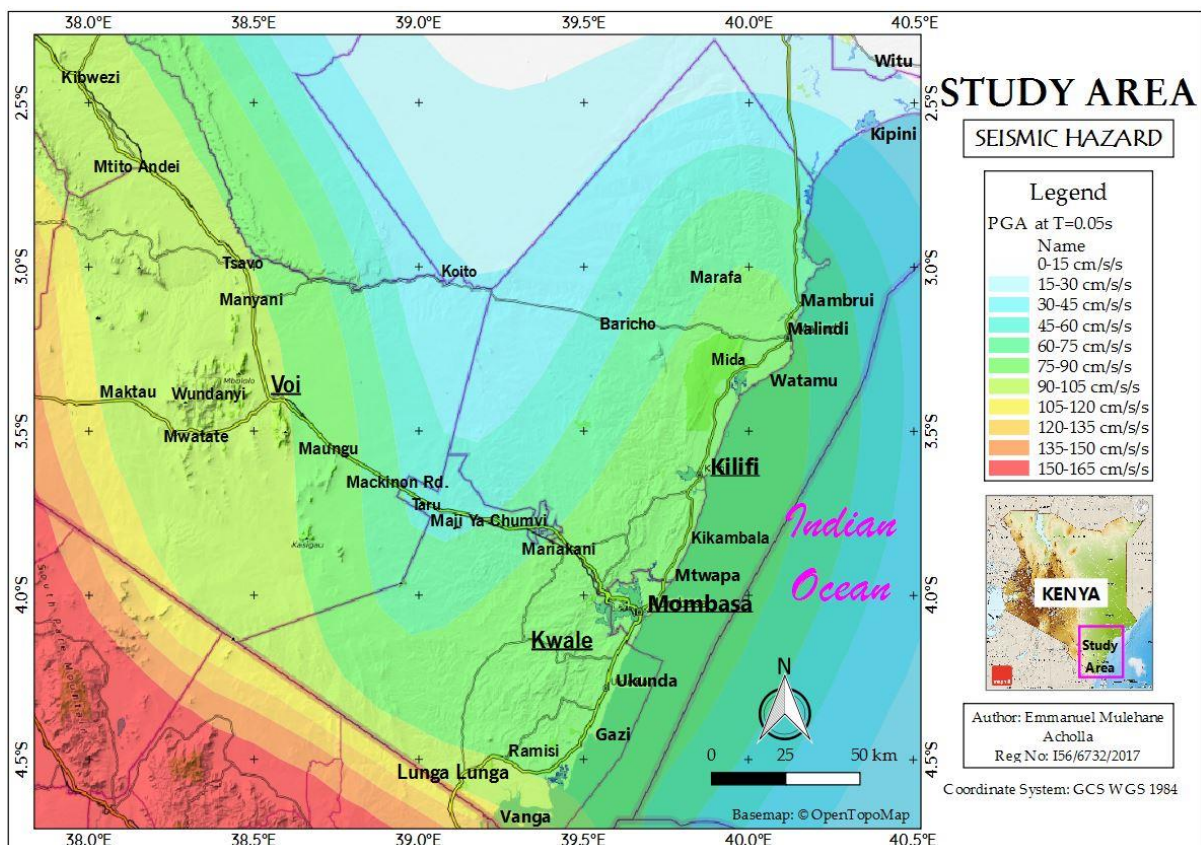


Figure 7-2 Ground accelerations in the study area at a 0.05s structural period

The preceding map shows that for a given structural duration of $T=0.05s$, the highest seismic hazard is expected at Vanga town in southern Kwale County, at 105-120 cm/s/s, followed by Voi at 90-105 cm/s/s. Ukunda, Mombasa City, Kilifi, Kwale, Malindi and Vanga towns all have the least expected seismic hazard ranging between 90-105 cm/s/s.

Therefore, earthquakes with short periods ($T=0.05s$) have the potential to cause the greatest damage in the Study Area, due to the associated high peak ground acceleration (PGA).

7.2.1.2 PGA at T=0.1seconds

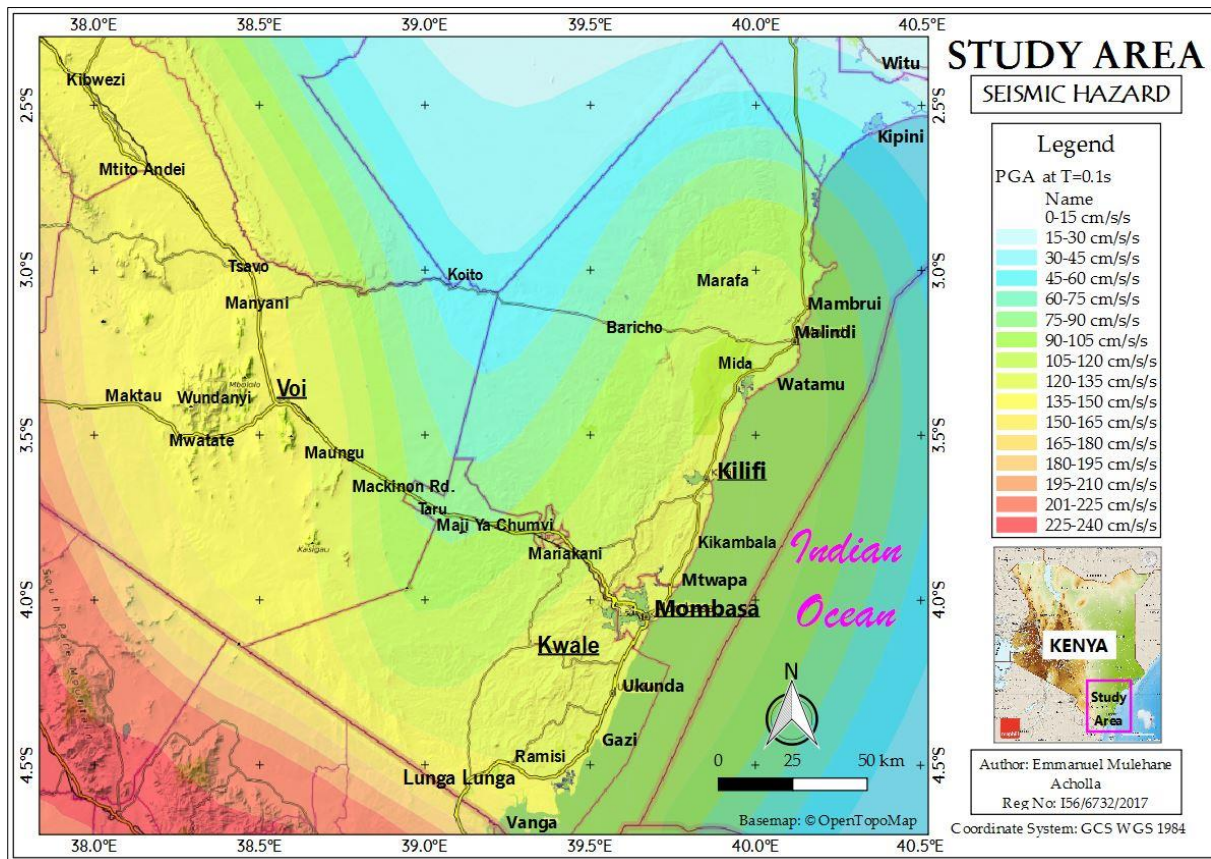


Figure 7-3 Ground accelerations in the study area at 0.1s structural period

The preceding map shows that for a given structural duration of $T=0.1s$, the highest seismic hazard is expected at Vanga town in southern Kwale County, at 165-180 cm/s/s, followed by Voi at 150-165 cm/s/s. Ukunda, Mombasa City, Kilifi and Kwale towns have an expected seismic hazard of 135-150 cm/s/s. Malindi and Ukunda towns have the least expected seismic hazard ranging between 120-135 cm/s/s.

Therefore, earthquakes with short periods ($T=0.1s$) have the potential to cause considerable damage in the Study Area, due to the associated high peak ground acceleration (PGA).

7.2.1.3 PGA at T=0.15 seconds

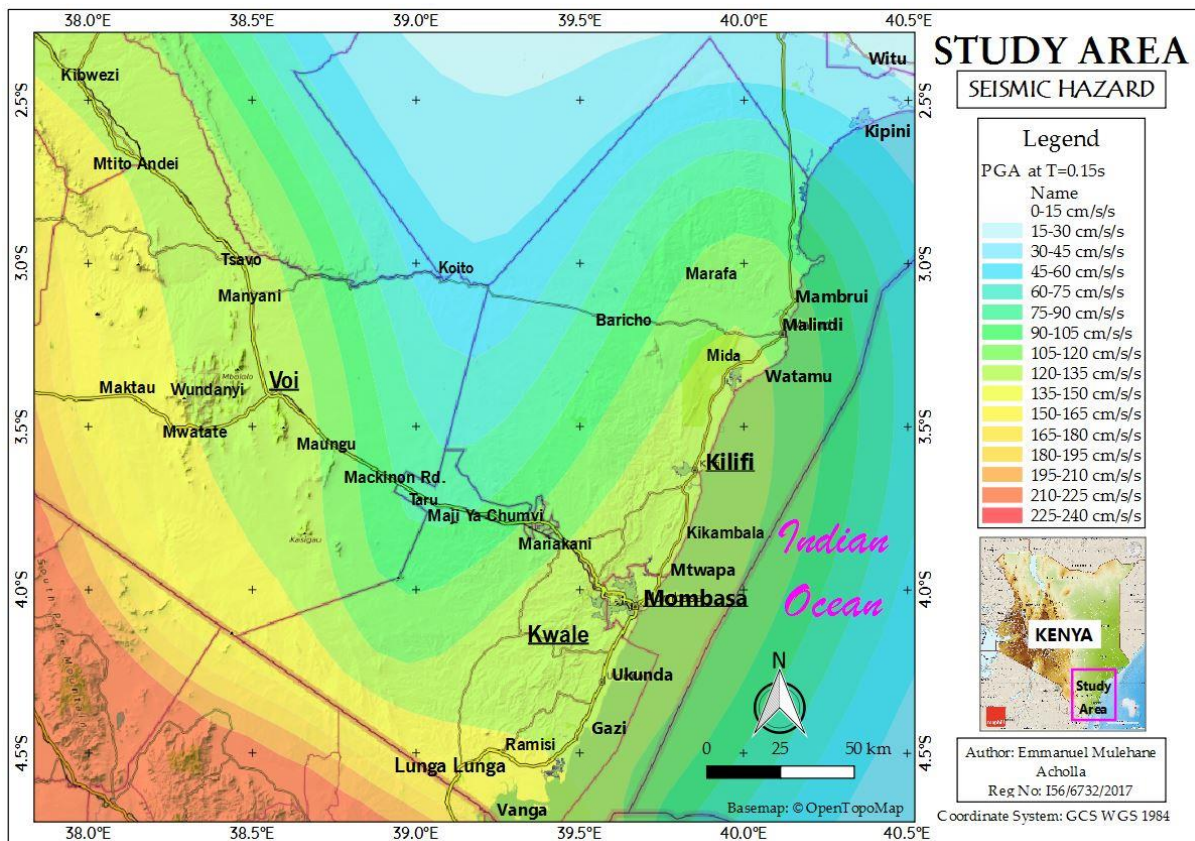


Figure 7-4 Ground accelerations in the study area at a 0.15s structural period

The preceding map shows that for a given structural duration of $T=0.15s$, the highest seismic hazard is expected at Vanga town in southern Kwale County, at 195-210 cm/s/s, followed by Voi at 180-195 cm/s/s. Ukunda, Mombasa City, Kwale, Kilifi and Ukunda towns have an expected seismic hazard of 165-180 cm/s/s. Malindi town has the least expected seismic hazard ranging between 150-165 cm/s/s.

Therefore, earthquakes with short-medium periods ($T=0.15s$) have the potential to cause appreciable damage in the Study Area, due to the associated moderate peak ground acceleration (PGA).

7.2.1.4 PGA at T=0.3 seconds

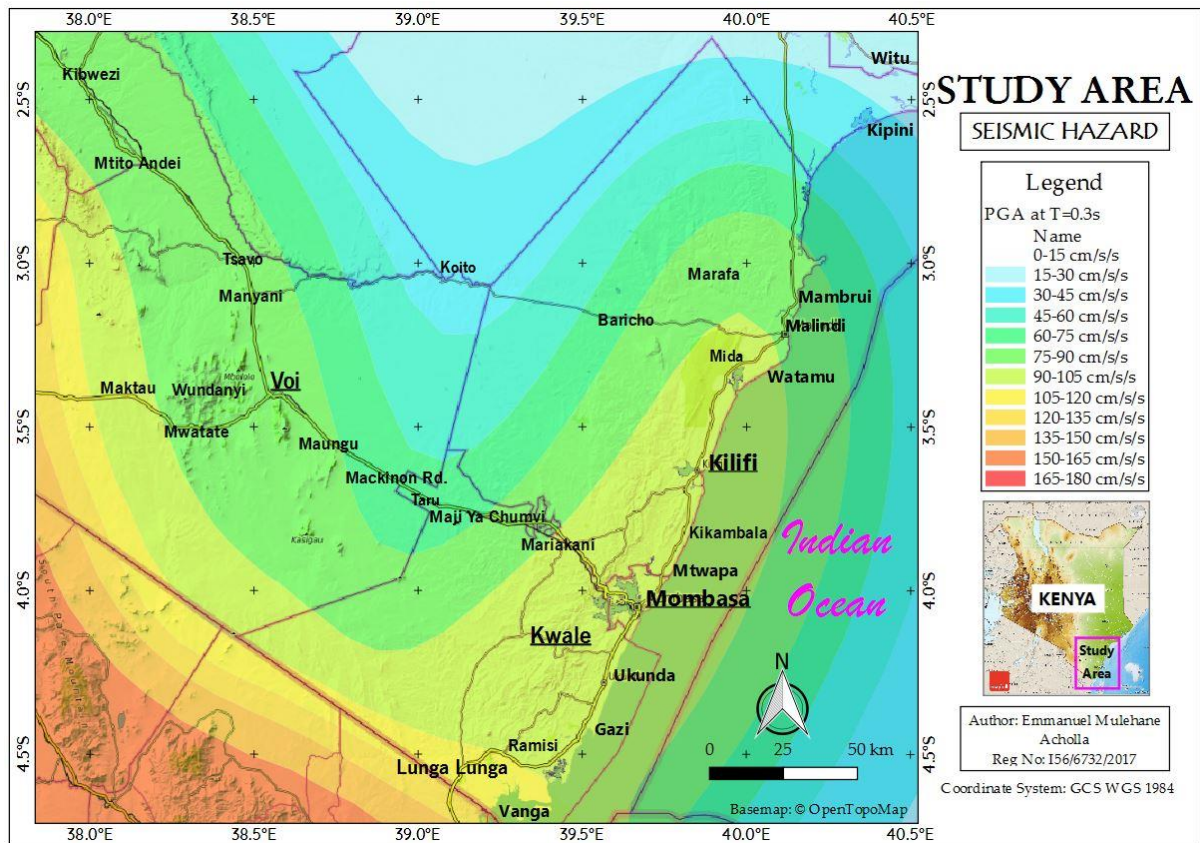


Figure 7-5 Ground accelerations in the study area at a 0.3s structural period

The preceding map shows that for a given structural duration of $T=0.3s$, the highest seismic hazard is expected at Vanga town in southern Kwale County, at 120-135 cm/s/s. Ukunda, Mombasa City, Kwale, Kilifi and Ukunda towns have an expected seismic hazard of 105-120 cm/s/s. Malindi and Voi towns have the least expected seismic hazard ranging between 90-105 cm/s/s.

Therefore, earthquakes with medium periods ($T=0.3s$) have the potential to cause appreciable damage in the Study Area, due to the associated moderate peak ground acceleration (PGA).

7.2.1.5 PGA at T=0.5 seconds

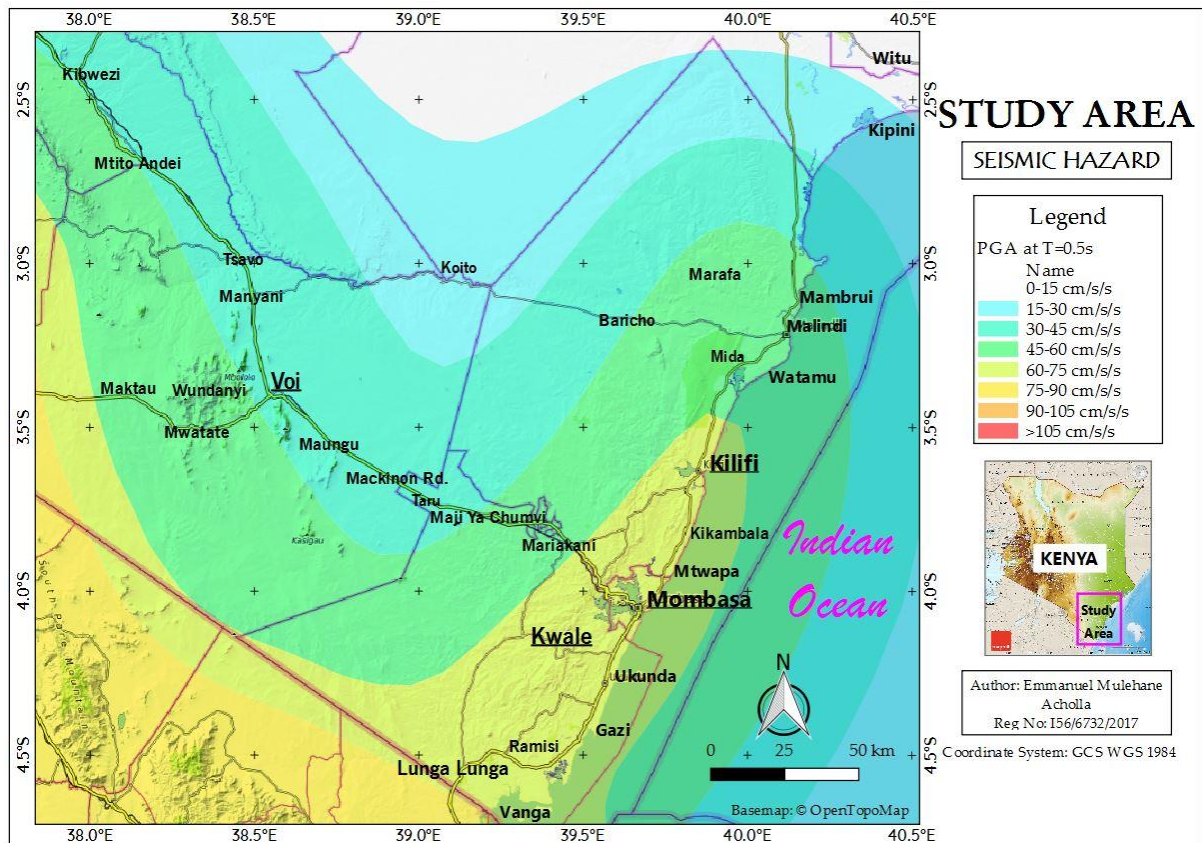


Figure 7-6 Ground accelerations in the study area at a 0.5s structural period

The preceding map shows that for a given structural duration of $T=0.5s$, the highest seismic hazard is expected at Vanga, Ukunda, Kwale, Mombasa City and Kilifi towns, at 90-105 cm/s/s. Voi town has the least expected seismic hazard ranging between 45-60 cm/s/s.

Therefore, earthquakes with medium-long periods ($T=0.5s$) have the potential to cause appreciable damage in the Study Area, due to the associated moderate peak ground acceleration (PGA).

7.2.1.6 PGA at T=1.0 seconds

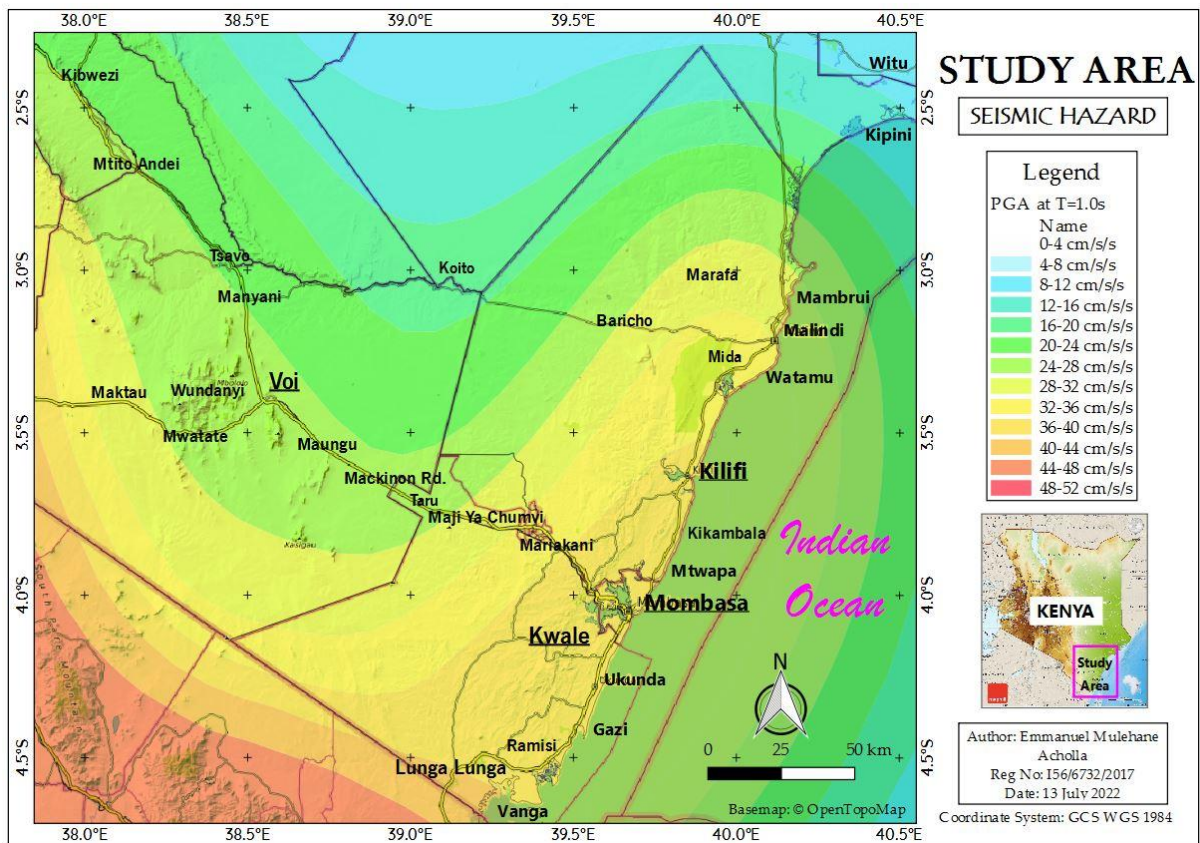


Figure 7-7 Ground accelerations in the study area at a 1s structural period

The preceding map shows that for a given structural duration of $T=1.0s$, the highest seismic hazard is expected at Vanga town in Southern Kwale County, at 44-49 cm/s/s. Ukunda, Kwale, Mombasa City, Kilifi and Watamu towns have an expected seismic hazard of 36-40 cm/s/s. Voi town has the least expected seismic hazard ranging between 28-32 cm/s/s.

Therefore, earthquakes with long periods ($T=1s$) have the potential to cause minor damage in the Study Area, due to the associated low peak ground acceleration (PGA).

7.2.1.7 PGA at T=2.0 seconds

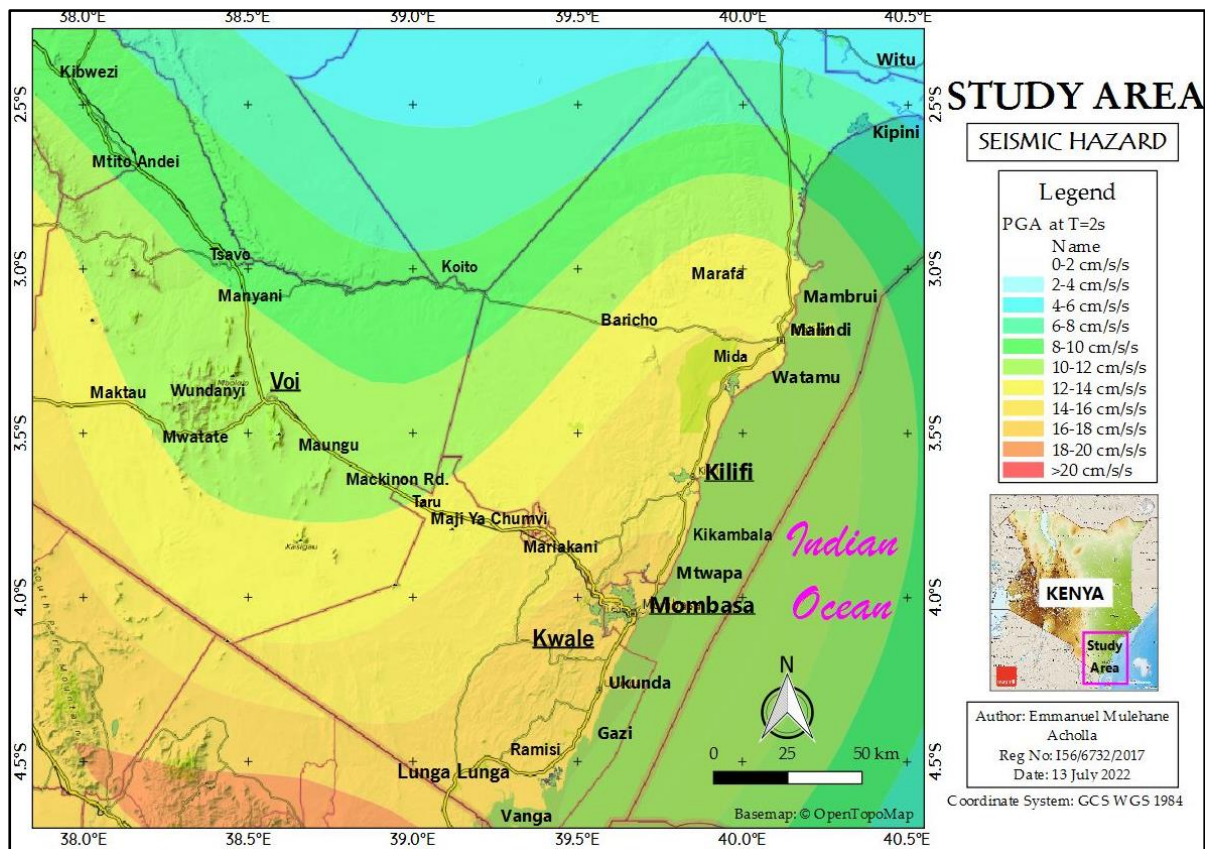


Figure 7-8 Ground accelerations in the study area at a 2s structural period

The preceding map shows that for a given structural duration of $T=2.0s$, the highest seismic hazard is expected at Vanga, Ukunda, Kwale town and Mombasa City, at 18-20 cm/s/s. At Kilifi and Watamu towns, the expected hazard is 16-18 cm/s/s. Voi town has the least expected seismic hazard ranging between 10-12 cm/s/s.

Therefore, earthquakes with long periods ($T>2s$) have the potential to cause the least damage in the Study Area, due to the associated very low peak ground accelerations (PGA).

7.2.2 UPDATED SEISMIC HAZARD MAP

The CRISIS 2015 software results for seismic hazard calculation were transferred to ArcGIS Pro 2.3.3 software and utilized to build an earthquake hazard map of the area, as shown in Fig 7-17 below, for a 10% exceedance chance in 50 years.

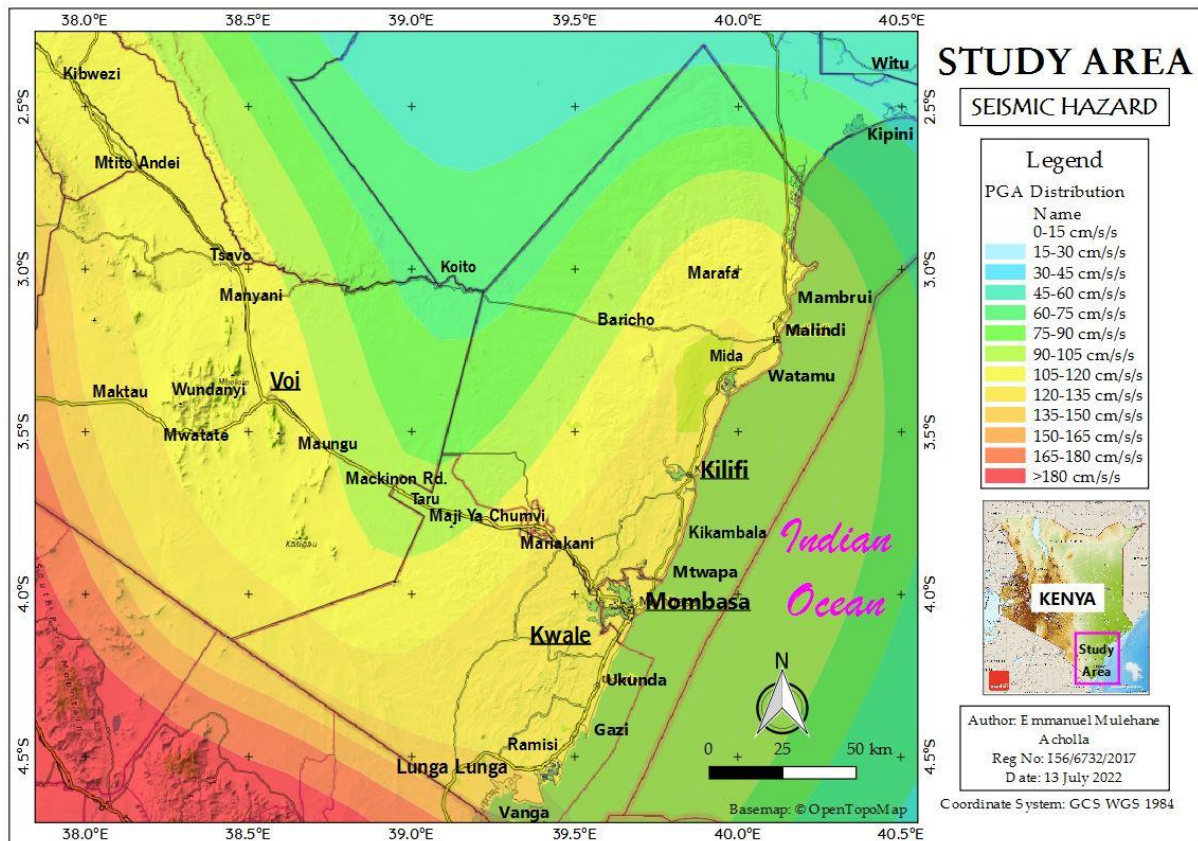


Figure 7-9 Seismic hazard map of the study area for a 10% Probability of Exceedance in 50 years

The preceding map shows that the lowest seismic hazard is expected in the northernmost part of Kilifi County, near Kipini town, at 15-30 cm/s/s. At Malindi Town, the expected hazard is 60-75 cm/s/s, similar to Voi town.

Kilifi town, Mombasa City, Ukunda, Kwale and Vanga towns all have an expected hazard ranging between 75-90 cm/s/s, with Vanga town having the highest, while Kilifi has the lowest of the three.

It should be noted, however that the areas depicted as having a low seismic hazard, such as Malindi town, may still experience moderate earthquakes in the near-distant future, which may cause damage.

7.3 HAZARD CURVES AND SPECTRA

Seismic hazard curves are a graphical representation of the probability of exceedance versus the calculated ground motion acceleration with a specified structural frequency and a fixed time frame. They allow the derivation of peak ground accelerations at specific towns with the associated range of probability.

Uniform Hazards Spectra (UHS) are a graphical representation of the peak ground motion acceleration versus the structural periods. They allow the derivation of the structural periods corresponding to the highest ground motion intensity level. This is critical for dynamic seismic assessment of civil engineering structures, whose structural UHS curve should plot within the site UHS curve.

In this study, graphs of earthquake hazard were derived for Malindi, Watamu, Kilifi, Mombasa, Kwale, Ukunda and Vanga towns for a 50-year time frame and for structural periods of $T=0.5s$. The uniform hazard spectra (UHS) are derived for a fixed probability of exceedance in 50 years for structural periods of 0.05s, 0.1s, 0.15s, 0.3s, 0.5s, 1.0s and 2.0s.

7.3.1 MALINDI

The highest probability of exceedance for Malindi town was observed at $1E+00$ (1 cm/s/s), while the lowest exceedance probability corresponds to $1E+02$ (100 cm/s/s) as shown in Fig 7-10 below. The highest ground motion intensity level was observed at structural period $T=0.05s$, while the lowest ground motion intensity level was observed at structural period $T=2.0s$.

Therefore, earthquakes with short periods ($T=0.05s$) have the potential to cause the greatest damage at Malindi town, due to the associated high PGA (130 cm/s/s), in contrast to earthquakes with longer periods ($T=2.0s$).

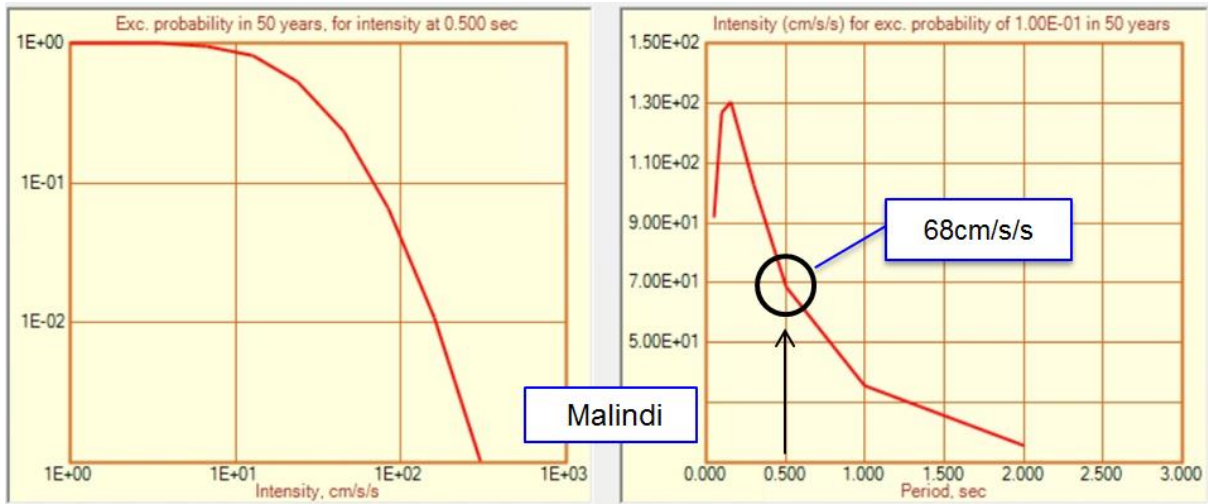


Figure 7-10 Seismic hazard curve & UHS for Malindi for 5% in 50-year PGA at T=0.5s

7.3.2 WATAMU

The highest probability of exceedance for Watamu town was observed at 1E+00 (1 cm/s/s), while the lowest exceedance probability corresponds to 1E+02 (100 cm/s/s) as shown in Fig 7-11 below. The highest ground motion intensity level was observed at structural period T=0.05s, while the lowest ground motion intensity level was observed at structural period T=2.0s.

Therefore, earthquakes with short periods (T=0.05s) have the potential to cause the greatest damage at Watamu town, due to the associated high PGA (138 cm/s/s), in contrast to earthquakes with longer periods (T=2.0s).

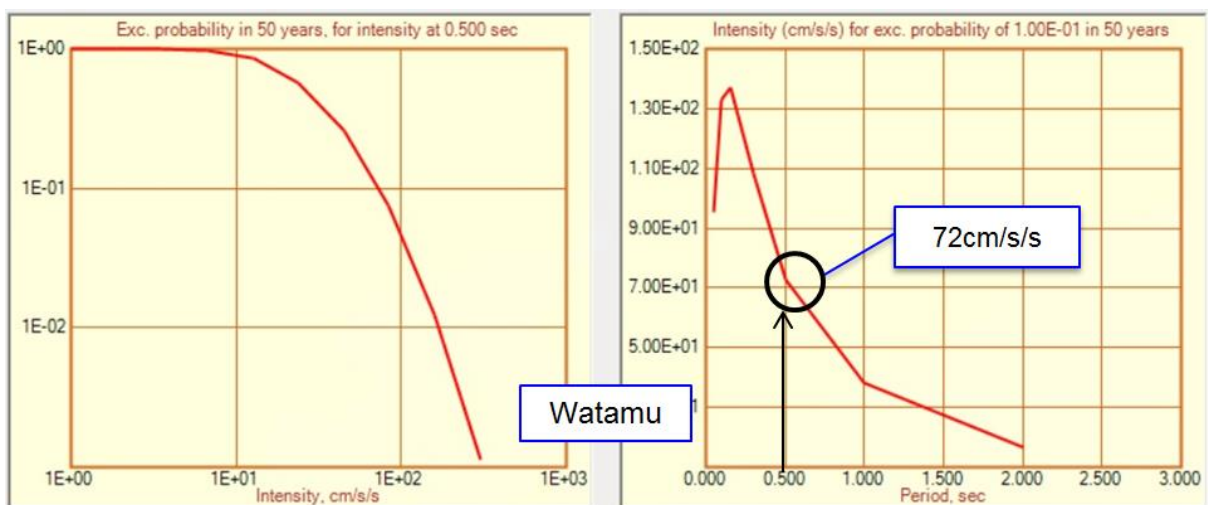


Figure 7-11 Seismic hazard curve & UHS for Watamu for a 5% in 50 year PGA at T=0.5s

7.3.3 KILIFI

The highest probability of exceedance for Kilifi town was observed at 1E+00 (1 cm/s/s), while the lowest exceedance probability corresponds to 1E+02 (100 cm/s/s) as shown in Fig 7-12 below. The highest ground motion intensity level was observed at structural period T=0.05s, while the lowest ground motion intensity level was observed at structural period T=2.0s.

Therefore, earthquakes with short periods (T=0.05s) have the potential to cause the greatest damage at Kilifi town, due to the associated high PGA (138 cm/s/s), in contrast to earthquakes with longer periods (T=2.0s).

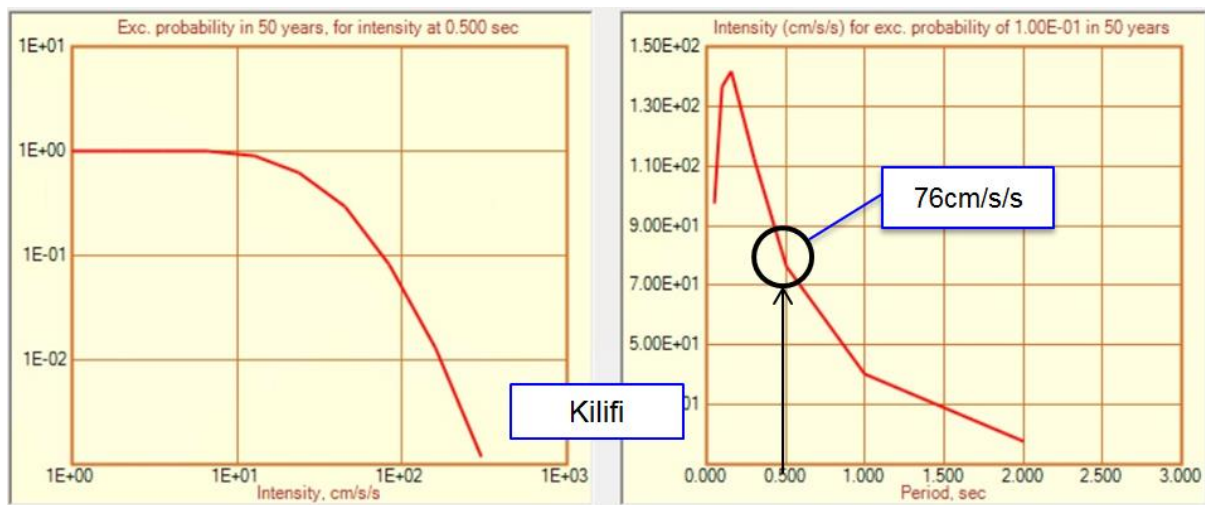


Figure 7-12 Seismic hazard curve and UHS for Kilifi for a 5% in 50 year PGA at T=0.5s

7.3.4 MOMBASA

The highest probability of exceedance for Mombasa City was observed at 1E+00 (1 cm/s/s), while the lowest exceedance probability corresponds to 1E+02 (100 cm/s/s) as shown in Fig 7-13 below. The highest ground motion intensity level was observed at structural period T=0.05s, while the lowest ground motion intensity level was observed at structural period T=2.0s.

Therefore, earthquakes with short periods (T=0.05s) have the potential to cause the greatest damage at Mombasa City, due to the associated high PGA (145 cm/s/s), in contrast to earthquakes with longer periods (T=2.0s).

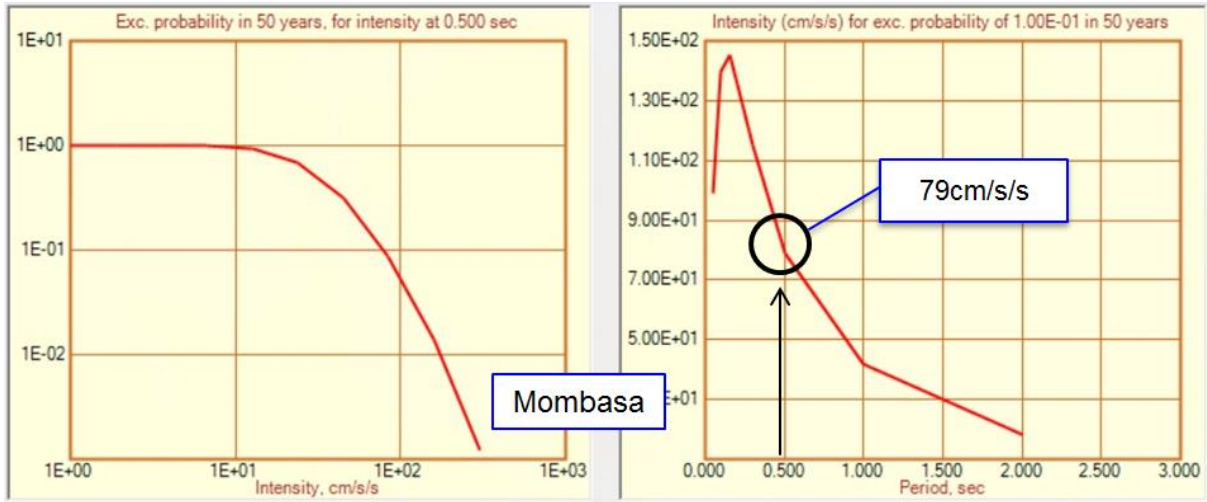


Figure 7-13 Seismic hazard curve & UHS for Mombasa for a 5% in 50 year PGA at T=0.5s

7.3.5 VOI

The highest probability of exceedance for Voi town was observed at 1E+00 (1 cm/s/s), while the lowest exceedance probability corresponds to 1E+02 (100 cm/s/s) as shown in Fig 7-13 below. The highest ground motion intensity level was observed at structural period T=0.05s, while the lowest ground motion intensity level was observed at structural period T=2.0s.

Therefore, earthquakes with short periods (T=0.05s) have the potential to cause the greatest damage at Mombasa City, due to the associated high PGA (145 cm/s/s), in contrast to earthquakes with longer periods (T=2.0s).

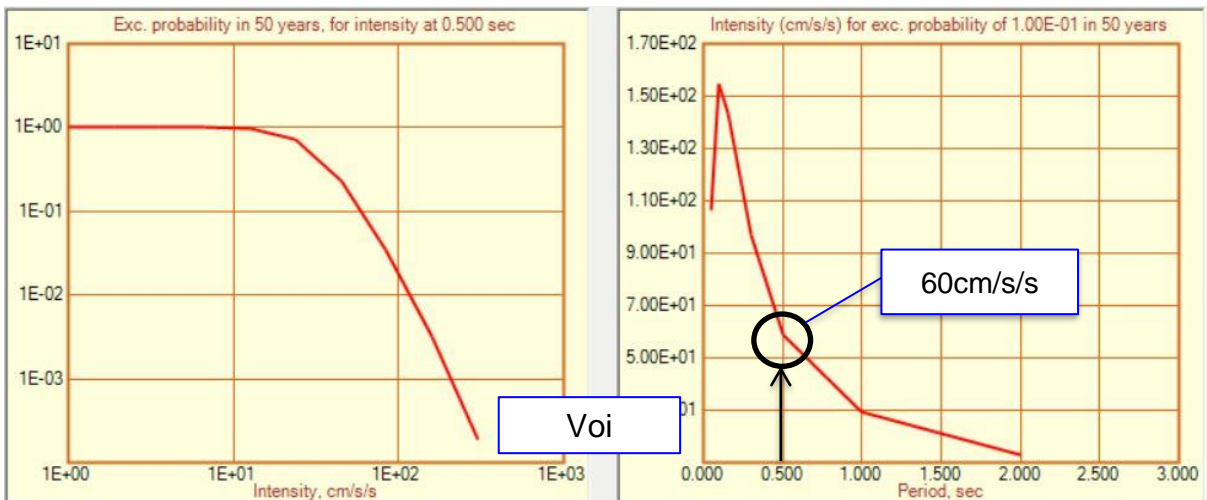


Figure 7-14 Seismic hazard curve & UHS for Voi for a 5% in 50 year PGA at T=0.5s

7.3.6 KWALE

The highest probability of exceedance for Kwale town was observed at 1E+00 (1 cm/s/s), while the lowest exceedance probability corresponds to 1E+02 (100 cm/s/s) as shown in Fig 7-14 below. The highest ground motion intensity level was observed at structural period T=0.05s, while the lowest ground motion intensity level was observed at structural period T=2.0s.

Therefore, earthquakes with short periods (T=0.05s) have the potential to cause the greatest damage at Kwale Town, due to the associated high PGA (148 cm/s/s), in contrast to earthquakes with longer periods (T=2.0s).

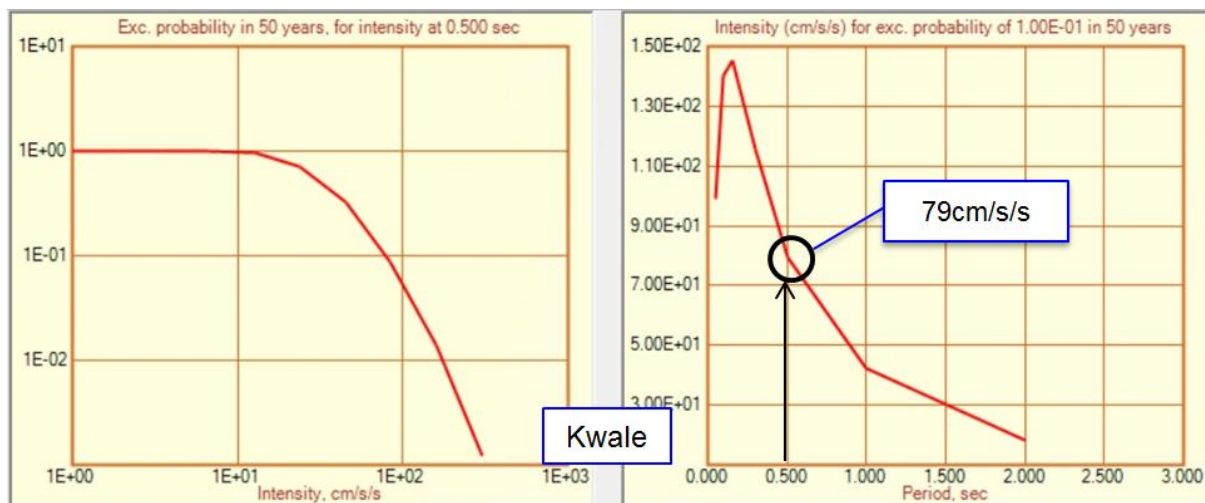


Figure 7-15 Seismic hazard curve & UHS for Kwale for a 5% in 50 year PGA at T=0.5s

7.3.7 UKUNDA

The highest probability of exceedance for Ukunda town was observed at 1E+00 (1 cm/s/s), while the lowest exceedance probability corresponds to 1E+02 (100 cm/s/s) as shown in Fig 7-15 below. The highest ground motion intensity level was observed at structural period T=0.05s, while the lowest ground motion intensity level was observed at structural period T=2.0s.

Therefore, earthquakes with short periods (T=0.05s) have the potential to cause the greatest damage at Ukunda town, due to the associated high PGA (148 cm/s/s), in contrast to earthquakes with longer periods (T=2.0s).

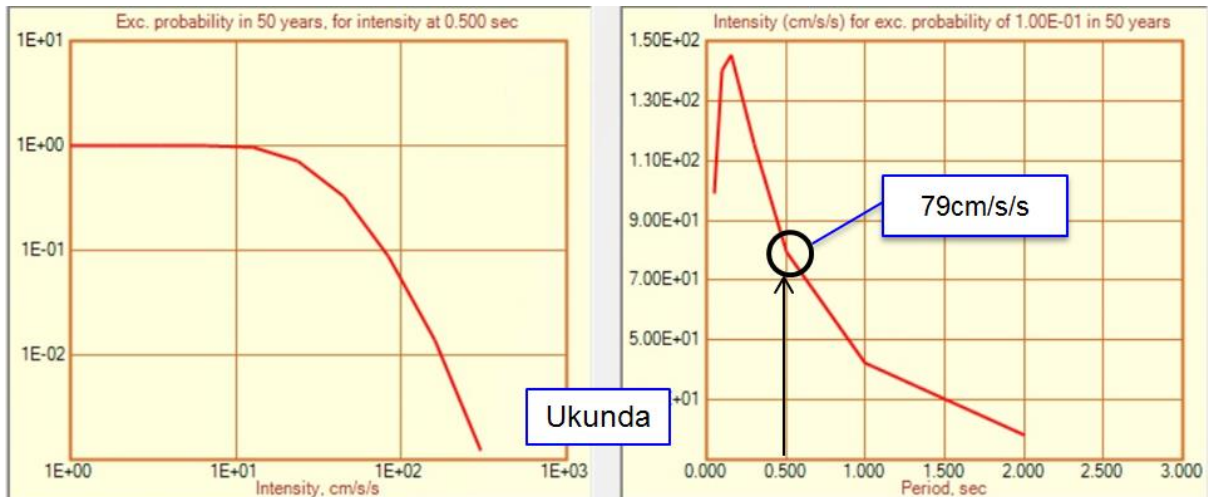


Figure 7-16 Seismic hazard curve & UHS for Ukunda for a 5% in 50 year PGA at T=0.5s

7.3.8 VANGA

The highest probability of exceedance for Vanga town was observed at 1E+00 (1 cm/s/s), while the lowest exceedance probability corresponds to 1E+02 (100 cm/s/s) as shown in Fig 7-16 below. The highest ground motion intensity level in the Study Area of 170cm/s/s was observed at structural period T=0.05s, while the lowest ground motion intensity level was observed at structural period T=2.0s.

Therefore, earthquakes with short periods (T=0.05s) have the potential to cause the greatest damage at Vanga town, due to the associated high PGA (178 cm/s/s), in contrast to earthquakes with longer periods (T=2.0s).

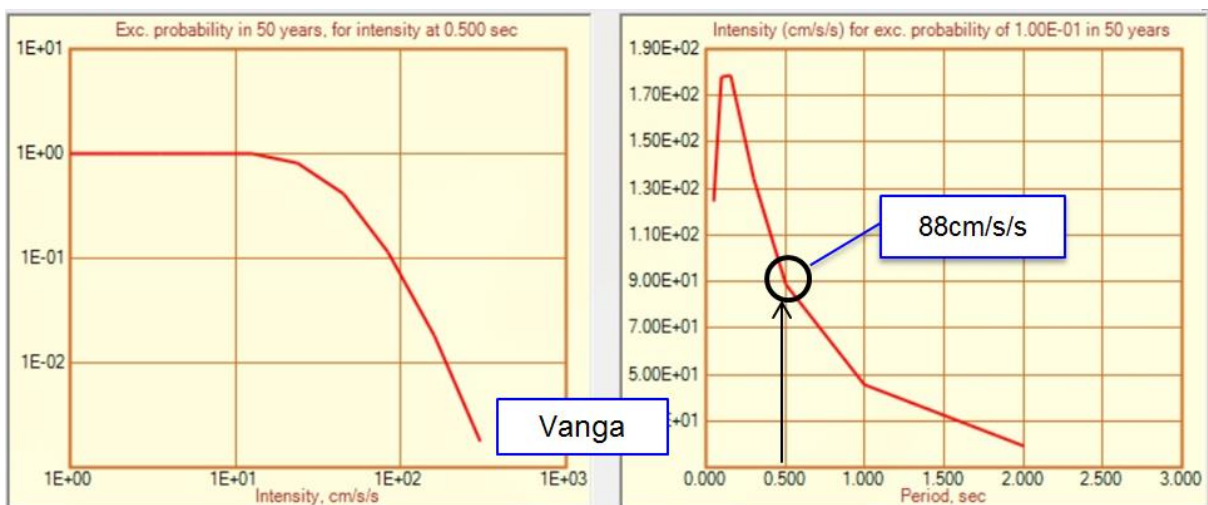


Figure 7-17 Seismic hazard curve & UHS for Vanga for a 5% in 50 year PGA at T=0.5s

8 DISCUSSIONS

8.1 SEISMIC SOURCES

8.1.1.1 *Faults*

Previous works done covering the study area (Giardini, 1992; Hayes et al., 2014; Lubkowski, 2014; GEM, 2016; Poggi et al., 2017, 2018; Jepkemoi, 2017) have not undertaken any field ground truthing to confirm the presence of faults or lineaments. The data used primarily came from geologic fault databases and geological mapping reports.

This study obtained data on geologic faults from a published geological map by the Ministry of Energy (1987). Afterwards a field ground truthing was carried out to confirm physical evidence of these faults and to deduce the predominant faulting regime in the study area. This was intended to inform the seismic source model in the seismic hazard computation.

Evidence of geological faults and lineaments exist in the study area. The geological faults and lineaments in the study area manifest as NE-SW trending river rapids in Kwale County, a NE-SW trending right-lateral elbow bend across river Nyore NW of Mombasa City and NE-SW aligned sag ponds at Vitengeni in Kilifi County. Except for the river rapids with 2m displacements in Kwale County, the rest of the manifestations are fault zones exposed at river beds.

The general trend and location of these fault manifestations agrees quite well with the published geological map by the Ministry of Energy (1987). However, the field ground truthing visit did not encounter physical evidence of the minor faults indicated on the mentioned map, nor the maps by Caswell et al (1953; 1956). These may be mapped through field geophysical methods.

An interesting phenomenon noted during the field ground truthing was the occurrence of geothermal hot springs at Maji Moto near Mwananyamala in Kwale County. These hot springs occur within a fault zone whose lithology is exposed at the nearby Ramisi River bed.

8.1.1.2 *Area Sources*

The latest works done in the study area like Poggi et al., (2017, 2018) and Jepkemoi (2017) have elected to use area seismic source zones rather than fault sources, mainly because the observed earthquakes could not be reliably associated with known geologic structures.

The same situation applies to the current study, which took place on a passive continental margin. However, this study explicitly carried out a field ground truthing to confirm any links between the instrumental earthquake epicenters and the positions of mapped geologic faults.

The results of the field visits confirmed that geologic faults in the study area are mainly normal or listric-normal faults, related to its setting on a passive continental margin occasioned by divergent tectonics during the Jurassic period. These geologic faults are mainly buried under sediment sequences, except at river beds where they are exposed. Surface manifestations encountered are benign and include NE-SW aligned sag ponds, elbow bends and river rapids.

A plot of instrumental earthquake epicenters in the study area covering the period from 1938 to 2019 shows that the epicenters are not located directly on the locations of the mapped geologic faults. This can be attributed to the listric-normal nature of these faults.

Post-field visit analysis indicated that the seismicity in the study area exemplifies a diffuse pattern, with most of the events occurring within a ~100 Km corridor extending NE-SW from northern Malindi to southern Kwale County. The zone covers the onshore and offshore parts of the study area. A second zone is found north of Mt. Kilimanjaro in the Tsavo area. It is curvilinear in a NW-SE trend and covers the westernmost tip of Kwale County. A third zone covers the Kilimanjaro volcano and the Manyara Rift. It is curvilinear in a NW-SE trend south of the study area. This zone has numerous moderate M5 and M6 earthquakes.

In this regard, a seismic Area Source Zone (ASZs) model was developed, consisting of these three seismicity corridors.

Previous works like Poggi et al., (2017, 2018) have assumed a single area source zone covering the study area. This generalization leads to an under-estimation of the contribution of the Juvenile Northern Tanzania Divergence and the offshore Davie Fracture on the earthquake activity, and thus earthquake hazard, in the study area. The present study has eliminated this generalization by clearly demarcating the specific source zones attributed to the Northern Tanzania Divergence, the Chyulu-Taita-Kilimanjaro volcano-seismic zone and the offshore Davie Fracture.

8.2 SEISMIC HAZARD

Previous work on seismic hazard assessment in the study region by the Global Seismic Hazard Assessment Program (Giardini, 1992), the US Geological Survey (Hayes et al., 2014), and Jepkemoi (2017) suggests a smaller earthquake hazard. GSHAP (1992) and USGS (2014) estimate a uniform seismic hazard level of 20cm/s/s in the area, but Jepkemoi (2017) forecasts

14cm/s/s to 18cm/s/s. Given that these studies did not undertake field visits to the study area, this is an underestimation of the inherent hazard.

The Global Earthquake Model (Pagani et al., 2018) assessed the world's seismic hazard based on PSHA. The resulting map predicts that the area has a seismic hazard level ranging between 50cm/s/s to 80 cm/s/s.

Previous work done by the Global Earthquake Model (Pagani et al., 2018) is considered by this author to be a close representation of the seismic hazard in the area. This is because it integrated a considerable body of scientists globally who contributed to the study. However, the seismic hazard map by GEM (2018) was designed with certain assumptions, chief being that a hard rock foundation underlies the entire study area and that the study area is covered by a single seismic source zone. Furthermore, it predicts that Malindi, Kilifi, Mombasa, Ukunda and Kwale towns all have the same seismic hazard level of 0.05-0.08g corresponding to 50 cm/s/s to 80 cm/s/s.

The present study reveals that the actual seismic hazard for the five (5) mentioned towns is not only higher (68 cm/s/s to 79 cm/s/s), but increases southwards from Malindi to Kwale. The study by GEM (2018) predicts the maximum acceleration in the study area to be at Vanga town, at 0.07-0.09g corresponding to 70-90 cm/s/s. The current study agrees with the prediction that Vanga town has the highest seismic hazard in the study area, but predicts a ground acceleration of 88cm/s/s. This can be attributed to the different attenuation relations applied in the two studies.

It is important to note, however, that despite Malindi town having the lowest seismic hazard levels in the study area, this does not completely preclude the possibility of a recurrence of the 1938 $M_s6.0$ earthquake at Kibiboni, 28 Km WNW of Malindi town. This is because earthquakes (or large aftershocks of ancient large earthquakes) that occur at passive continental margins have unusually long recurrence intervals, and may still cause damage, despite a computed low seismic hazard level.

8.3 HAZARD CURVES AND SPECTRA

Previous works done covering the study area by Lubkowski (2014), Jepkemoi (2017), and Poggi et al., (2017) have derived seismic hazard curves for only one town in the study area, that is, Mombasa City. While Mombasa city is the most densely populated city in the study area, in the recent past other areas of the study area have witnessed increased population growth and significant capital investments, like Malindi, Kilifi and Ukunda.

This study has derived graphs of earthquake hazard for Malindi, Watamu, Kilifi, Mombasa, Voi, Kwale, Ukunda and Vanga towns considering a 10% exceedance probability in a 50-year time frame and for a structural period of $T=0.5s$. For shaking durations of 0.05s, 0.1s, 0.15s, 0.3s, 0.5s, 1.0s, and 2.0s, uniform hazard spectra (UHS) have also been calculated for a set chance of exceedance of being surpassed in 50 years.

It was observed that the highest probability of exceedance for Malindi, Watamu, Kilifi, Mombasa City, Kwale, Ukunda and Vanga towns was at $1E+01$ (10 cm/s/s), while the lowest exceedance probability corresponds to $1E+02$ (100 cm/s/s). It was also observed that the highest ground motion intensity (hazard) level of 170 cm/s/s at all the towns in the Study Area was observed at the structural period $T=0.05s$, while the lowest ground motion intensity level was observed at structural period $T=2.0s$.

These observations agree quite well with the observations of the aforementioned authors. Therefore, short-period earthquakes have the greatest potential to cause considerable damage in the study area.

Deriving earthquake hazard distribution graphs for specific places within the area, such as Likoni in Mombasa, remains a priority. This will provide site-specific seismic hazard curves to be incorporated into future strategic civil infrastructure projects, like the proposed Mombasa Gate suspension Bridge at Likoni.

9 CONCLUSIONS AND RECOMMENDATIONS

9.1 CONCLUSIONS

The current study successfully used the probabilistic seismic hazard assessment (PSHA) approach to quantify the earthquake hazard in the area of study in terms of maximum horizontal ground shaking with a 10% chance of exceedance over a 50-year timeframe. Three goals were established to accomplish this task.

The first objective was to demarcate the earthquake sources that caused the seismicity in the area. It is clear from this study that earthquakes in/around the Study Area occur in three distinct zones (ASZs), influenced by the offshore Davie Fracture Zone (DFZ), the Northern Tanzania Divergence Zone (NTDZ) and the Chyulu-Taita Hills zone. The geologic faults within these zones are predominantly normal, or listric-normal faults with a general NNE-SSW trend, and a SE dip direction.

The second objective was to compute the peak horizontal earthquake ground accelerations for the study area in terms of annual probabilities of exceedance and extract the hazard curves for all major towns and cities. PGA in the Study Area was computed for a 10% exceedance probability in 475 years in cm/s/s, for spectral periods between 0.05 to 2 seconds. Seismic hazard spectra (UHS) indicate that earthquakes with short periods ($T < 0.5s$) have the potential to cause the greatest damage in the Study Area, due to the associated high PGA.

The final objective was to develop an updated earthquake hazard map of the area. This study successfully developed this map, with a 10% likelihood of being surpassed in 50 years in maximum horizontal shaking units of cm/s/s. The map indicates that the earthquake hazard in the area increases significantly from Malindi town in the north (68cm/s/s) to Vanga town in the south (88cm/s/s).

9.2 RECOMMENDATIONS

The following are the recommendations of the present study:

- a) The Government of Kenya should update the Kenyan Seismic Building Code to incorporate probabilistic seismic hazard analysis, which may necessitate the acquisition of more data and deployment of a wider broadband seismic network in the Coast region of Kenya to capture more microseismic activity, particularly in view of future strategic projects like nuclear power plants.
- b) The Government of Kenya (KeNHA) and Japan (JAICA) should undertake a probabilistic earthquake hazard assessment at the proposed Mombasa Gate Bridge site, and translate the same into its seismic design, considering that the 1990 Mw5 earthquake which occurred 33 Km S.E of Mombasa may have occurred on an active fault related to the Davie-Walu Fracture Zone.
- c) The County Governments whose jurisdictions are covered by the present study area should consider undertaking seismic risk analysis using the peak ground acceleration (PGA) data available from this study, in preparation for the development of County Seismic Building Codes. The County Governments should then enforce this Code in the construction industry within their respective jurisdictions to ensure earthquake resilience.
- d) The Nuclear Power & Energy Agency (NuPEA) in undertaking site studies for a nuclear power plant in Kenya, should consider prioritizing Kilifi County in view of its lower seismic hazard level *ceteris paribus*.
- e) Passive rifted continental margins which exhibit a high level of seismic activity and/or residual tectonic activity which can be attributed to reactivation of existing faults (e.g. Kenya's Indian Ocean coastline) should be re-classified as passive-aggressive continental margins. This will pave way for the development of attenuation relations that are specific to passive continental margins to allow for more accurate earthquake ground motion calculations during future seismic hazard analyses.
- f) Developers of probabilistic seismic hazard analysis (PSHA) software like CRISIS 2015™v4.1 should include a provision in their respective "Site Effects" modules to allow for the analysis of sites with a thick succession of lithologies (e.g. sedimentary stratification) with different seismic wave velocities, rather than being restricted to one underlying lithology (assumed uniform bedrock) with a fixed seismic wave velocity.

9.3 AREAS FOR FURTHER RESEARCH

This study postulates that the NNE-SSW curvilinear alignment of offshore earthquake epicenters south of Watamu town may result from an offshore fault separating the Mombasa High from the Tembo Trough (Simiyu, 2020), whose approximate location is illustrated in Appendix 11.3. The instrumental earthquakes may result from elastic accommodation of the strain generated by the nearby Davie-Walu Fracture Zone.

Therefore, there is a need to undertake detailed bathymetric and marine geophysical mapping of the offshore part of the area of study (offshore part of Watamu-Kilifi-Mombasa coastline) to properly constrain this structure in order to improve future seismic and/or tsunami hazard analyses or modelling.

10 REFERENCES

Abuodha, P.A.W. (2003) *Geomorphology of the Kenyan Coast: Not as a result of sea level change alone*. Kenya Marine Fisheries Research Institute, Mombasa, Kenya.

Agricultural University, Wageningen. 227 pp., 34 tbs, 32 figs, 160 refs,

Ahmad, N. (2016) *Steps for conducting Probabilistic Seismic Hazard Analysis using GIS and CRISIS tools*. Earthquake Engineering Center, University of Engineering and Technology, Peshawar, Pakistan.

Akkar, S., Bommer, J.J., 2007. *Empirical prediction equations for peak ground velocity derived from strong-motion records from Europe and the Middle East*. Bull. Seismol. Soc. Am. 97, 511-530.

Amu Power (2018) *Project Site*. [Online] Available at: <https://www.amupower.co.ke/contact.html>

Analysis. Sci. Rep. 7, 44171; doi: 10.1038/srep44171.

Baker, J.W. (2008) *An introduction to Probabilistic Seismic Hazard Analysis (PSHA)*. Version 1.3. Cambridge University Press, Cambridge, England.

Bechtel Corporation. (2017) *Bechtel selected to build first expressway in Kenya*. [Online] Available from: <https://www.bechtel.com/newsroom/releases/2018/08/bechtel-to-build-first-expressway-in-kenya> [Accessed: 25th February, 2018]

Bourbie, T., Coussy, O., Zinszner, B., 1987. *Acoustics of Porous Media*. Gulf Publishing Company, 27 Rue Ginoux 75737, Paris, France.

Caswell, P.V., Baker, B.H., (1953). *Geology of the Mombasa-Kwale Area*. Degree Sheet 69. Mines and Geological Department. Nairobi, Kenya.

Caswell, P.V. (1956). *Geology of the Kilifi-Mazeras Area*. Degree Sheet No. 66, SE Quarter. Report No. 34. Geological Survey of Kenya. Nairobi, Kenya.

Climate-Data.org (2018) [Online] Available from <https://en.climate-data.org> Accessed on 4th July 2018

- Condie, K.C., (1997). *Plate Tectonics and Crustal Evolution*. Fourth Edition, Butterworth-Heinemann, Jordan Hill, Oxford OX2 8DP, United Kingdom
- Cornell, C. A., Banon, H., and Shakal, A. F. (1979). *Seismic motion and response prediction alternatives*. *Earthquake Engineering & Structural Dynamics*, 7(4), 295-315.
- Delvaux, D., Barth, A. (2010) *African Stress pattern from formal inversion of focal mechanism data*. *Tectonophysics*, No. 482, pp. 105-128
- Dirkx, R. (2017) *Observations on Tectonic Evolution and Prospectivity of Madagascar Offshore Basins Based on Interpretation of New Seismic Data*. AAPG/SEG International
- Emishaw, L., & Abdelsalam, M. G. (2019). *Development of late Jurassic-early Paleogene and Neogene-Quaternary rifts within the Turkana Depression, East Africa from satellite gravity data*. *Tectonics*, 38. <https://doi.org/10.1029/2018TC005389>
- English and Dutch summaries, 1 map (1: 500 000).
- Giardini, D. (1999) *The Global Seismic Hazard Assessment Program (GSHAP)*. *Annals of Geophysics*. Vol. 42, No. 6.
- Global Earthquake Model (2016) *A seismic hazard model for Sub-Saharan Africa*. Technical Report, DOI: 10.13117/GEM.REG.TR2016.01
- Gupta, I.D. (2002) *The State of the Art in Seismic Hazard Analysis*. *ISSET Journal of Earthquake Technology*, Paper No.428, Vol.39, No.4, pp. 311-346
- Gutenberg, B., Richter, C. F. (1944). *Frequency of earthquakes in California*. *Bulletin of the Seismological Society of America*, 34(4), 185-188.
- Hayes, G.P., Jones, E.S., Stadler, T.J., Barnhart, W.D., McNamara, D.E., Benz, H.M., Furlong, K.P., Villasenor, A. (2014). *Seismicity of the Earth 1900-2013: East African Rift*. US Geological Survey Open-File Report 2010-1083-P, 1 sheet, scale 1:8,500,000. ISSN 2331-1258.
- McDonald, A. M., Dochartaigh, B.E.o., Bonsor, H.C., Davies, J., Key, R. (2010) *Developing quantitative aquifer maps of Africa*. *British Geological Survey International Report*, No. IR/10/103, pp34.

International Seismological Centre. (2015) *On-line Bulletin*. [Online] Available from: <http://www.isc.ac.uk> International Seismological Centre, Thatcham, United Kingdom. [Accessed 4th January, 2018]

Japan International Cooperation Agency (2020). *Signing of Japanese ODA Loan Agreement with the Republic of Kenya: Contributing to the stimulation of regional economic activities by the construction of a bridge at Mombasa, a gateway to East Africa*. Published on 11th December 2019. URL: https://www.jica.go.jp/english/news/press/2019/20191211_41_en.html. Last Accessed: 15th December 2019.

Jepkemoi, S.K. (2017). *Seismic Source Zone Model Definition and Characterization: Implication for seismic hazard assessment in Kenya*. MSc Dissertation. University of Nairobi, Nairobi, Kenya

Kanda, I., Njue, E., Suwai, J. (2012). *Opportunities for Direct Use of Medium Enthalpy Geothermal Resources in Mwananyamala Geothermal Prospect, Kenya*. Proceedings of the 4th African Rift Geothermal Conference. 21-23 November, 2012. Nairobi, Kenya.

Katumwehe, A.B., Abdelsalam, M.G., Atekwana, E.A, Lao-Davila, D.A., 2015. *Extent, kinematics and tectonic origin of the Precambrian Aswa Shear Zone in eastern Africa*. Gondwana Research, <http://dx.doi.org/10.1016/j.gr.2015.03.007>

Kenya National Highways Authority (2019). *Feasibility Study in the Mombasa Gate Bridge Construction Project, Mombasa County*. KeNHA, P.O Box 49712-00100, Nairobi, Kenya.

Kindt, R., van Breugel, P., Lilleso, J.P.B., Gachathi, F., Omondi, W., Jamnadass, R., Graudal, L. (2011) *Potential Natural vegetation of eastern Africa. Vol.8. Atlas and Tree Species Composition for Kenya: Forest and Landscape working paper xx-2013*. Available from www.sl.life.ku.dk [Accessed 9th July 2018].

Kivuti N. (1995) *Stratigraphy, depositional history and environments of deposition of Cretaceous through Tertiary strata in the Lamu Basin, South East Kenya and implications for reservoirs for hydrocarbon exploration*. Sedimentary Geology. Vol96, pp.43-71.

Lay, T., Wallace, T.C. (1995) *Modern Global Seismology*. Academic Press, San Diego CA, USA. ISBN-13: 978-0-12-732870-6.

Lombardi, A. M. (2017). SEDA: A software package for the Statistical Earthquake Data

Lubkowski Z., Villani, M., Coates, K., Jirouskova, N., Willis, M. (2014). *Seismic Design Considerations for East Africa*. Second European Conference on Earthquake Engineering & Seismology. Istanbul, 2014.

Mbede E.I., Dualeh, A. (1997) *The coastal basins of Somalia, Kenya and Tanzania*. African Basins, Sedimentary Basins of the world, 3, edited by R.C. Selley, pp.211-233, Elsevier Science B.V, Amsterdam, Netherlands.

McGuire R.K. (2004) *Seismic Hazard and Risk Analysis*. Earthquake Engineering Research Institute Monograph No. MNO-10.

Midzi, V., Hlatywayo, D.J., Chapola, L.S., Kebede, F., Atakan, K., Lombe, D.K., Turyomurugyendo, G., Tugume, F.A. (1999) *Seismic Hazard Assessment in Eastern and Southern Africa*. Annali Di Geofisica, Vol. 42, No. 6.

Ministry of Agriculture. (1980) *Exploratory Soil Map of Kenya*. Kenya Soil Survey, Nairobi, Kenya. Available at: <https://es.dac.jrc.ec.europa.eu/resource-type/national-soil-maps> [Accessed: 9th July 2018]

Morley, C.K. (1999) *Geoscience of rift systems - Evolution of East Africa*. AAPG Studies in Geology. Series No. 44, pp 242.

Mulwa, J.K., Kimata, F., Duong, N.A. (2013) *Seismic Hazard*. In, Developments in Earth Surface Processes, Vol. 16, pp. 267-292, Amsterdam, Netherlands.

Mumma, A., Lane, M., Kariu, E., Tuinhof, A., Hirji, R. (2011) *Kenya Groundwater Governance Case Study*. Water Papers, 71726. Available at: www.worldbank.org/water [Accessed 4th July 2018]

Nyaberi, M.D., Rop, B. K. (2014) *Petroleum prospects of Lamu Basin, South East Kenya*. Journal Geological Society of India. Vol. 83, pp.414-422.

Nuclear Power & Energy Agency (2022). *Kenya signs its fourth country programme framework for cooperation with the IAEA*. [Online] Available from: <http://www.nuclear.co.ke/index.php/press-release/news?start=6>

Oosterom, A.P., 1988. *The Geomorphology of Southeast Kenya*. Doctoral Thesis,

- Ordaz, M., Martinelli, F., Aguilar, A., Arboleda, J., Meletti, C., & D'Amico, V. (2015). *CRISIS2015 Program for computing seismic hazard*. Instituto de Ingeniera, UNAM, México.
- Ordaz, M., Martinelli, F., Aguilar, A., Arboleda, J., Meletti, C., & D'Amico, V. (2014). *CRISIS User's Manual*. Instituto de Ingeniera, UNAM, México.
- Pagani, M., Garcia-Pelaez, J., Gee, R., Johnson, K., Poggi, V., Styron, R., Weatherill, G., Simionato, M., Viganò, D., Danciu, L., Monelli, D. (2018). *Global Earthquake Model (GEM) Seismic Hazard Map* (version 2018.1 - December 2018), DOI: 10.13117/GEM-GLOBAL-SEISMIC-HAZARD-MAP-2018.1
- Pamukcu, O.A., Dogru, F., Cirmik, A., Gones, D., (2021) Seismic a and b-values and crustal parameters of Samos Island-Aegean Sea, Lesvos Island-Karaburun, Kos Island-Gokova Bay earthquakes. *Turkish Journal of Earth Sciences*, vol. 30, pp. 833-850.
- Phethean, J., Kalnins, L., Hunen, J, Biffi, P.G, Davies, McCaffrey, K.J.W. (2016) *Madagascar's escape from Africa: A high resolution plate reconstruction for the western Somali Basin and implications for supercontinent dispersal*. *Geochemistry, Geophysics, Geosystems*, vol.17, Issue 12, pp. 5036-5055.
- Pluijm, B., Marshak, S. (2004). *Earth Structure: An Introduction to Structural Geology & Tectonics*. Second Edition. WW Norton & Company. ISBN 0-393-92467-X
- Poggi, V, Durrheim, R., Tuluka, G.M., Weatherhill, G., Gee, R., Pagani, M., Nyblade, A., Delvaux, D. (2017) *Assessing seismic hazard of the East African Rift: a pilot study from GEM and AfricaArray*. *Bulletin of Earthquake Engineering*, vol. 15, issue 11, pp. 4499-4529.
- Reeves, C.V., Teasdale, J.P., Mahanjane, E.S. (2016) *Insight into the Eastern Margin of Africa from a new tectonic model of the Indian Ocean*. In, *Transform Margins: Development, Controls and Petroleum systems*, Geological Society of London, Special Publications vol. 431.
- Ring, U. (2014) *The East African Rift System*. *Austrian Journal of Earth Sciences*. Vol 107/1, pp.132-146
- Saria, E., Calais, E., Stamps, D.S., Delvaux, D., Hartnady, C.J.H. (2014) *Present-day kinematics of the East African Rift*. *Journal of Geophysical Research, Solid Earth*, vol. 119, pp.1-17.

Stein, S., Wyssession, M. (2003) *An Introduction to Seismology, Earthquakes, and Earth structure*. Blackwell Publishing, 350 Main Street, Malden, MA 02148-5020, USA.

United Nations Office for the Coordination of Humanitarian Affairs, (2007). *Earthquake Risk in Africa: Modified Mercalli Scale*. [Online] Available from: https://www.preventionweb.net/files/7483_OCHAROCEAEarthquakesv2071219.pdf
[Accessed: 25th February 2018]

United States Geological Survey. (2018) *Earthquake Hazards Program*. Available at: <https://earthquake.usgs.gov/earthquakes/search/> (Accessed 24-02-2018)

Wanjala, C.S. (2020) *Assessing the hydrocarbon potential of the offshore Lamu Basin using nuclear well logs*. Master's Thesis submitted to the Institute of Nuclear Science & Technology, University of Nairobi, Kenya.

Weatherhill G.A, Pagani M., Garcia J., (2016) *Exploring earthquake databases for the creation of magnitude-homogeneous catalogues: tools for application on a regional and global scale*. International Journal of Geophysics, pp. 206:1652–1676.

Wolin, E., Stein, S., Pazzaglia, F., Kafka, A., (2011) *Mineral, Virginia, earthquake illustrates seismicity of a passive-aggressive margin*. Geophysical Research Letters, Issue 2, vol. 39

Worku, A. (2017) *The Status of Basic Design Ground Motion provisions in seismic design codes of Sub-Saharan African Countries: A Critical Review*. Journal of the South African Institution of Civil Engineering, vol. 56, No.1, pp. 40-53, Paper 977.

11 APPENDICES

11.1 COMBINED EARTHQUAKE CATALOG (USGS & ISC, AD1938-2020)

Year	Month	Day	Hour	Min	Sec	Lat	Lon	Depth	Mag
1938	7	21	9	10	42	-3	40	35	6
1967	10	14	23	29	29	-3.3758	38.0388	14.2	5.7
1968	5	20	13	0	15	-3.0932	37.089	10	5
1969	4	18	16	12	1	-3.2611	36.4671	10	4.6
1971	1	5	0	58	15	-4.5653	36.7153	10	4
1972	10	30	16	13	43	-3.4381	36.5919	10	4.6
1972	11	7	9	16	48	-3.2692	36.6876	10	4.3
1973	3	29	13	50	33	-3.1999	39.0712	10	4.5
1975	7	28	12	58	41	-3.6749	36.1456	10	4.7
1975	8	2	22	53	35	-2.7727	37.4738	10	5.1
1975	8	5	20	59	35	-2.4952	38.7149	10	4.6
1975	11	29	10	16	7	-2.7757	36.8302	10	4.7
1975	12	23	7	23	56	-3.1925	37.098	10	4.6
1975	12	26	4	6	13	-3.3512	36.5279	10	4.4
1976	1	9	23	13	53	-3.222	36.6385	10	4.4
1976	1	19	17	30	22	-2.9557	37.2092	10	4.9
1976	1	21	22	24	16	-2.9174	36.7369	10	4.5
1976	2	5	7	46	25	-2.8566	37.3599	10	4.2
1976	2	9	20	4	45	-2.9832	37.2403	10	4.5
1976	11	29	20	42	22	-2.5463	37.1614	10	4.2
1977	3	25	0	44	21	-2.7505	37.2291	10	4.3
1978	4	5	17	46	11	-1.7134	36.998	10	4.7
1978	7	26	0	30	17	-5.025	37.8811	10	4.6
1980	12	4	21	5	47	-2.2386	39.3495	10	4.3
1983	5	9	16	15	21	-4.2789	37.7325	17.5	5.4
1984	10	7	3	55	56	-4.0063	37.8008	10	4.8
1986	9	27	4	50	15	-4.1864	37.6881	10	4.6
1988	3	13	9	47	42	-5.4113	36.7278	10	4.6
1990	3	13	23	5	29	-4.0307	39.9259	10	5.3
1990	5	7	6	24	31	-4.306	39.8199	10	3.9

1991	1	1	21	37	2	-3.199	38.178	10	4.2
1992	2	25	20	10	27	-6.8723	39.8734	10	4.2
1994	3	7	2	29	41	-3.76	37.312	15	3
1994	3	24	19	41	50	-3.47	39.579	13.2	3.4
1994	4	1	8	58	16	-6.329	41.408	13.1	3.2
1994	5	20	23	11	40	-3.197	37.015	18	2.3
1994	6	7	9	11	4	-4.703	39.252	8.1	2.8
1994	7	11	4	59	50	-2.712	37.653	36	1.7
1994	7	15	17	29	54	-2.841	37.732	27.4	2.9
1994	7	24	17	59	4	-0.461	38.226	15	3.1
1994	8	6	10	37	38	-3.163	36.122	24.8	2.4
1994	8	6	15	36	37	-3.168	36.152	24.5	2.1
1994	8	11	17	2	57	-2.937	38.078	16.1	2.4
1995	1	10	23	7	29	-3.78	36.48	50	3
1995	2	27	12	22	47	-2.9306	39.9749	10.5	4.9
1995	4	8	19	48	54	-4.117	37.586	38	3.5
1995	5	6	3	22	50	-3.783	36.996	34.1	3.1
1995	5	13	9	23	17	-2.571	37.319	38	3
1995	5	16	9	24	19	-1.027	37.206	36.4	3
1995	5	16	16	5	45	-5.376	37.075	38	2.9
1995	6	4	5	12	4	-4.9	39.818	19.8	3
1995	6	30	0	50	32	-1.868	39.367	15	3.3
1995	7	21	1	58	55	-5.053	39.407	15	3.7
1995	7	31	18	58	31	-1.103	38.432	15	3.6
1995	9	27	10	38	27	-2.998	36.445	15	3
1995	10	13	1	9	56	-2.24	36.78	8	2.7
1995	10	21	1	39	3	-1.99	36.69	8	3.1
1995	10	21	6	34	48	-3.63	37.17	36	3.2
1995	11	1	23	14	33	-1.33	39.5	34	3.8
1995	11	2	13	54	8	-2.62	36.4	10	2.4
1995	11	4	0	19	36	-2.97	36.15	15	3.9
1995	11	12	9	50	53	-4.12	37.41	18	3.2
1995	11	15	7	34	5	-3.73	36.52	8	3.3
1995	11	29	21	51	28	-3.24	37.49	15	3.4
1995	12	5	0	25	24	-2.12	36.44	18	2.4
1995	12	5	4	26	11	-4.43	39.2	14	4

1995	12	8	21	24	47	-2.19	36.52	15	2.9
1995	12	8	21	41	14	-2.16	36.51	15	2.7
1995	12	8	23	40	49	-4.5647	38.7557	10	5
1995	12	9	0	16	41	-4.5871	38.6678	15	4.2
1995	12	13	22	14	25	-3.91	36.46	8	3.9
1995	12	19	0	30	25	-2.96	36.56	12	3
1995	12	19	1	1	42	-4.57	36.49	15	4.1
1995	12	23	8	54	48	-2.56	36.42	12	2.7
1995	12	23	15	26	5	-3.39	36.87	9	3.4
1995	12	27	4	58	9	-2.07	36.49	15	2.8
1995	12	27	8	56	58	-2.97	36.83	8	3.2
1995	12	29	2	38	3	-2.6419	36.4492	9	2.9
1995	12	30	6	48	9	-3.53	39.03	8	3.3
1996	3	5	2	36	20	-2.263	36.513	10	2.4
1996	3	7	18	33	3	-3.439	37.546	10	3
1996	3	24	10	28	28	-1.871	36.667	10	2.2
1996	3	30	3	23	28	-2.333	37.34	13.1	2.8
1996	4	18	12	14	32	-3.034	37.754	12.9	2.9
1996	4	23	20	2	33	-3.863	36.086	10.1	3.4
1996	5	13	21	54	8	-1.428	37.696	10	1.7
1996	5	16	3	40	45	-4.173	36.48	38	3.4
1996	5	19	10	46	46	-3.041	36.146	13	3.6
1996	6	8	23	9	23	-3.046	36.415	28.9	2.3
1996	6	11	17	12	30	-3.005	36.363	32.9	3.1
1996	6	18	5	25	27	-2.944	36.869	38	2.7
1996	6	29	14	19	44	-2.815	37.714	10	2.2
1996	7	1	18	36	43	-6.041	39.131	10	3.8
1996	7	5	15	24	54	-1.826	38.22	10	2.2
1996	7	23	22	45	17	-3.827	36.219	13	4.1
1996	8	4	2	34	42	-3.052	39.021	28.4	3.1
1996	8	7	22	40	55	-3.031	36.146	13	2.7
1996	8	14	3	18	28	-2.079	36.439	10	1.6
1996	8	14	21	15	33	-2.418	40.086	13.1	3.3
1996	8	22	0	29	47	-3.115	36.495	5.6	2.5
1996	8	22	18	55	35	-2.968	36.433	38	2.6
1996	8	23	0	53	44	-1.798	38.647	24	2.4

1996	8	30	3	16	44	-2.409	36.341	10	1.3
1996	8	31	7	28	25	-2.924	37.871	10	1.3
1996	8	31	16	48	34	-3.175	38.082	5.4	2.8
1996	10	10	17	29	6	-3.583	36.461	12.6	3.4
1996	10	14	20	48	35	-2.916	36.348	12.3	3.3
1996	10	25	1	5	32	-3.049	39.374	37	2.9
1996	10	25	1	12	45	-2.672	39.704	10	3.9
1996	11	1	0	42	6	-2.579	38.46	9.8	2.4
1996	11	2	7	2	42	-3.005	38.255	5.8	3.1
1996	11	13	20	32	37	-3.573	36.184	12.9	3.3
1996	11	13	23	36	21	-2.858	37.89	18.2	2.3
1996	11	22	17	9	31	-2.704	37.651	13	3.7
1996	12	2	2	27	47	-2.966	36.273	11.5	2.9
1996	12	7	9	23	33	-2.979	39.449	11.7	3.2
1996	12	9	8	59	15	-2.191	38.094	10	2.3
1996	12	13	2	32	14	-2.272	36.432	10	1.7
1996	12	15	16	52	31	-3.23	36.445	6.1	4.1
1996	12	19	0	20	10	-1.747	37.937	50.5	2.4
1996	12	21	2	39	35	-2.057	37.735	10	2.2
1996	12	21	6	52	50	-2.188	37.02	10	3.2
1996	12	26	13	13	21	-1.262	37.038	10	1.3
1996	12	29	4	40	2	-3.169	38.583	10	2.6
1996	12	31	15	15	48	-4.7501	36.3247	35.3	3.9
1997	1	25	14	39	50	-1.979	37.826	31.7	3.1
1997	2	7	5	55	42	-3.705	36.429	6.7	3.1
1997	2	13	14	19	0	-3.3324	36.7756	7	3.1
1997	2	15	1	33	1	-1.814	37.564	14.1	3.3
1997	3	14	7	57	50	-2.6087	37.5864	22.3	3
1997	3	23	5	50	4	-3.007	36.265	23.3	3.8
1997	4	1	13	36	8	-2.9535	37.26	33	3.8
1997	5	22	7	39	51	-3.148	37	10.5	3.5
1997	6	9	2	38	30	-6.4361	39.356	10	4.2
1997	6	30	23	41	53	-3.439	37.522	10.4	3.1
1997	8	16	14	44	29	-3.836	36.669	29.7	3
1997	9	23	15	41	27	-4.188	37.66	12	3.5
1997	10	20	9	16	48	-2.749	37.651	10	3.2

1997	10	20	10	49	16	-3.703	37.381	12.9	3
1997	10	21	5	54	37	-2.781	37.654	10	3.1
1997	11	27	22	32	11	-2.837	37.486	22.1	3.2
1997	12	9	17	6	39	-2.492	37.688	11.1	3
1998	7	7	3	21	8	-3.186	36.222	20.7	1.8
1998	7	21	23	4	37	-2.34	36.325	14	1.6
1998	7	31	2	7	24	-3.549	39.547	9.1	1.6
1998	9	12	19	20	52	-3.143	38.081	11.5	4
1998	10	2	7	55	43	-2.401	39.248	10	2.9
1998	10	7	5	18	9	-2.468	36.489	10	2.6
1998	10	7	12	0	15	-1.996	36.552	10	2.8
1998	10	19	10	45	29	-1.634	36.893	14.1	3.2
1998	11	3	18	32	44	-1.214	38.698	14	2.5
1998	11	19	4	24	5	-3.072	37.118	10	4.5
1998	11	20	23	25	49	-3.076	37.133	26.5	3.4
1998	11	28	9	1	1	-2.28	36.565	10	2.6
1998	12	20	12	25	57	-3.215	39.981	6.7	2.8
1999	4	12	20	0	48	-5.048	37.279	13	3.4
1999	4	21	20	54	5	-3.024	37.255	12.7	2.6
1999	6	1	3	13	52	-3.098	36.247	6.7	3.2
1999	6	4	1	55	54	-3.252	36.105	38	3.3
2005	1	15	5	13	12	-5.9797	39.187	35.3	5
2006	6	17	21	53	8	-4.1699	39.6202	10	3.9
2007	7	15	11	24	21	-3.1145	36.2383	14.5	5.2
2007	7	15	20	42	12	-2.8693	36.2234	16.8	5.2
2007	7	16	22	42	41	-2.7751	36.1889	6.4	4.2
2007	7	17	10	34	34	-2.7838	36.2763	11.7	3.9
2007	7	17	14	10	43	-2.8335	36.2745	15.7	5.6
2007	7	17	18	27	51	-2.809	36.2488	8.6	4.9
2007	7	18	0	22	46	-2.8455	36.3722	10	4.3
2007	7	18	10	7	49	-2.8118	36.2258	10	3.7
2007	7	20	18	14	13	-2.9207	36.3111	8.9	4.2
2007	7	25	17	3	46	-2.8782	36.1886	10	4.2
2007	7	25	23	18	47	-2.7463	36.2385	18.5	4.2
2007	7	27	21	59	3	-2.8088	36.1816	10	3.7
2007	7	28	20	11	34	-2.7267	36.2186	10	3.9

2007	7	30	11	54	53	-2.4809	36.3395	11.7	4
2007	7	30	13	17	9	-2.8424	36.3616	10	3.8
2007	7	31	21	9	21	-3.0437	36.2636	10	4.5
2007	8	18	7	44	2	-2.9044	36.1694	17	5
2007	8	20	2	56	47	-2.7922	36.2114	7.3	5.2
2007	8	20	6	38	43	-2.3565	36.4379	10	4.3
2007	8	22	14	32	21	-2.7515	36.19	10	3.7
2007	8	25	2	8	37	-2.8476	36.3337	10	3.7
2007	8	30	18	49	35	-2.6724	36.2176	10	4
2007	9	10	0	26	43	-2.6982	36.2165	10	4.7
2007	12	23	12	56	12	-4.0311	39.2165	6	4.9
2008	2	14	6	16	27	-2.8355	36.3944	10	4.2
2008	2	14	11	5	29	-2.5312	36.3793	10	3.7
2008	2	14	15	31	2	-4.8058	39.3111	10	3.9
2008	4	30	13	42	56	-7.2127	39.6288	10	3.7
2009	10	14	22	10	10	-2.1957	37.427	10	3.5
2010	4	12	0	29	29	-3.4885	40.0402	10	3.6
2011	5	29	3	8	40	-2.406	39.5059	10	4
2011	6	10	8	28	13	-6.9916	39.5498	10	4.6
2012	4	17	2	1	20	-2.0556	37.5447	10	4.3
2012	4	25	21	56	20	-3.8712	37.8394	10	3.8
2012	11	30	8	46	53	-4.5784	36.2937	10	4
2013	8	21	8	30	24	-3.2937	36.3455	10	4.2
2014	2	19	19	40	43	-4.2819	38.6236	10	3.2
2015	9	8	23	43	25	-7.1583	39.5684	10	4.8
2016	3	22	10	56	17	-4.3984	35.9659	10	4.8
2016	7	13	3	1	14	-5.5088	35.966	10	5.1
2016	7	21	17	15	9	-5.6644	35.9952	10	4.5
2017	2	5	9	54	40	-5.0291	39.2566	14.98	4.5
2017	10	30	12	14	33	-5.4845	35.8673	10	4.5
2017	12	4	23	56	58	-5.6269	36.1336	10	4.4
2018	3	3	4	40	9	-7.6209	38.1373	10	4.7
2018	8	8	16	51	11	-2.0577	37.6557	10	3.4
2018	10	5	9	11	49	-5.4517	35.8542	10	4.4
2019	2	7	8	52	38	-3.3005	37.3751	10	3.7
2019	3	24	16	21	15	-3.0654	38.162	10	4.7

2020	8	12	17	13	16	-7.33	39.813	17.55	6.0
-------------	---	----	----	----	----	-------	--------	-------	-----

11.2 FIELD GROUND TRUTHING SCHEDULE

DAY	ACTIVITY
Day 1: 16th March 2019	Travel from Nairobi to Mombasa by bus. Accommodation and set up at Mtwapa Town.
Day 2: 17th March 2019	Hire of field vehicle and driver. Calibration of GPS.
Day 3: 18th March 2019	Field visit to Outcrop A, Quarry A and Quarry B.
Day 4: 19th March 2019	Field visit to River Bend A and Quarry C.
Day 5: 20th March 2019	Travel to Ukunda Town and set up. Hire of field vehicles and driver.
Day 6: 21st March 2019	Field visits to Outcrop B and River Rapids
Day 7: 22nd March 2019	Field visits to River Bend B, Hot spring A and Quarry D.
Day 8: 23rd March 2019	Review of fieldwork, travel back to Mombasa City and travel back to Nairobi.

11.3 LOCATION OF POSTULATED OFFSHORE FAULT

